Spatial Power Combining with a Linear Array and Lens Combination for Millimeter Wave Satellite Communications

by

Irfan Kadri B.Eng

A thesis submitted to the Faculty of Graduate Studies and Research in partial fulfillment of the requirements for the degree of

Master of Applied Science

Ottawa-Carleton Institute for Electrical Engineering
Department of Electronics
Carleton University
Ottawa, Ontario, Canada

December, 2003

Your file Votre référence
ISBN: 0-612-89846-6
Our file Notre référence
ISBN: 0-612-89846-6

ABSTRACT

The design and implementation of a linear array employing spatial power combining for millimeter wave satellite communications is discussed in this thesis. A spatial power combined linear array and lens combination has several advantages over conventional reflector and feed based antennas. Spatial power combining allows high power transmission without costly high power amplifiers and complex cooling mechanisms. This is achieved by using multiple lower power and lower cost amplifiers in parallel. These amplifiers are closely integrated with the radiating elements. The radiated power then combines in free space, resulting in a high power, high gain beam. A lens is added to the linear array to yield a beam similar to that of a reflector antenna.

The theory of spatial power combining, microstrip patch antennas and arrays is discussed. The design, implementation and testing of a working active antenna is then detailed. The resulting spatially combined linear active array with lens shows a gain of 42.53 dB with an EIRP of 53 dBm at 30 GHz. The radiation pattern shows a pencil beam as desired with cross-pol levels 30 dB below the beam peak. This is achieved in a system that measures 0.15 m x 0.15m x 0.205 m. The linear array and lens combination is also shown to be much more economical and easier to manufacture and cool than a comparable reflector based antenna.

ACKNOWLEDGMENTS

I would like to acknowledge the support of the Communications Research Centre for their assistance in providing the facilities for this research alongside Carleton University. The financial support of the National Science and Research Council and Carleton University is gratefully acknowledged.

On an individual basis, the assistance rendered by the following people has been invaluable in making this research possible: From Carleton University Professor Langis Roy, for guidance with the writing of the thesis; Mike Britton and Joey Bray for their invaluable discussions on microwave theory; Muhammad Arsalan for his desktop publishing skills; from the Communications Research Center, Soulideth Thirakoune for all his help and especially his patience while using the anechoic chamber; John Bradley for all his assistance with the amplifiers and mechanical drawings for the design and Professor Aldo Petosa for his inspiration and innovation, his guiding hand has steered the design through difficulties that often looked insurmountable. On a personal note I would like to thank my dear friend Denise Fung, for being there to help me rise to the challenge. To all I offer my deepest gratitude.

Finally I wish to dedicate this thesis to the memory of my mother. I hope I have made you proud.

TABLE OF CONTENTS

LIST OF FIGURES

LIST OF TABLES

CHAPTER 1

INTRODUCTION

1.1 Motivation and Introductory Remarks

Extremely high frequency (EHF) communications involves the utilization of microwave frequencies in the 30 to 300 GHz range. EHF communications systems have found widespread use, especially in the military, and are currently proliferating in commercial applications. Some of the advantages of using the EHF band versus lower frequency bands include:

- Frequency availability – The EHF band has the capability of providing wideband communications and frequency availability to its user.
- Size and weight – The small operational wavelengths of EHF frequencies, on the order of millimeters allows for smaller compact transceivers and antennas. To further reduce the size it has been proposed to integrate monolithic microwave integrated circuit (MMIC) amplifiers with the antennas thus resulting in a completely integrated antenna/transceiver system.
- Ease of deployment – The small size and lightweight of EHF transceivers allows them to be portable and thus easily and quickly deployed in difficult to reach remote areas.

Due to these advantages EHF communications systems are widely being touted for use for not only for commercial satellite communications but also for potential future terrestrial point-to-point wireless links. This is better illustrated by Figure 1.1 below which shows how EHF communication can be used to connect not only major urban areas with satellite links but also in parallel terrestrial EHF wireless links can be used to service rural and remote areas. This is of great significance to the Canadian geographical situation, as it will enable the equitable delivery of broadband services to all regions of the country

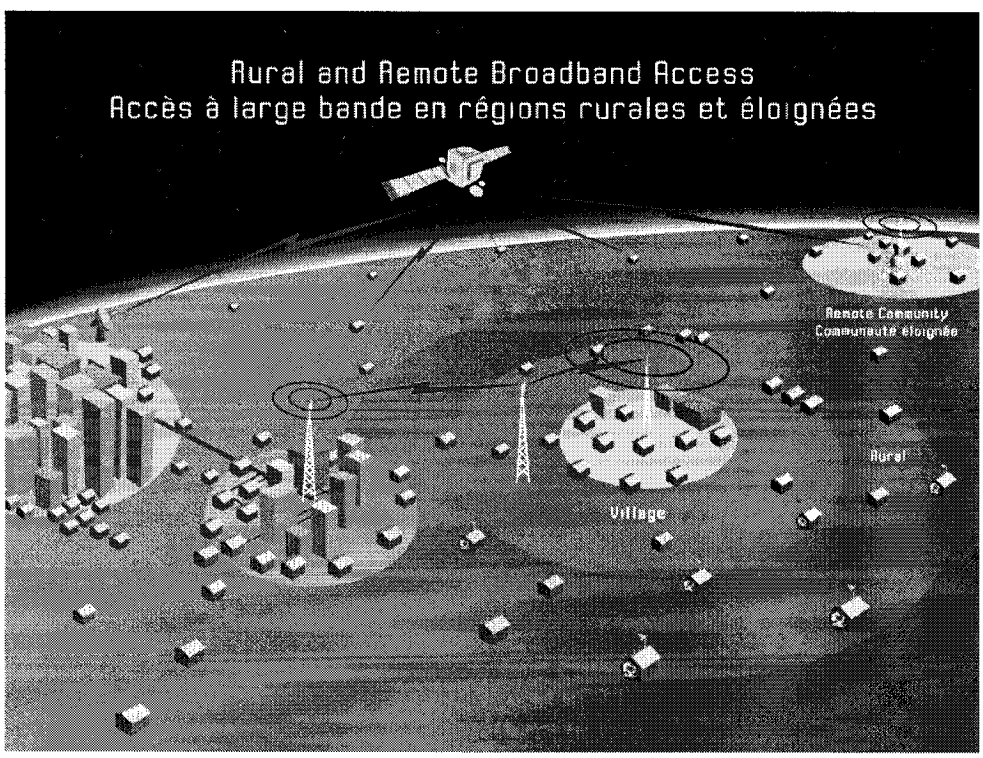

Figure 1.1: EHF Satcom and Terrestrial system [*Chou02*]

One disadvantage of EHF systems is that transmissions are more dependant on atmospheric conditions than at lower frequencies. Propagation studies have shown that the major factor affecting EHF transmission is rain attenuation. However when properly designed with adequate gain margins for

the geographic areas of intended use, EHF systems will provide satisfactory link availability performance. To further reduce the impact of varying atmospheric conditions, circular polarized transmission are utilized. This allows the link to be active even if polarization transformation occurs.

In order to maintain a good gain margin it becomes necessary to use high power amplifiers. At EHF frequencies conventional designs usually employ single high power amplifiers in the transmit chain to achieve the required gain margin. There are significant drawbacks to this approach however. Single high-power EHF amplifiers are costly to design and manufacture, and require significant active cooling to operate optimally. Should the amplifier fail, the entire communications system shuts down, i.e. there is no failsafe.

Spatial power combining is envisaged as a technique to overcome this bottleneck in EHF communications. It proposes to replace a single high performance amplifier and antenna, with arrays of distributed low cost, low power amplifiers and antennas called "active antennas" operating in parallel. The motivation for the present study arises from the need to assess how spatial power combining techniques can be employed to provide a more efficient, less costly method of achieving higher power at EHF frequencies – as applicable to portable terminals for EHF SATCOM or for potential future EHF terrestrial wireless applications. By using the spatial power-combining alternative it is possible to make use of cheaper, lower-power amplifiers in conjunction with economical printed circuit antennas such as microstrip patches. Such a structure would be easier to thermally manage. Also if a single amplifier were to fail, the

system can still continue to operate due to spatial diversity albeit with reduced performance.

For some of the upcoming EHF satellites (operating at 20/30 GHz and requiring circular polarization), it is estimated that the ground terminal should provide an EIRP of at least 45 dBW. The amount of power required from the amplifiers will then depend on the gain of the antenna and the efficiencies associated with power combining. For example, if a 40 dB gain antenna (reflector or reflect array) is used, then 5 dBW of power has to be generated at the output of the spatial power-combining array assuming the spatial power combiner to be 100% efficient.

1.2 Thesis Objectives

The general area of EHF spatial combining is quite large, encompassing areas such as beam shaping, thermal management, MMIC circuit design, packaging and environmental protection, among many other issues. The main objectives of this thesis are as follows:

- To study spatial power combining techniques and configurations based on active antenna arrays.
- To design practical broadband microstrip antenna elements for operation at EHF frequencies.
- To study and implement arrays of antennas for beam shaping as a viable alternative to conventional horn and reflector antenna assemblies.

- To implement practical methods of integrating active devices with microstrip antenna elements in order to output higher power more efficiently.
- As a result of the above, to design and implement a practical active antenna system for a 20 GHz receive – 30 GHz transmit, portable SATCOM terminal.

It is thus hoped to further the use of microstrip antenna elements with integrated MMIC's in EHF communications systems. The potential benefits of this would be the realization of low cost, compact SATCOM terminals that not only enhance the utilization of EHF frequencies for SATCOM networks but also bring closer to reality, future broad band terrestrial wireless networks

1.3 Thesis Organization

Chapter 2 provides an introduction and overview of power combining techniques and a summary of successful experimental demonstrations of antenna arrays that have employed spatial power combining. The chapter then covers a review of the theory and terminology of patch antenna design and the theory behind antenna arrays as will be required for better understanding of the work in the chapters to follow.

Chapter 3 focuses on the first attempt at designing a spatially combined array in the form of a planar array architecture. The chapter compares the use of horn antennas versus microstrip antennas as feed elements for a reflector dish. Various configurations of passive planar arrays are explored, the advantages and disadvantages of the various configurations are evaluated and finally the

challenges in implementing a feed design and power splitting network are presented.

Chapter 4 continues the work presented in chapter 3 and presents the evolution of the planar array architecture into a linear array architecture. The linear array configurations designed are presented with simulated and measured results. The work done to allow for easier integration of active devices into the linear array architecture is also shown in this chapter. The chapter then shifts to describing the design of a practical 20/30 GHz circularly polarized transmit/receive passive array, as opposed to a simple linearly polarized 30 GHz transmit design, that was previously studied. Once again simulated and measured data are shown and compared.

Chapter 5 presents the actual integration of the active devices with the linear array. It begins with a description and tradeoff study of the amplifiers available for use. The measured results of the amplifier chosen for this project are shown. Finally the measured results from the design of an active array using spatial power combining are presented.

Chapter 6 is a summary of the work carried out showing the impact of the thesis results. Also offered are suggestions for future research that may be carried out in this area.

Also of note is the work shown in Appendix E. A complete Fresnel lens design is shown as well as original methods to make Fresnel lenses multi-frequency capable.

CHAPTER 2

OVERVIEW OF SPATIAL POWER COMBINING AND RELATED DESIGN CONSIDERATIONS

This chapter is an overview of the underlying concepts useful in the design process. The theory covered is relevant to the entire design cycle as it not only sets the boundaries of what can be achieved but it also provides impetus for the evolution of the design. The three concepts that will be covered are the theory, methods and applications of spatial power combining; the theory and design of microstrip patches; and the theory and the use of arrays.

2.1 Spatial Power Combining

In the antenna array to be designed, spatial power combining techniques are utilized mainly to obtain large gain and for shaping the beam pattern.

Spatial power combining is a technique whereby power is combined in beams or modes in free space rather than via transmission lines. It is a novel approach that aims to provide the advantages of solid-state technology for millimeter wave frequencies *[Harv00]*. Recent research into the area has resulted in a number of successful demonstrations of spatial combined amplifier elements from frequencies of 10 GHz (P_{out} = 150 W) to 60 GHz (P_{out} = 36 W). A survey of the more promising architectures is provided in Section 2.2.

Combining by using transmission line circuits is inherently limited due to the losses in the lines and combining structures. Examining the corporate feed in Figure 2.1(a) it can be seen that as additional elements are added, the length of the transmission lines and number of combining nodes increase. The losses of the structure increase non-linearly with the complexity of the circuit. Eventually these exceed the increment power of the added amplifiers and the overall output power decreases *[Harv00]*.

Spatial power combining as illustrated in Figure 2.1(b) avoids line losses by eliminating the combining nodes. The output power of the amplifiers is combined in beams in free space. This can result in more efficient amplification of the input signal.

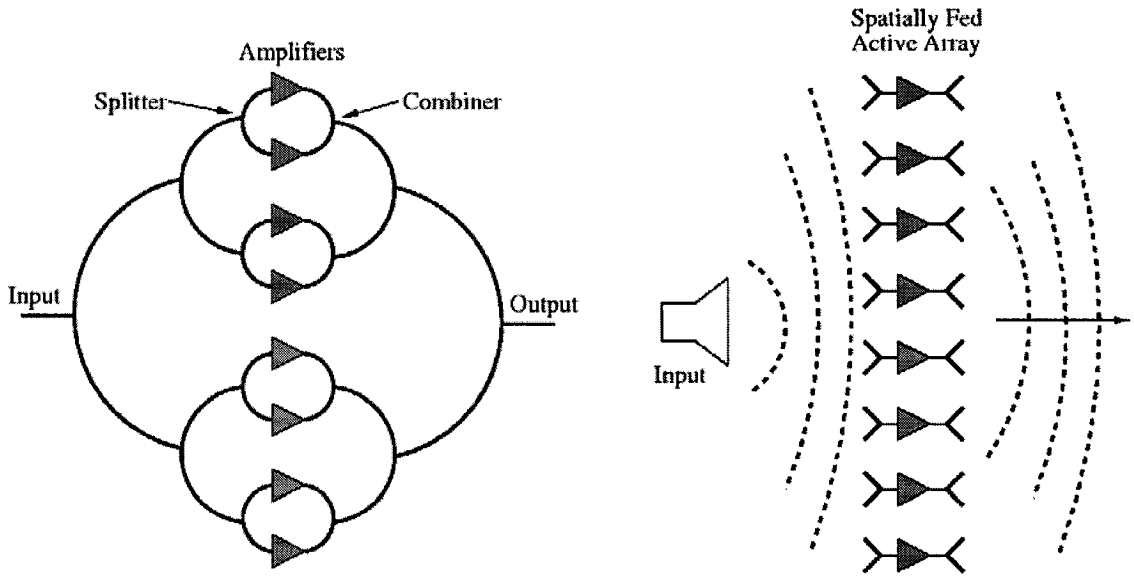

Figure 2.1: a) Circuit power combining. b) Spatial Power Combining[*Deli02*]

However due to the complexity inherent in the design of a spatially combined array, the technique is best suited to high power high frequency applications with arrays consisting of a large number of elements *[Deli02]*. At lower frequencies i.e. < 10 GHz, the line losses are not significant enough to warrant the use of spatial power combining.

2.2 Spatial Power Combiner Architectures

The two classic array topologies for spatial power combining are the tile and the tray architecture. These configurations are examined in the following sections with their associated advantages and disadvantages.

2.2.1 Tile Architecture

The tile architecture involves the use of radiating elements with integrated amplifiers placed perpendicular to the direction of wave propagation as in Figure 2.2(a). The wave is received on one side, amplified by the active device and then

radiated normal to the surface on the other side. The tile architecture is exemplified by two emerging topologies, the grid spatial power combiner and the active array tile power combiner. Two implementations of the tile architecture are shown in Figures 2.2(b) and 2.2(c) *[Deli02].*

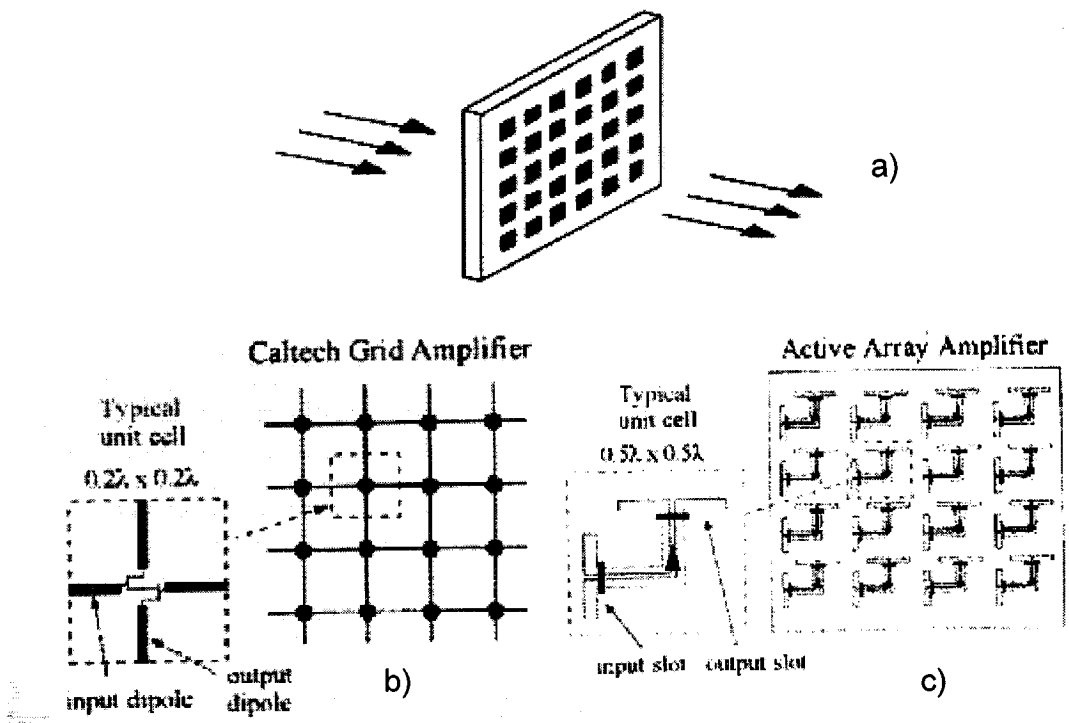

Figure 2.2: a) Tile Architecture b) Grid Combiner c) Active tile combiner

In the grid implementation, active devices (usually differential transistor pairs) are integrated at the vertical and horizontal intersections of a metallic mesh. The array then couples to a wave propagating normal to the surface. To achieve isolation between the input and output of the spatial power combiner the incoming and outgoing waves are orthogonally polarized. Recently reported grid amplifiers are monolithically fabricated and typically utilize dipole elements as the receive/transmit antennas. Due to the nature of fabrication, grid amplifiers yield small cell sizes (average unit cell sizes are in the order of 0.1λ x 0.1λ) and lower

power per cell than is possible from a single differential pair (due to cross coupling). However the grid can be densely packed, which allows for moderate gain and power handling on a single chip. This is very desirable in applications where inexpensive mass produced amplifiers are required.

An active tile array uses larger unit cells with each element of the array composed of an antenna integrated directly with an active device such as an MMIC. The individual cells are placed closer than half a wavelength. Thus the combination of all the cells forms a periodic antenna array structure. The wave is received on one side, amplified by the active device and then radiated normal to the surface on the other side. In the designs demonstrated to date, the antenna elements have consisted of dipole or slot antenna elements. This can be extended to patch elements as is proposed in the present research.

The active tile array is easily amenable to the addition of other active devices such as frequency multipliers and phase shifters, thereby greatly adding to the functionality of the structure.

2.2.2 Tray Architecture

The tray approach differs from the tile approach in that the wave is fed parallel to the antenna elements. This approach is ideally suited for use with traveling wave or endfire type antennas. Multiple trays can be stacked on top of the other to form a two dimensional array. A circuit that is perpendicular to the plane of the antenna array amplifies the input signal. This is subsequently radiated from the other side of the tray as shown in Figure 2.3

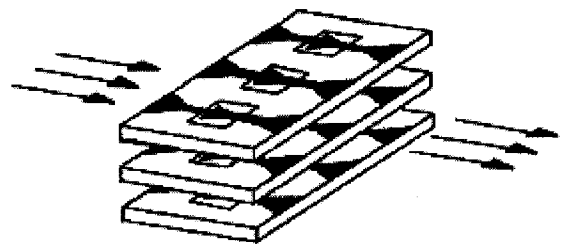

Figure 2.3: Tray Architecture

The tray approach allows for improved functionality since circuit integration is done directly along the path of signal propagation. It also provides the greatest isolation between the active circuits. Of the two architectures the tray is also the simplest for implementing thermal management schemes. *[Harv00]*

2.2.3 Survey of Experimental Demonstrations

A brief survey of the designs reported to date is given in Table 2.1. The capabilities of spatial power combining techniques are shown, especially with regards to the output power and bandwidths that are possible.

Table 2.1: Summary of power combining experimental demonstrations *[Harv00]*

Organization	Technique	Number of Elements	Output Power – EIRP	Frequency and Bandwidth	Bias Condition
University of California Santa Barbara	Tray	Eight trays with 32 MMIC's	150 W	8 to 11 GHz	8 V @ 60 A
Lockheed Martin/ NC State	Tile	45 elements double sided	25W	800 MHz @ 34 GHz	Not reported
Caltech/Rockwell	Grid	512 p-HEMT transistors	5W CW	1.3GHz @ 37 GHz	2.7 V @ 6.5 A
Sanders	Tray	272 MMIC's	35 CW	4GHz @ 61 GHz	Not reported

It is clear from the above results that free space power combining is a very viable approach for large power handling at millimeter wave frequencies.

Although not summarized above, the linearity and distortion characteristics of the amplifiers are also very promising due to operation of the individual devices at low power. For example the Caltech/Rockwell grid amplifier system demonstrated a third order intercept point of 45 dBm.

2.2.4 Potential Applications

The power handling and linearity of free space power combiners means that they have the potential to compete with Traveling Wave Tubes (TWT) amplifiers especially in satellite communication applications *[Harv00]*. However this is still an area that needs to be explored as TWT's are quite firmly entrenched as the device of choice in microwave power modules due to their ruggedness in the harsh environment of space.

Another more promising application of free space power combining amplifiers is in the area of airborne communications transponders. Transponders mounted on dirigibles and aerostats are being touted as more economical alternatives to the more expensive and difficult to deploy, communication satellites *[Harv00]*.

Other potential areas of applications include the use of free space power combiners in small size radars. Due to the compactness of the amplifier arrays they can be integrated in radars such as missile seekers where space is of a premium. Many of the proposed next generation missile seekers are being fitted with mm-wave seekers due to their all-weather capability and increased precision e.g. the AMRAAM air-to-air missile *[Harv00]*. Arrays of free space power combiners could be fitted with phase shifters to allow for dynamic beam steering. The compatibility of the phase shifters with the amplifiers offers tremendous

advantages in that it can replace mechanical gimbals for beam steering and the integral antenna of the free space power combiner could replace the parabolic dish in the nose of the missile. Conceivably this could lead to weight, size and cost savings of up to 50%.

2.3 Patch Antenna Theory and Design Methodology

The basic radiating element to be used for the design of the array was the microstrip patch. An understanding of its basic theory and underlying principles is necessary in order to better understand the choice of this element in the overall design and its impact on the antenna system. This will be further seen in Chapters 3 and 4.

Microstrip patches are commonly used antenna elements *[Shaf93]*. They consist of a metallic patch suspended above a grounded substrate of height *h* and relative permittivity of ε_r.

Microstrip antennas find widespread usage as they are low profile and can be designed to be conformal; are light weight and inexpensive to manufacture using printed circuit board etching techniques; are operational over a wide range of frequencies (typically 1-40GHz); can be fed using a variety of methods; can generate either linear or circular polarization; are easily combined to form linear or planar arrays and are amenable to integration of active components allowing for more complex operations such as beam forming and scanning.

There are different analytical models to predict the behavior of patch antennas. These include the transmission line model, cavity model and full wave analysis *[Bala82]*.

Although the transmission line model is the least accurate of the three, it is the easiest to use and offers a good guideline for the initial design of patch antennas. Commercial electromagnetic simulators such as Ensemble *[Ens80]* are useful to subsequently refine the design and optimize for the desired results.

2.3.1 Patch Feed Mechanisms

There are various methods of exciting a patch. Some of the common ones are illustrated below:

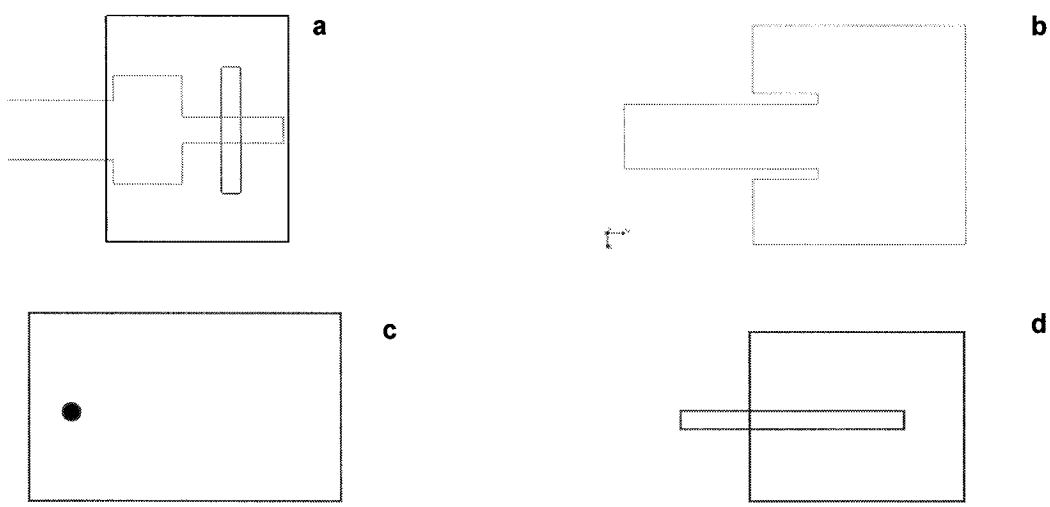

Figure 2.4: Various feed mechanisms for a patch – a. aperture coupled patch, b. direct feed patch, c. probe fed patch d. proximity fed patch

The direct feed and probe-coupled patch have a physical connection between the feed transmission line and the radiating element. As such they are more suited to low frequency applications < 10GHz as the feed radiation tends to interfere with the patch pattern for higher frequencies.

The aperture coupled and proximity fed patch on the other hand electro magnetically couple energy from the feed lines to the radiating element. This in

turn makes them more useful for higher frequency applications as the feed is physically separate from the patch.

2.3.2 Patch Design Parameters

Effective dielectric constant

The transmission line model replaces the inhomogeneous configuration of the microstrip patch, in which the fields are concentrated both in air and within the substrate, into a homogenous configuration. This is accomplished by combining the effect of the air and the substrate into a new medium with an effective dielectric constant ε_{eff}. The static value of ε_{eff} is given by *[Bala82].*

$$\varepsilon_{eff} = \frac{\varepsilon_r + 1}{2} + \frac{\varepsilon_r - 1}{2}\left(1 + 10\frac{h}{w}\right)^{-1/2} \qquad \textbf{[2.1]}$$

Major Patch Dimensions

Shown in Figure 2.5 are the most important dimension of a patch antenna. The values for these dimensions can be calculated using the equations shown in Section 2.3.4 through 2.3.6.

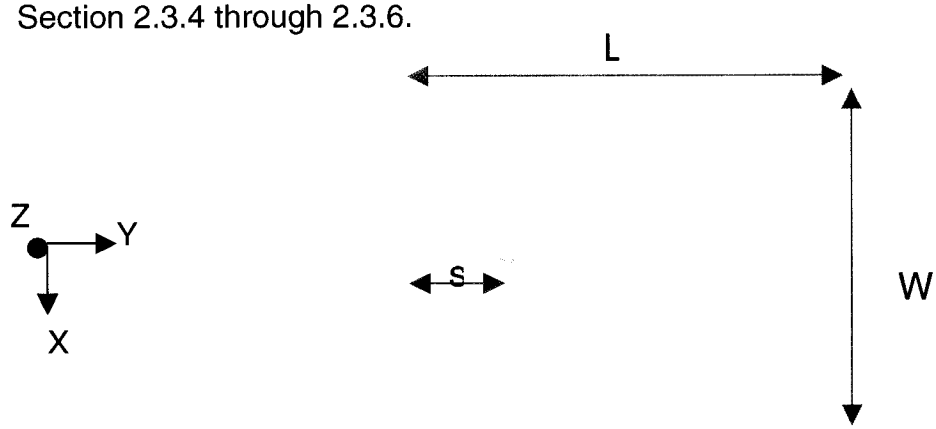

Figure 2.5: Major dimensions for a patch

Resonant Length

The resonant length (see Figure 2.5) of the patch antenna can be calculated to a first approximation by using the equation for a half wavelength transmission line *[Bala82]*:

$$L \approx \frac{\lambda_o}{2\sqrt{\varepsilon_r}} \qquad \textbf{[2.2]}$$

However due to the presence of fringing fields the patch appears electrically larger than its physical area by a factor of *2(ΔL+ΔW)*. *ΔL* and *ΔW* can be determined using *[Bala82]*:

$$\Delta L = \frac{0.412h(\varepsilon_{eff} + 0.3)\left(\frac{W}{h} + 0.264\right)}{(\varepsilon_{eff} - 0.258)\left(\frac{W}{h} + 0.8\right)} \qquad \textbf{[2.3]}$$

$$\Delta W = \frac{\ln 4}{\pi} h = 0.4413h \qquad \textbf{[2.4]}$$

The length of the can then be calculated using *[Bala82]*:

$$L_{eff} = (L + 2\Delta L) \qquad \textbf{[2.5]}$$

For the dominant mode the resonant frequency of the antenna is then given by *[Bala82]*:

$$f_o = \frac{c}{2L_{eff}\sqrt{\varepsilon_{eff}}} \qquad \textbf{[2.6]}$$

Patch Width

The second dimension of the patch that requires calculation is the width. The width affects the patch input impedance and the bandwidth. The width of the patch to a first approximation can be calculated using *[Bala82]*:

$$W = \frac{c}{2f_o}\sqrt{\frac{2}{\varepsilon_r + 1}} \qquad \textbf{[2.7]}$$

Location of Feed Point

The final part of designing a patch antenna is the location of the feed point. This is important in that it determines the input impedance of the patch. Ensuring that the impedance of the transmission line feeding the patch is equal to that of the patch will minimize mismatch losses.

The transmission line model lumped equivalent values for conductance G_s and susceptance B_s of a patch, of width W are given by*[Bala82]*:

$$G_s = \frac{W}{120\lambda_O}\left(1 - \frac{1}{24}(k_0 h)^2\right)$$

$$B_s = \frac{W}{120\lambda_O}\left(1 - 0.636\ln(k_0 h)\right)$$

$$k_o = \frac{2\pi}{\lambda} \qquad \textbf{[2.8]}$$

The location of the feed point as a function of the offset distance s from the edge of the patch is then given by *[Bala82]*:

$$R_{in}(s) = \frac{1}{2G_s}\cos^2\left(\frac{\pi}{L}s\right) \qquad \textbf{[2.9]}$$

At the resonant frequency the input impedance is purely resistive and is given by *[Bala82]*:

$$R_{in} = \frac{1}{2G_s} \qquad [2.10]$$

2.3.3 Radiation Patterns for a Patch

The radiation pattern is one of the most important characteristics of an antenna. The far field radiation pattern for a patch antenna can be described by the two components of the E-field. For a patch in the XY plane with θ measured from the Z-axes and ϕ from the X-axes the E-field is given by *[Bala82]*:

$$\begin{aligned} E_\theta(\theta,\phi) &= \frac{-\sin(W_k)\cos(L_k)}{W_k}\frac{\cos\phi(\varepsilon_{eff} - \sin^2\theta)}{\varepsilon_{eff} - \sin^2\theta\cos^2\phi} \\ E_\phi(\theta,\phi) &= \frac{\sin(W_k)\cos(L_k)}{W_k}\frac{\varepsilon_{eff}\cos\theta\sin\phi}{\varepsilon_{eff} - \sin^2\theta\cos^2\phi} \\ W_k &= 0.5kW\sin\theta\sin\phi \\ L_k &= 0.5k(L + 2\Delta L)\sin\theta\cos\phi \end{aligned} \qquad [2.11]$$

where W = width of the patch

and L is the length of the patch

The total E-field is therefore *[Bala82]*:

$$E_\theta(\theta,\phi) = \sqrt{E_\theta{}^2(\theta,\phi) + E_\phi{}^2(\theta,\phi)} \qquad [2.12]$$

When plotted the resulting pattern as shown in Figure 2.6

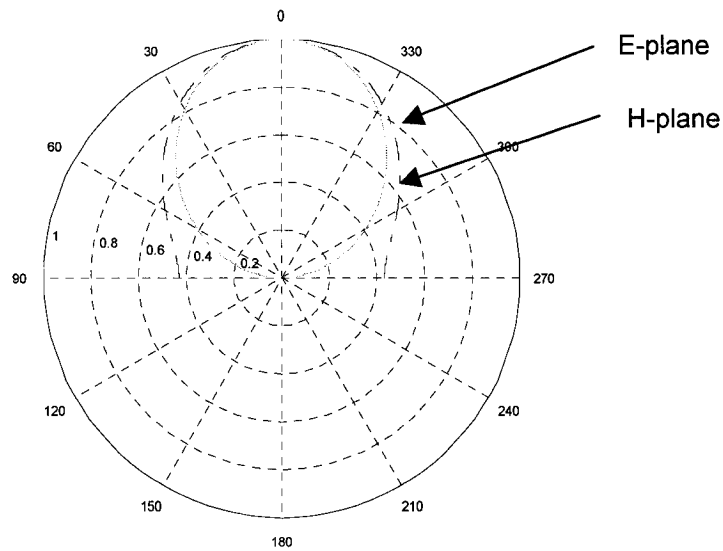

Figure 2.6: Patch radiation pattern

With the E-plane being the pattern cut for $\phi = 0^0$ and the H-plane being the pattern for $\phi = 90^0$ with respect to the patch shown in Figure 2.5. Typically the gain for a patch antenna is between 5 and 6 dB *[Hans98]*

2.4 Array Theory

The previous section concentrated on the theory behind a single element patch. In order to obtain more degrees of freedom in the design of the desired antenna beam shape, the basic patch elements may be placed in arrays. The placement of the individual patches so that their patterns combine/interfere correctly is governed by array theory. This section is a brief overview of the parameters that govern the behavior of an array.

Antenna arrays are often used to combine a number of low gain, wide beam width elements into an antenna with a higher gain i.e. a more focused radiation pattern. Patch elements are ideal for linking together to form arrays because of the ease in which an array of patches can be manufactured.

The radiation pattern of an array can be very carefully tailored by adjusting the number of elements, the location i.e. spacing between elements, the orientation of the elements and the amplitude and phase of the signal fed to each element.

Manipulating the above design parameters allows characteristics of the antenna array to be controlled such as the location of the beam peak, sidelobe levels and the location of the nulls.

In addition to the above benefits of using an array, arrays can be mated with active elements such as phase shifters to allow for dynamic beam steering. This is often known as a phased array.

An array works via the principle of array multiplication, that is the far field radiation pattern of an array is the product of two patterns:

Array Pattern = Element Pattern x Array Factor

2.4.1 Uniformly Excited Linear Arrays

The excitation of an array consists of the amplitude and phase at each element. This discrete distribution is known as the aperture distribution. For a uniformly excited array every element in the array has a constant amplitude excitation but may have a variable scan phase. An example of a linear array can be seen in Figure 2.7.

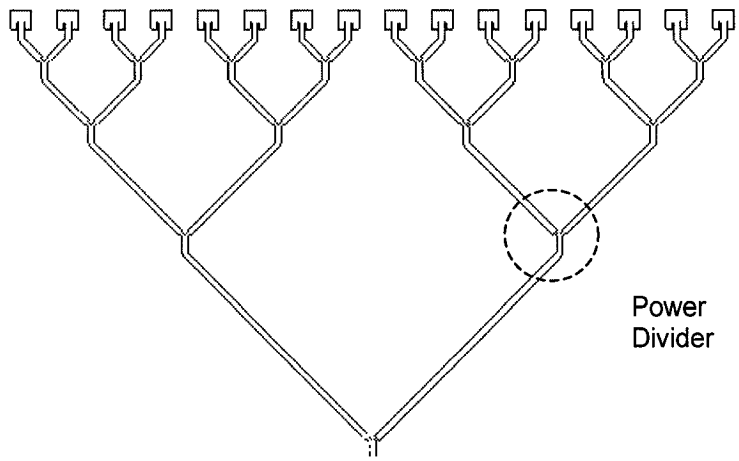

Figure 2.7: A corporate fed linear array

Array Factor for Linear Arrays

In the far field the contribution of each element to the array factor can be given as *[Bala82]*:

$$AF(\theta) = \sum_{n=1}^{N} A_n e^{j((n-1)kd\cos\theta+\beta_n))} \qquad \textbf{[2.13]}$$

where k = $2\pi/\lambda$, d is the inter element spacing, β_n is the phase excitation, A_n is the amplitude excitation, N is the number of radiating elements and θ is the scan angle from boresight.

A uniformly excited array with linear phase progression, has $A_n = A_0$ and $\beta_n = (n-1)\ \beta$. Many practical arrays are excited in this fashion. The array factor then simplifies to *[Bala82]*:

$$AF(\theta) = A_0 \sum_{n=1}^{N} e^{j(n-1)(kd\cos\theta+\beta)} \qquad \textbf{[2.14]}$$

Taking the Fourier transform of the array factor, the magnitude of the array factor becomes *[Bala82]*:

$$|AF(\psi)| = A_0 \frac{\sin(N\psi/2)}{\sin(\psi/2)} \quad \textbf{[2.15]}$$

where $\psi = kd\cos\theta + \beta$

In general for a large number of elements N, the main lobe narrows, the number of sidelobes are equal to N-2 and the nulls occur at $\psi = \pm 360^0/N$. This is an important consideration and the effect of it will more clearly be seen in Section 4.11.

Grating Lobes

As discussed above the values of N, d and β are the prime factors that determine the array pattern. In order to ensure that all the power is focused into a single main beam, d and β have to be chosen properly.

Spacing the elements of an array too far apart will produce additional main beams called grating lobes. This is undesired as it directs power away from the main lobe. Grating lobes occur because the larger spacing allows the waves from each element to add in phase at both the grating lobe angle as well as at the main beam angle. To avoid grating lobes the designer must impose restrictions on the maximum allowable element spacing. This is set by the equation *[Bala82]*:

$$d_{\max} = \frac{\lambda}{1 + |\cos(\theta_{\max})|} \quad \textbf{[2.16]}$$

where θ_{max} is the max scan angle of the main beam as measured from the array axis. In general spacing the elements at up to half a wavelength will preclude grating lobes except for extreme scan angles.

Beam Width of Broadside Linear Arrays

A broadside array is one in which the main beam is perpendicular to the array axis. To achieve a broadside array β must be set equal to 0 i.e. the signal path length to or from any element in the array is equal. The location of the beam half power points can be determined by setting the array factor given by equation 2.15 equal to 0.5*[Bala82]*:

$$\theta_h = \cos^{-1}\left(\pm\frac{1.391\lambda}{\pi N d}\right) \quad for \rightarrow \pi d/\lambda << 1 \qquad [2.17]$$

Directivity of Broadside Linear Arrays

For a broadside array the directivity is equal to *[Bala82]*:

$$D = \frac{1}{\frac{1}{N} + \frac{2}{N}\sum_{m=1}^{N-1}\frac{N-m}{mkd}\sin(mkd)} \qquad [2.18]$$

Increasing the number of element N increase the directivity. Increasing the inter-element spacing d also increases the directivity but only up to a certain point, after which the directivity drops off dramatically.

2.4.2 Planar Arrays

Combining linear arrays in two dimensions results in planar arrays. Planar arrays introduce further degrees of freedom for beam shaping and further boost gain as compared to linear arrays. A common arrangement for a planar array can be seen in Figure 2.8.

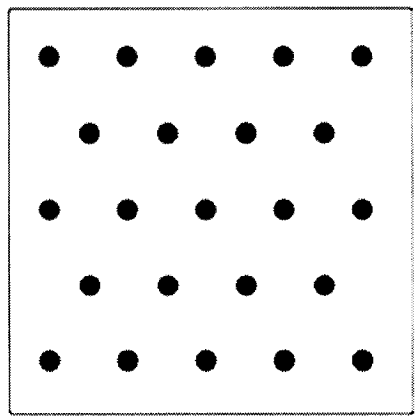

Figure 2.8: Planar Array – Triangular Lattice

A triangular lattice is often used as it allows greater inter element spacing than a rectangular lattice, without introducing grating lobes *[Bala82]*.

Array Factor for Planar Arrays

The general array factor for a planar array is given by *[Bala82]*:

$$AF = \sum_{i=1}^{K} A_i e^{-j\psi_i}$$
$$\psi_i = kx_i \sin\theta\cos\phi + ky_i \sin\theta\sin\phi + \beta_i \qquad \textbf{[2.19]}$$

For a rectangular lattice of uniform amplitude with linear phase progression β_x and β_y along their respective axis the array factor can be written as the product of two linear arrays given by *[Bala82]*:

$$AF = A_0 \frac{\sin(\frac{M}{2}\psi_x)\sin(\frac{N}{2}\psi_y)}{\sin(\frac{\psi_x}{2})\sin(\frac{\psi_y}{2})} \qquad \textbf{[2.20]}$$

where ψ_x and ψ_y are similarly defined as to ψ_i in equation 2.19, except in their respective axes and M and N are integers.

2.5 Feed Networks and Design Considerations for Arrays

The question of how the elements are excited with a particular amplitude and phase has not yet been addressed. Feed networks provide each element with the required excitation. These consist of power dividers/combiners, which take the power from one port and distribute it to all the required ports, i.e. the array elements.

The feed network is often the major stumbling block in array design. Although an array may seem feasible and elegant at first, it is often the case that the required power division cannot be achieved within the feed network.

The two main types of feeds are series feeds, where the array elements are in series along a transmission line, and shunt feed where the array elements are in parallel with a feed network

We will focus mainly on the shunt feed in particular the corporate feed network as shown in Figure 2.7. In a corporate feed each element is equidistant to the input port. These feeds are attractive in that they are relatively wideband. However they occupy much more space and are more lossy due to the line lengths required.

2.5.1 Power Dividers

Highlighted in Figure 2.7 is a power divider. Its purpose is to split the power appropriately at a junction of a feed network from one input signal into two or more signals of lesser power. The power division does not have to be equal as will be seen in Section 3.6.

There are various kinds of power dividers. The ones relevant to this thesis are the T-junction power divider and the Wilkinson Power divider.

T-Junction Power Divider

This is a simple 3 port network that can be modeled as a junction of three transmission lines. Figure 2.9 shows a Y-junction power divider that has the same principles of operation as a T- junction divider. A Y-junction is used as opposed to a T-junction at high frequencies due to the excessive substrate power loss in the latter at the apex of the T.

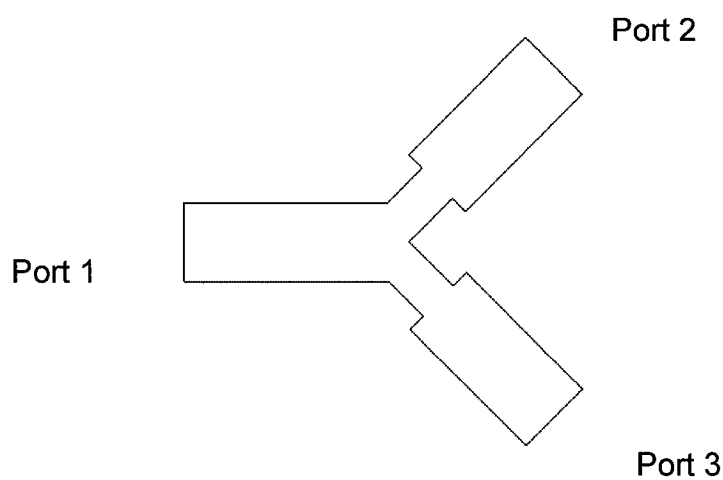

Figure 2.9: A corporate feed structure

Power enters the junction at port 1 and is split between ports 2 and 3. The division is achieved because of the ratio of the characteristic impedances between the transmission line connecting port 2 and that connecting port 3. This is given by the equation *[Poza98]*:

$$\frac{P_2}{P_3} = \frac{Z_{O3}}{Z_{O2}} \qquad \textbf{[2.21]}$$

Assuming a lossless junction *[Poza98]*:

$$P_1 = P_2 + P_3 \qquad [2.22]$$

As well we require the junction to be input matched at all three ports in order to minimize reflection loss. This means that *[Poza98]*:

$$Z_{O1} = \frac{Z_{O2} Z_{O3}}{Z_{O2} + Z_{O3}} \qquad [2.23]$$

The equations, although useful as a starting point in the design of a T-junction, do not paint a completely accurate picture. In general a three-port network cannot be lossless, reciprocal and matched at all ports *[Poza98]*. However a junction implemented in microstrip, which is in itself a lossy medium can allow for physically realizable devices. These equations can be further refined to include the effect of an arbitrary Y-junction angle as described in *[Mehr78]*.

Wilkinson Power Divider

Wilkinson power dividers offer an advantage over T-junction power dividers in that they can be designed to offer good isolation between ports. This is very useful in that when all the output ports are matched the divider is lossless and only reflected power is dissipated. As shown in Figure 2.10 a shunt resistor is connected between ports 2 and 3 to dissipate any reflected power at the output ports, thus maintaining good isolation.

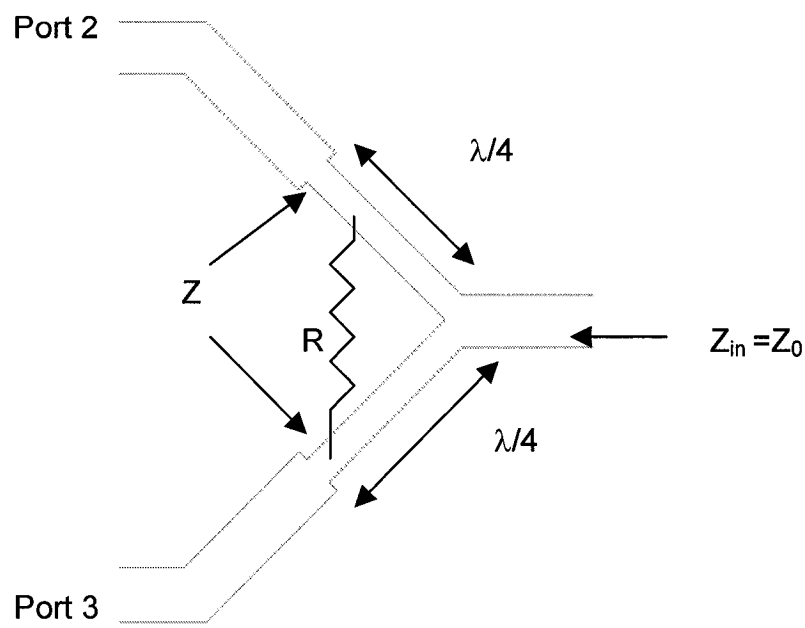

Figure 2.10: Wilkinson power divider

The power division ratio between ports 2 and 3 is defined as $\mathbf{K^2 = P_3/P_2}$. The following equations then apply for the design of the divider *[Poza98]*:

$$Z_{O3} = Z_O\sqrt{\frac{1+K^2}{K^3}}$$
$$Z_{O2} = K^2 Z_{O3} = Z_O\sqrt{K(1+K^2)}$$
$$R = Z_O\left(K + \frac{1}{K}\right) \qquad \textbf{[2.24]}$$

2.5.2 Mutual Coupling in Arrays

Mutual coupling is the term applied to the undesirable interaction between elements in an array whereby energy from one element impinges on its adjacent elements. Mutual coupling places a restriction on how close elements in an array can be placed, for the closer the elements the greater the mutual coupling. The effects of mutual coupling include distortion in the radiation pattern, input

impedance change in the element resulting in greater mismatch loss, limiting scan performance of an array and limiting the amount of gain that can be generated from an array of aperture area Ae. This last effect is known as the gain paradox.

Since mutual coupling is such a difficult phenomenon to analyze, its effect on the array can be studied through the use of an electromagnetic simulator such as Ensemble.

CHAPTER 3

PLANAR FEED ARRAY ARCHITECTURE

Commonly used feeds for planar reflectors or parabolic reflectors are pyramidal or corrugated horns. The horn is used to deliver as much energy as possible onto the primary antenna for subsequent reflection into a focused high gain beam. Typically a single horn with a single high-gain, high-power amplifier in the signal path to boost the power is used. An alternate way of performing the same function is to use a microstrip array with multiple lower power amplifiers as shown in Figure 3.1. This method of using an active distributed microstrip feed, allows the utilization of spatial power combining techniques to achieve similar gain as the single horn, while significantly reducing the complexity associated with the design of horn feeds.

The focus of this chapter is the design and implementation of a 30 GHz microstrip planar array in which the advantages of a planar array versus a horn for a reflector feed and the challenges associated with the design of planar arrays for use as feed antennas, will be discussed.

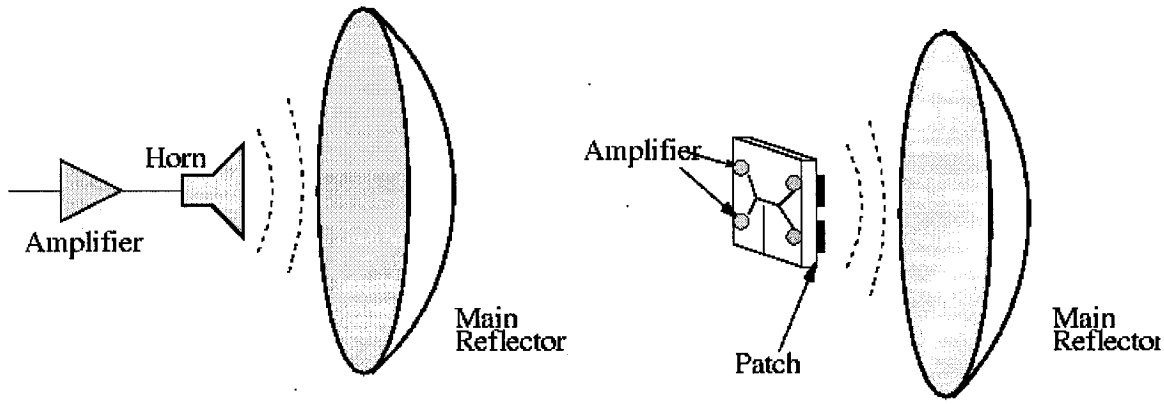

Figure 3.1: Horn feed to Array feed

3.1 Microstrip Arrays versus Horns as Feeds

Planar arrays are typically combinations of individual linear arrays. By appropriately choosing the number of elements and their placment, it is possible to illuminate the entire reflector via spatial combining techniques. The multiple elements are placed in an array in such a fashion that they emulate the power distribution provided by a horn feed. The benefits to be gained from using a planar array to mimic a horn feed include:

- Ease of manufacturing – Corrugated horns are difficult and expensive to machine. The tolerance requirements are extremely high. By comparison microstrip arrays are easily and inexpensively manufactured using printed circuit board techniques.
- Size – Horn feeds occupy a large volume thus adding to the size and mechanical complexity of the entire reflector antenna system. A similar aperture size microstrip array on the other hand is significantly shallower in depth allowing for a more compact antenna system.

- Cost – In order to boost the output power of a horn feed, amplifiers have to be added to it in a series fashion. This in turn dictates the use of high-power, high-gain amplifiers. Such high performance amplifiers significantly increase the cost of the feed. On the other hand, a planar array can utilize a number of low-power, low-gain amplifiers employed in parallel. The same overall power can be achieved by distributing the amplifiers over the array, and then spatially combining their power as compared to an active horn feed. However, considerable cost savings are achieved by the use of lower performance amplifiers e.g. four ¼ watt amplifiers would generally cost less than one 1 watt amplifier.
- Redundancy and Degradation – A single active horn by nature has no redundancy at all. Should the amplifier fail the entire feed fails. In contrast for a distributed active planar array the chances of all the amplifiers failing at the same time is much smaller (barring catastrophic circumstances). In the event of an amplifier failure the degradation of the signal is only fractional as compared to a horn feed where degradation would be total. Degradation due to element failure has been studied at length, and it has been shown that it can occur very gracefully for a parallel type structure *[Rutl99].*
- Thermal Management – The use of microwave power amplifiers often necessitates cooling. This is a significant problem as it greatly limits the freedom of the antenna designer in that allowance has to be made for thermal management devices such as heat sinks when designing

the feed. Distributing lower power amplifiers allows easier application of simple and economical thermal management schemes.

3.2 Microstrip Arrays as Feeds – Challenges & Goals

A planar array as a feed for a planar reflector has been previously implemented with a four-element array *[Shak02] [Shak00]* as shown in Figure 3.2.

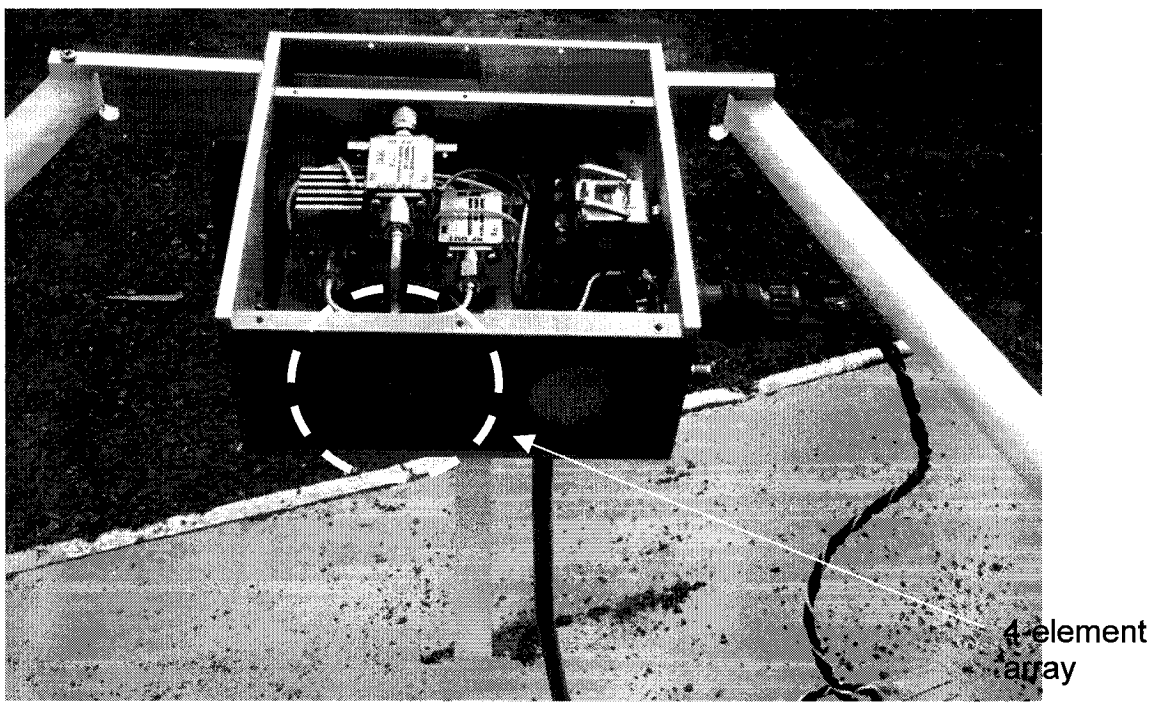

Figure 3.2: Four element planar array feed

The problem with a four-element array is that it was only possible to embed one amplifier per element to boost the gain for a total of four devices only. A larger number of elements were desired, as this would allow more embedded amplifiers thus allowing for a greater EIRP from the antenna.

The initial goal of this thesis was to design an eight or greater element array with a beamwidth of $40^0 \times 40^0$, which is required to illuminate an 0.45 m by

0.45 m reflector. This however is not as simple as just enlarging the initial array so as to obtain eight elements, since the horn feed pattern is to be emulated. A number of issues arise. Recall from array theory that more elements have the effect of decreasing the beamwidth, this results in the conflicting requirements of a large number of elements with a broad beam pattern. In order to satisfy both requirements a tradeoff has to be carried out between the two.

As well as adjusting the number of elements, the placement of the elements will be a major factor since the distance d between elements also affects beamwidth (See equation 2.17). To have a large beamwidth it is necessary to place the elements as close as possible to each other. There is a limit to how close the elements can be placed without overlapping the patches (array theory assumes ideal infinitesimal elements whereas in a real antenna the elements have finite sizes). The distance d also affects mutual coupling between the patches, further limiting how small d can be (see Section 2.5.2).

The third factor that can be adjusted to obtain the desired beamwidth is the use of unequal amplitude weightings on the individual patches. This method allows greater power to some patch elements and reduced power to others. In general, distributing more power to the inner elements while reducing the power of the periphery or edge elements will allow for a greater beamwidth *[Peto99]*). The challenge with this approach is that appropriate power splitters must be designed in order to distribute the power as required. At millimeter wave frequencies this is often difficult, especially for high division ratios. This will be more fully discussed in Section 3.6.

Finally adjusting the relative phase β between the elements allows for slight increases in beamwidth at the expense of increased ripple levels in the principal beams *[Bala82]*.

Although all the above factors can be manipulated, they have a major impact on the design of a feed network for the planar array itself. The feed network becomes a much greater challenge from a design perspective than the planar array and its intrinsic elements. The planar array feed network has to be capable of delivering the correct amplitude and phase at the spatial location of each patch element, while also allowing sufficient room for the amplifiers to be placed. All of this has to be achieved in the smallest footprint possible.

3.3 Planar Array Configurations

A number of planar array configurations have been explored in order to fulfill the above requirements. Initially the array configurations were studied using ARPS *[Arps00]*, which graphically present the pattern for various array configurations. This program uses the simple linear array equations and does not take into account any higher order electromagnetic phenomenon such as mutual coupling. However it is still useful in obtaining a first cut design, which can then be optimized using a full electromagnetic simulator such as Ensemble.

The main parameters of a planar array assessed were the number of elements, the amplitude weightings of the elements, the phase variance between the elements, the placement of the elements and the symmetry of placement of the element. Symmetrical arrays can be defined as arrays with elements equidistant in both the X and Y planes. Asymmetrical arrays have variable

spacing in the separate planes i.e. the separating between elements in the X plane is not necessarily the separation in the Y plane.

In order to maintain consistency the same patch element was used as a building block for every array. At 30 GHz the basic patch element on a Duroid board with ε_r of 2.2 and thickness t of 0.0762 mm, is 3.5 mm by 3.5 mm. When the array configuration is finally determined, the patch can be further optimized if necessary. Figures 3.3 and 3.4 below are generic representations of the two main array configurations studied – an odd element array and an even element array. This distinction was made due to the difference in feed design for odd and even arrays. The exact locations of the patch elements will be specified in the subsequent sections with respect to the coordinate system shown.

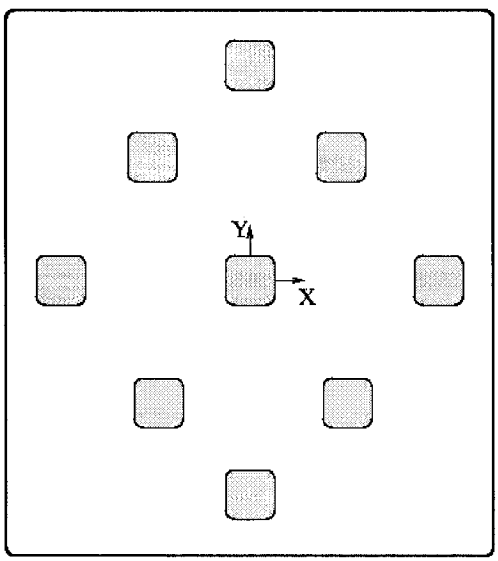

Figure 3.3: Generic 9 element lattice

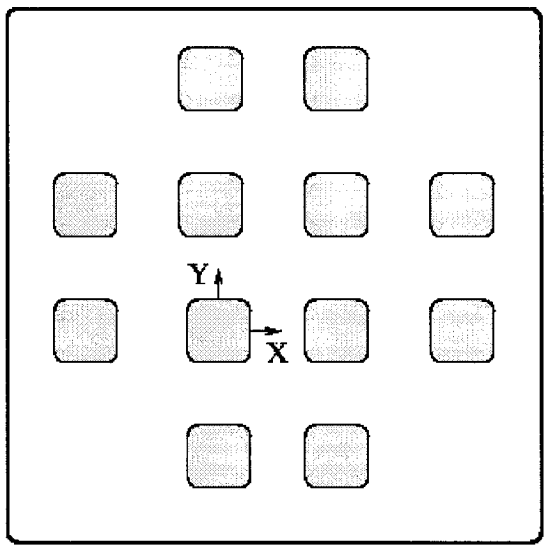

Figure 3.4: Generic 12 element lattice

To reiterate, the goal of this study is to obtain a 40^0 x 40^0 beamwidth at 30 GHz while using the largest number of elements possible. The array designs presented below are the best subset of all array configurations explored.

3.3.1 9 Element Lattice A – Symmetric, Equal Amplitude and Phase

The first configuration consists of equal amplitude and phase excitation in order to provide a basic reference array. Table 3.1 provides the element coordinates and excitations, while Figure 3.5 shows the resulting radiation pattern. The element spacing was chosen to be as tight as possible without overlap occurring.

Table 3.1: Nine element lattice A configuration

Element Number	X-ordinate [mm]	Y-ordinate [mm]	Amplitude [V]	Phase [degrees]
1	-3.5	-4	1	0
2	3.5	-4	1	0
3	3.5	4	1	0
4	-3.5	4	1	0
5	0	-8	1	0
6	8	0	1	0
7	0	8	1	0
8	8	0	1	0
9	0	0	1	0

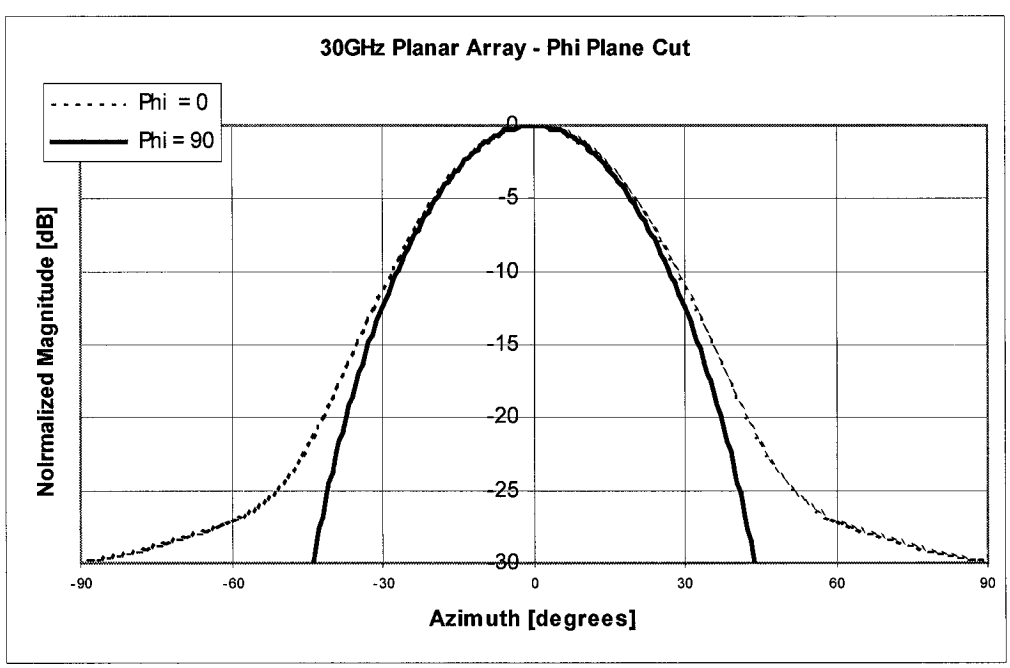

Figure 3.5: 9 Element Planar Array A

The results show an E-plane 3 dB beamwidth of 30.9^0, and an H-Plane 3 dB beamwidth of 30.2^0,which does not satisfy the requirements.

3.3.2 9 Element Lattice B – Asymmetric, Equal Amplitude and Phase

Lattice B consists of equal amplitude and phase excitation with the array stretched out in the Y-dimension to see the effect on the E and H-plane beamwidths. As before Table 3.2 provides the element coordinates and excitations, while Figure 3.6 shows the resulting radiation pattern.

Table 3.2: Nine element lattice B configuration

Element Number	X-ordinate [mm]	Y-ordinate [mm]	Amplitude [V]	Phase [degrees]
1	-3.5	-3.5	1	0
2	3.5	-3.5	1	0
3	3.5	3.5	1	0
4	-3.5	3.5	1	0
5	0	-8.5	1	0
6	6.25	0	1	0
7	0	8.5	1	0
8	-6.25	0	1	0
9	0	0	1	0

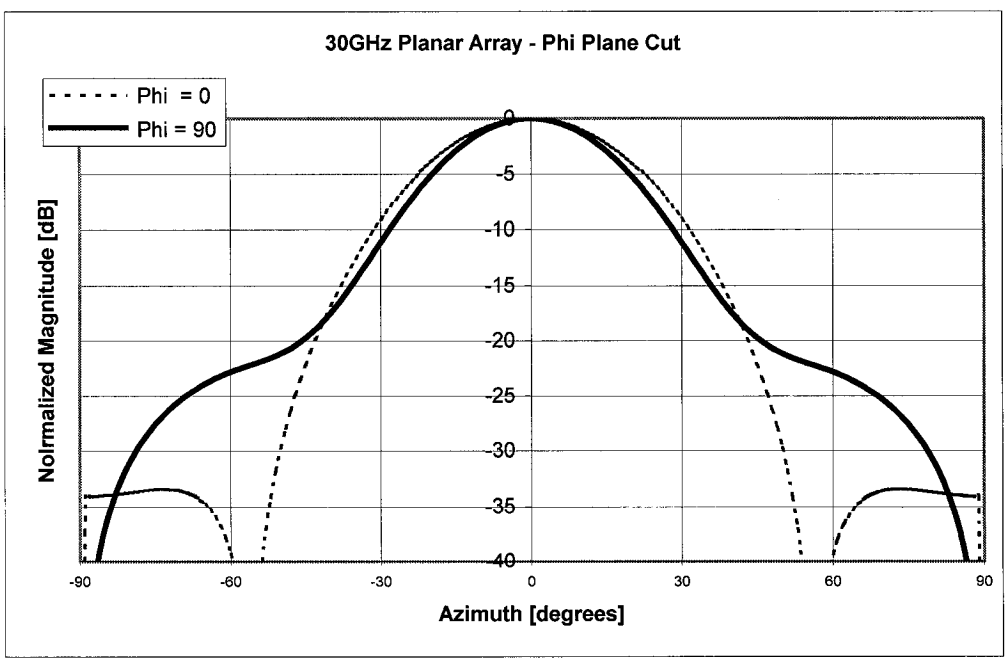

Figure 3.6: 9 Element Planar Array B

The results show an E-plane beamwidth of 35.0^0, and an H-plane beamwidth of 30.4^0,which is an improvement but still not good enough.

3.3.3 9 Element Lattice C – Asymmetric, Unequal Amplitude and Equal Phase

Lattice C varies all the parameters except phase. Table 3.3 provides the element coordinates and excitations, while Figure 3.6 shows the radiation patterns.

Table 3.3: Nine element lattice C configuration

Element Number	X-ordinate [mm]	Y-ordinate [mm]	Amplitude [V]	Phase [degrees]
1	-0.35	-0.35	0.6	0
2	0.35	-0.35	0.6	0
3	0.35	0.35	0.6	0
4	-0.35	0.35	0.6	0
5	0	-0.85	0.2	0
6	0.625	0	0.2	0
7	0	0.85	0.2	0
8	-0.625	0	0.2	0
9	0	0	1	0

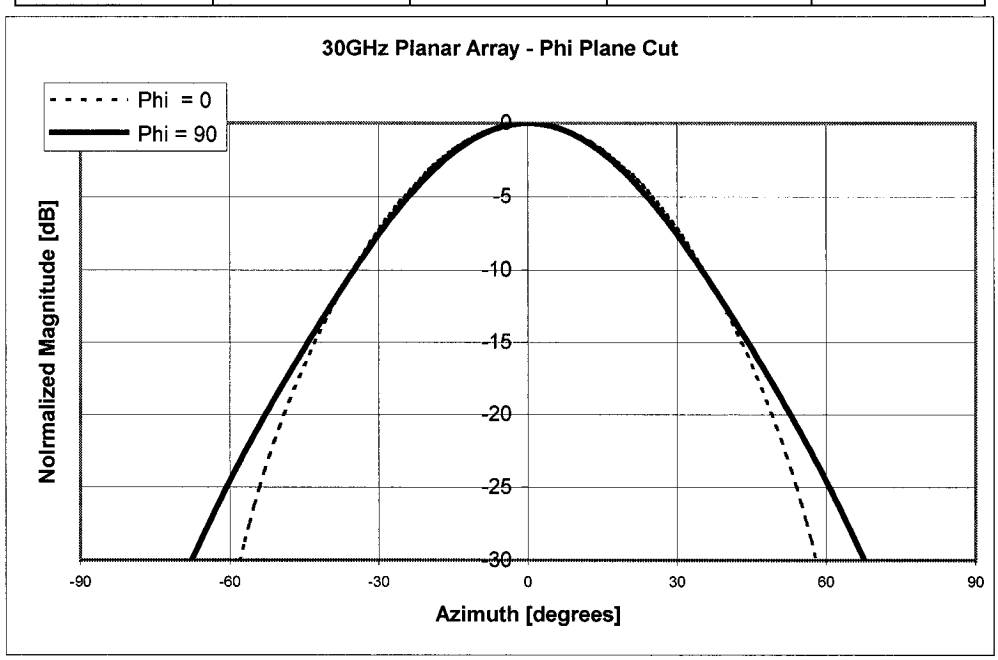

Figure 3.7: Nine Element Planar Array C

The results show an E-plane beamwidth of 38.86^0, and an H-plane beamwidth of 36.88^0,which is very close to the target beamwidth.

3.3.4 12 Element Lattice A – Symmetric Equal Amplitude and Phase

The first 12-element was also used as a reference array. Table 3.4 provides the element coordinates and excitations. Figure 3.5 shows the radiation patterns. The element spacing was chosen to prevent overlap.

Table 3.4: Twelve element lattice A configuration

Element Number	X-ordinate [mm]	Y-ordinate [mm]	Amplitude [V]	Phase [degrees]
1	0	0	1	0
2	4.5	0	1	0
3	9	0	1	0
4	-4.5	0	1	0
5	0	-4.5	1	0
6	4.5	-4.5	1	0
7	-4.5	4.5	1	0
8	0	4.5	1	0
9	4.5	4.5	1	0
10	9	4.5	1	0
11	0	9	1	0
12	4.5	9	1	0

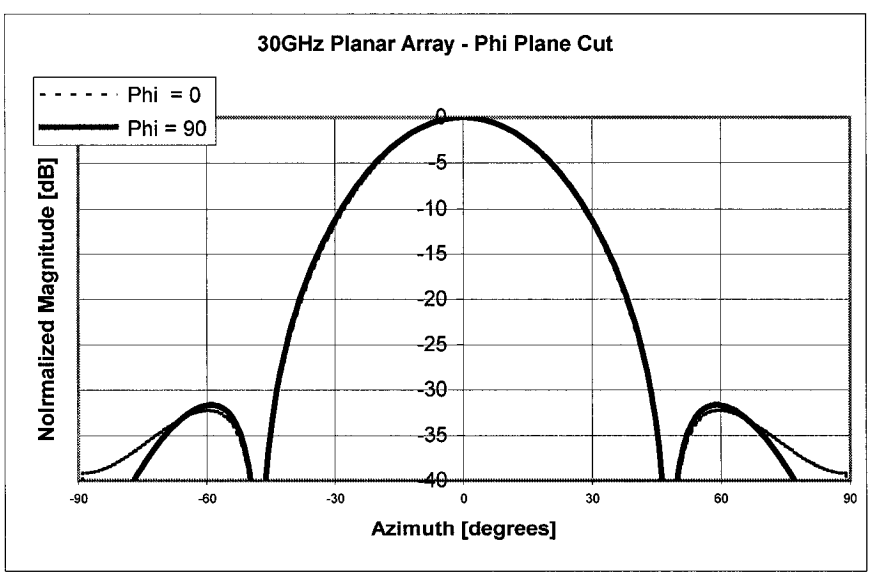

Figure 3.8: 12 Element Planar Array A

The results show an E-plane beamwidth of 31.3^0, and an H-Plane beamwidth of 32.0^0,which is very far from the targeted beamwidth

3.3.5 12 Element Lattice B–Symmetric, Unequal Amplitude and Phase

12-element lattice B was an improvement on the previous array. Chainging the amplitude improved the beamwidth in the 9 element array so this was studied as shown in Table 3.4 with the results in Figure 3.5.

Table 3.5: Twelve element lattice B configuration

Element Number	X-ordinate [mm]	Y-ordinate [mm]	Amplitude [V]	Phase [degrees]
1	0	0	2.5	-45
2	4.5	0	2.5	-45
3	9	0	1	45
4	-4.5	0	1	45
5	0	-4.5	1	45
6	4.5	-4.5	1	45
7	-4.5	4.5	1	45
8	0	4.5	2.5	-45
9	4.5	4.5	2.5	-45
10	9	4.5	1	45
11	0	9	1	45
12	4.5	9	1	45

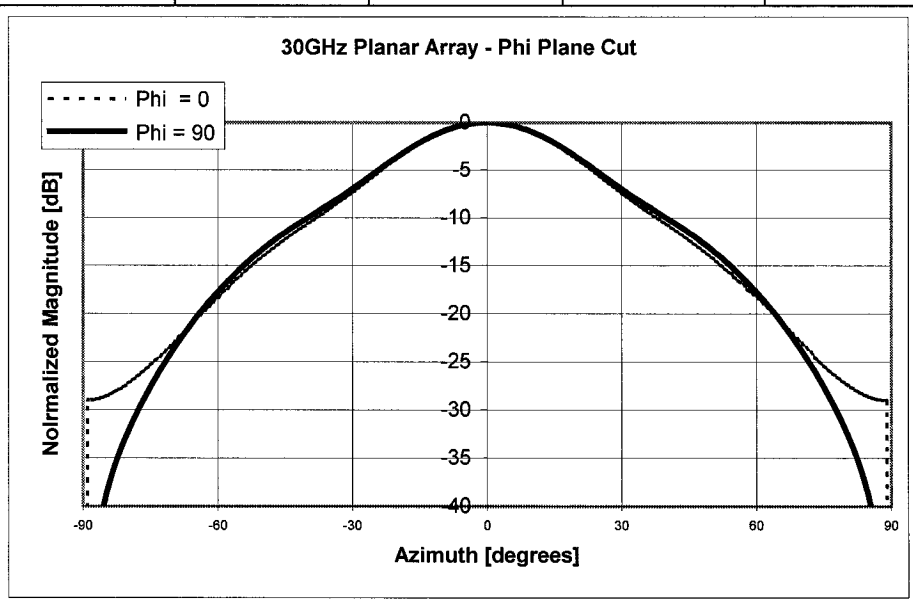

Figure 3.9: 12 Element Planar Array B

The results were better with an E-plane beamwidth of 35.2^0 and H-Plane beamwidth of 36.2^0.

3.3.6 Summary of Results and Discussion

Table 3.6 summarizes the results of the arrays presented in the previous sections.

Table 3.6: Summary of planar array performance for the various configurations

Number of Elements	Amplitude	Phase	Spacing	E-Plane Beamwidth	H-Plane Beamwidth
9	Equal	Equal	Symmetric	30.91	30.24
9	Equal	Equal	Asymmetric	35.00	30.43
9	Unequal	Equal	Asymmetric	38.86	36.88
12	Equal	Equal	Symmetric	31.35	32
12	Unequal	Unequal	Symmetric	35.24	36.25

The designs above are by no means an exhaustive search of all possible combinations of arrays that could yield the required beamwidth. There remains no easy way to obtain the right array combination for the required beamwidth except by trying out different configurations.

However based on the above results the two most promising arrays are the 9-element array with asymmetric spacing and unequal amplitude weighting and the 12-element symmetric array with unequal amplitude and phase weighting. They both have the widest beamwidth even though they are not far from the target beamwidth of 40^0. However, due to the difficulty in designing a feed network for an odd number of elements, only the 12-element array is considered further. The design of the feed network for this array is described in the following section.

3.4 Planar Array Feeds

In order to simplify the feed network design, a uniform amplitude distribution network is first implemented. This approach is adopted to allow for

easy routing of the microstrip transmission lines to the twelve patches. Once an appropriate routing is determined, only small modifications are then necessary to incorporate the non-uniform power divisions. The layout for the uniform amplitude feed network is shown in Figure 3.10.

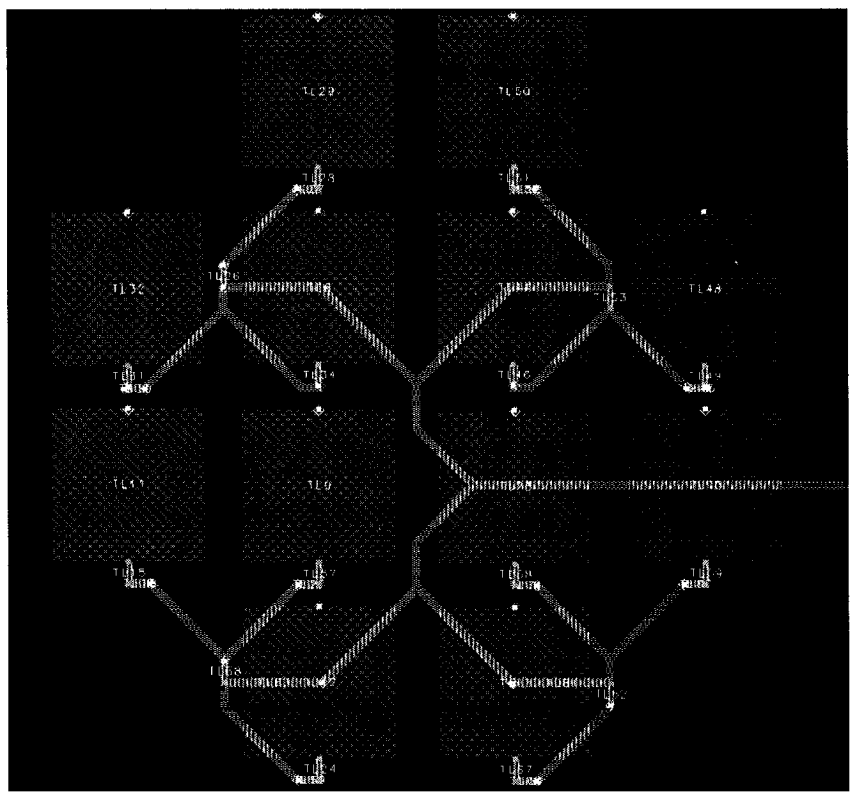

Figure 3.10: Feed design A for 12 elements

Every junction is shaped as a Y rather than a conventional T due to the frequency of operation as discussed in Section 2.5.1. This entails a more complicated feed geometry.

Referring to Table 3.5, which shows the required amplitude weightings for the 12 elements of the array, a power ratio between the inner four and the outer 8 elements of $(2.5/1)^2 = 6.25$ is needed. Using the design in Figure 3.10, the power division ratio becomes $(2.5^2+1^2)/1^2 = 7.25$, which is even more difficult,

since the last junction must split between one outer patch and an inner plus outer patch. Such power division is difficult to realize in microstrip technology. To ease these concerns, the feed is reorganized as shown in Figure 3.11

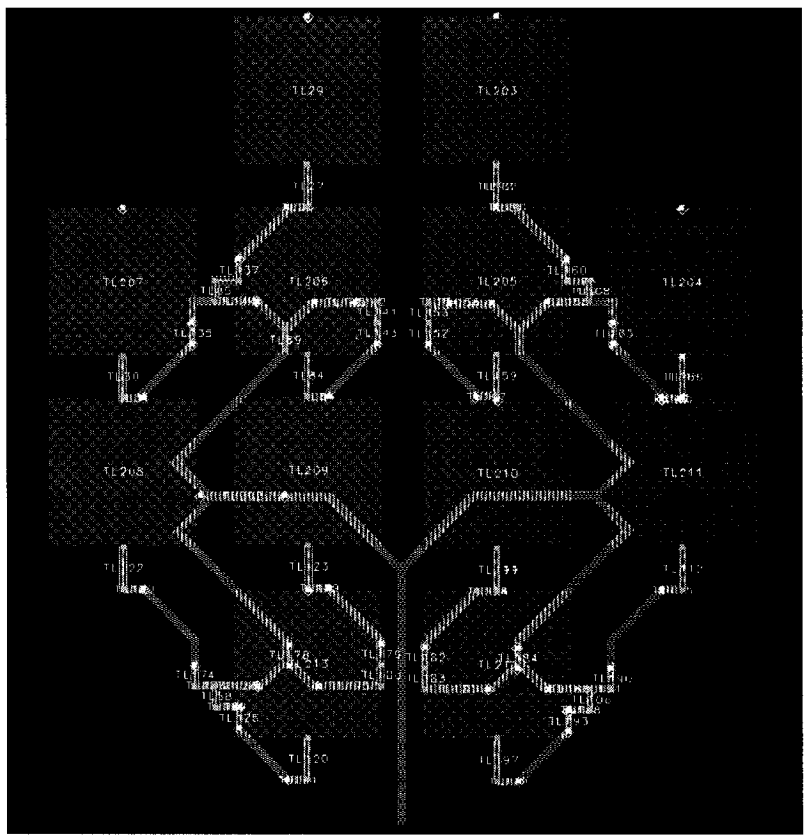

Figure 3.11: Feed design B for 12 elements

Using this new feed configuration, the power split ratio at the last junction is reduced to a much more achievable value of $2.5^2/(1^2+1^2) = 3.125$.

3.5 Power Splitters

This section describes the design of the various power splitters required to achieve the desired amplitude distribution at the microstrip patch elements. Wilkinson power splitters are chosen as they provide the best isolation between

ports and they are also the easiest to integrate into the proposed feed in terms of area occupied

A sketch of a microstrip Wilkinson power divider is shown in Section 2.5.1 a similar one is repeated in Figure 3.12 for convenience.

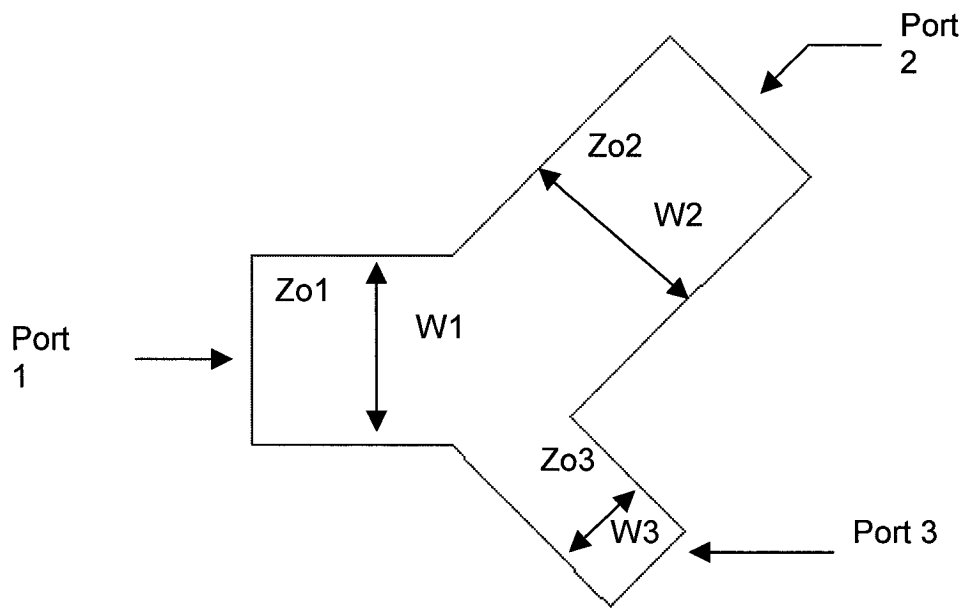

Figure 3.12: Wilkinson power divider – Geometry definitions

Using equation 2.25, the theory covered in Sections 2.12.1 and 2.12.2 and the required amplitudes, the impedance for the splitter sections can be determined. The corresponding line widths are calculated using a MATLAB program given in Appendix C. These values are summarized in Table 3.7.

Table 3.7: Unequal power split - Parameters

P_2	P_3	K^2	K	Z_{01} [Ω]	Z_{02} [Ω]	W_2 [mm]	Z_{03} [Ω]	W_3 [mm]
1	1	1	1	50	70.71	1.35	70.71	1.34
1	2	2	1.414214	50	51.49	2.24	102.99	0.6394
1	3	3	1.732051	50	43.87	2.84	131.61	0.3445
1	4	4	2	50	39.53	3.28	158.11	0.1962
1	5	5	2.236068	50	36.63	3.65	183.14	Not achievable due to etching tolerances
1	6	6	2.44949	50	34.51	3.95	207.04	
1	7	7	2.645751	50	32.86	4.21	230.03	
1	8	8	2.828427	50	31.53	4.45	252.27	

Note: W1 is sized to obtain 50Ω at the port 1 input

Since the design equations do not include the effects of junction discontinuities, an EM simulator - Ensemble was used to analyze the junctions and to adjust the parameters in order to obtain the desired power splits.

3.5.1 Wilkinson 1:1 divider

These junctions were not constructed as they have already been characterized previously and perform as expected.

3.5.2 Wilkinson 1-2 divider

EM analysis based on the values in Table 3.7 reveal that for the line impedances calculated the actual power split obtained is a 1:1.8 rather than 1:2. The S-parameters are shown in Figure 3.13. It is seen that the input return loss $|S_{11}|$ is near -20dB at 30 GHz, indicating nonetheless a good impedance match.

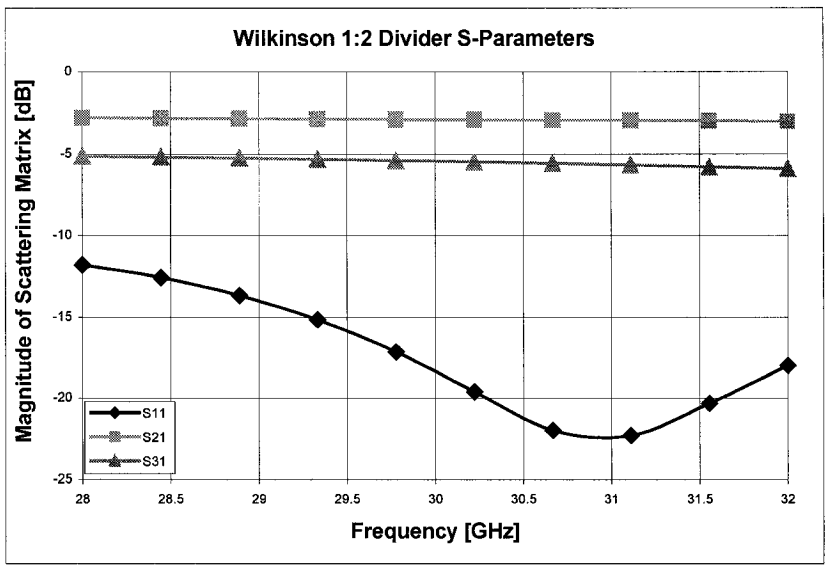

Figure 3.13: Wilkinson 1:2 Divider

3.5.3 Wilkinson 1:3 divider

Figure 3.14 shows the S-parameters for a 1:3 power divider. The division obtained was 3.27 which is slightly higher than that desired. Again a good impedance match is obtained

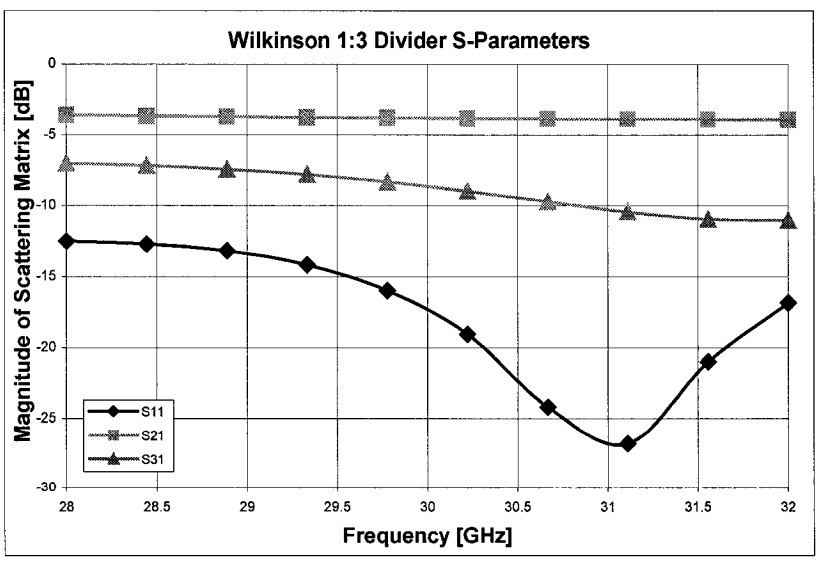

Figure 3.14: Wilkinson 1:3 Divider

3.5.4 Higher ratio dividers

Wilkinson divider equations of Section 2.5.1 do not hold well for higher divider ratios. As an example the element in Figure 3.15 is simulated, with an expected power division of 1:4 based on the line impedances. However, EM analysis shows a division ratio of 1:8

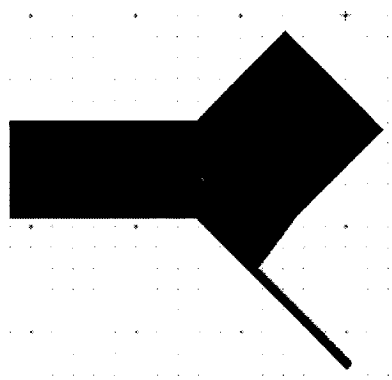

Figure 3.15: High ratio power divider

This can be seen by examining the S-parameters in Figure 3.16

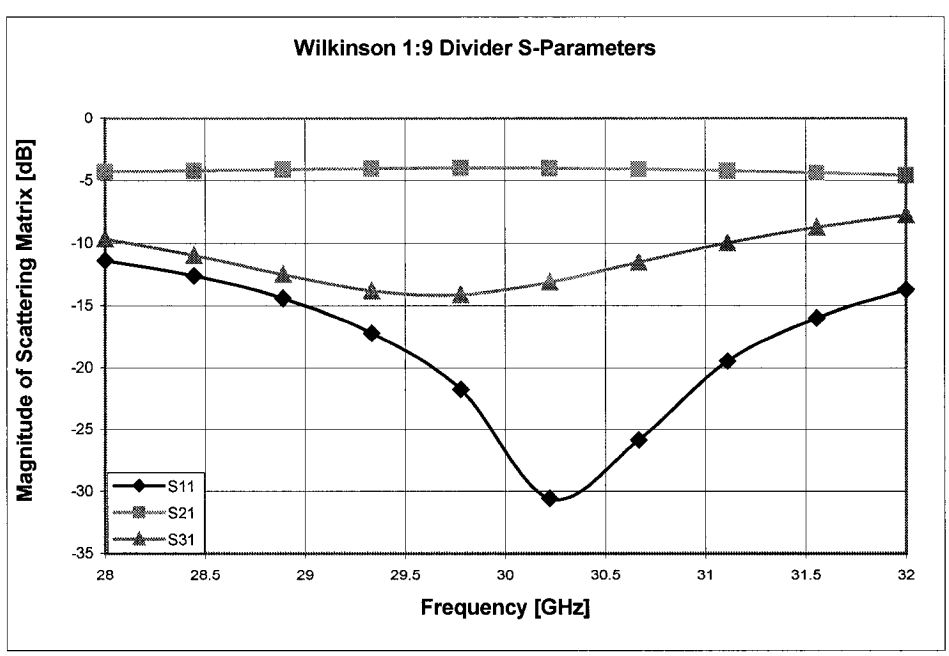

Figure 3.16: Wilkinson 1:9 Divider

Comparison of the port characteristic impedances with the resulting S-parameters quickly reveals a discrepancy. It is clearly evident that for the port

impedance designed, the power division ratio should be much lower than that calculated by the simulator. This brings into question the results obtained from Ensemble. It was often found that higher power division ratios could be achieved by "tweaking" the divider geometry while still using line impedances that were quite different than shown by calculations. This raises serious questions about the effect of splitter geometry on the resulting power division. In effect, there is no predictable way of laying out a power splitter to obtain the required power split of at least 1:4.

3.6 Conclusion

Considerable difficulty was encountered in even approaching a feasible feed solution for the planar array required. The large mismatches in the widths of the two different junctions introduced second order effects that are not easily explained. Not only was it extremely difficult to obtain the 1:4 ratio required it was also not possible to easily integrate the splitters into the feeds due to space constraints. The only possible way to feed the elements would be to place them far apart. However this would mean that the beamwidth requirements are met. Placing the elements closer would require that the feed lines to the inner elements be so thick that overlap would occur.

The planar array approach was more challenging than initially expected. It was not physically possible to design a planar array that had closely spaced elements with significantly different amplitude weightings between elements. A different approach was in order to meet the requirements.

CHAPTER 4:

LINEAR ARRAY ARCHITECTURE – PASSIVE DESIGN

As discussed in Chapter 3, a planar array design could not meet the required specifications of illuminating a reflector with the required beam shape. In addition to the difficulty in obtaining suitable radiation characteristics, there remained challenging issues in designing a practical feed network. An alternate concept in the form of a linear array is therefore examined. Instead of using a planar array to produce a circularly symmetric pattern that would illuminate the reflector, a linear array would be used in combination with a lens to form the beam without a reflector.

From array theory, a linear array is known to produce a fan shaped pattern with a narrow beam in the array plane and a wide beam in the orthogonal element plane. A one-dimensional linear lens as in Figure 4.1 can then be used to focus the broad element pattern to yield a narrow pencil beam over all planes as shown in Figure 4.2. The linear array has the advantage of being simpler to

implement than the planar configuration and has the capability for wide angle scanning in the array plane, should such functionality be required.

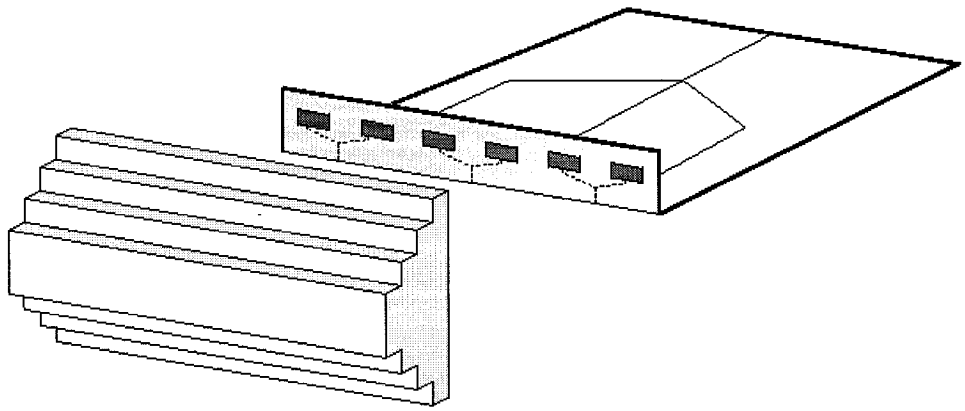

Figure 4.1: Linear array with 1D lens – Isometric view

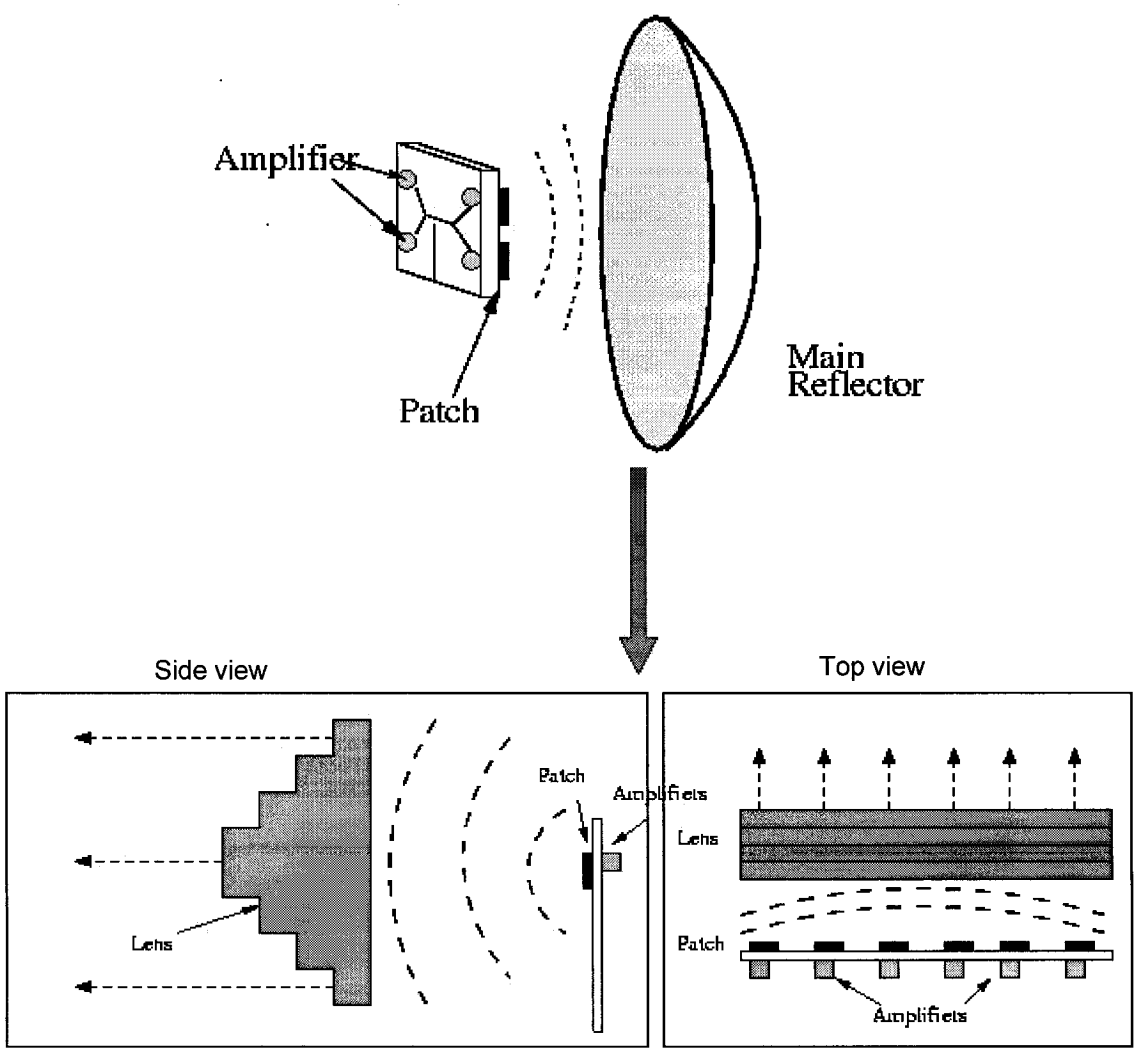

Figure 4.2: Planar array to linear array with 1-D lens

Typically, non-uniform amplitude weightings are used on linear arrays for sidelobe suppression. A uniformly weighted linear array, on the other hand, can only suppress sidelobes to a maximum of -13 dB *[Bala82]*. However, uniform amplitude excitation has other advantages, it especially simplifies the feed and power splitter design and will be adopted here.

The focus of this chapter is the design of a passive (without amplifiers), version of the linear array. The array is designed for a center frequency of 30 GHz with a bandwidth of 0.5 GHz. As well the cross-pol levels must be at least 15 dB below the co-pol levels. In order to meet these specifications various element and linear array configurations were explored. These include surface-fed and aperture fed patches as well as H-plane, E-plane and bent arrays. The latter sections of the chapter also present the necessary design work to make the array dual frequency capable with circular polarization. This would allow for 20 GHz receive and 30 GHz transmit operation with CP waves, as required for SATCOM applications.

4.1 Surface Fed Array

In section 2.3.1, several methods of feeding a microstrip patch are presented. The first design for the linear array involves a surface fed array of 16 elements. A surface fed patch has the radiating elements, feed and power distribution on the same layer. Sixteen elements were chosen as this would allow a 2^N number of amplifiers to be easily integrated. This method of feeding the patch is chosen, as the equations for a surface fed patch are readily available and the manufacturing easily done.

4.1.1 Single Element Surface Fed Patch

The first step in the linear array realization is the design of a single radiating element. Equations 2.1 through 2.10 are used to determine the initial dimensions of the microstrip patch based on a substrate with ε_r = 2.2 and a thickness t of 0.762mm. A commercial electromagnetic simulator (Ensemble), is then used to adjust the basic patch dimensions in order to optimize performance. Figure 4.3 shows the various parameters to be adjusted. A matching $\lambda/4$ transformer having L_{trans} and W_{trans} provides the required input impedance of 50 Ω at 30 GHz.

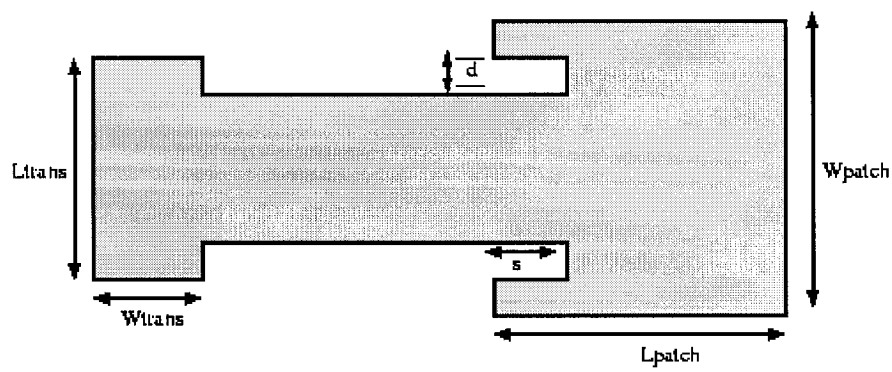

Figure 4.3: Surface fed patch with transformer

An example calculation for the design of a surface fed patch can be seen in Appendix B. The optimized width and length of the patch are 2.5 mm and 3.3 mm respectively. The final patch results from Ensemble are shown in Figure 4.4 for return loss and Figure 4.5 for the radiation pattern.

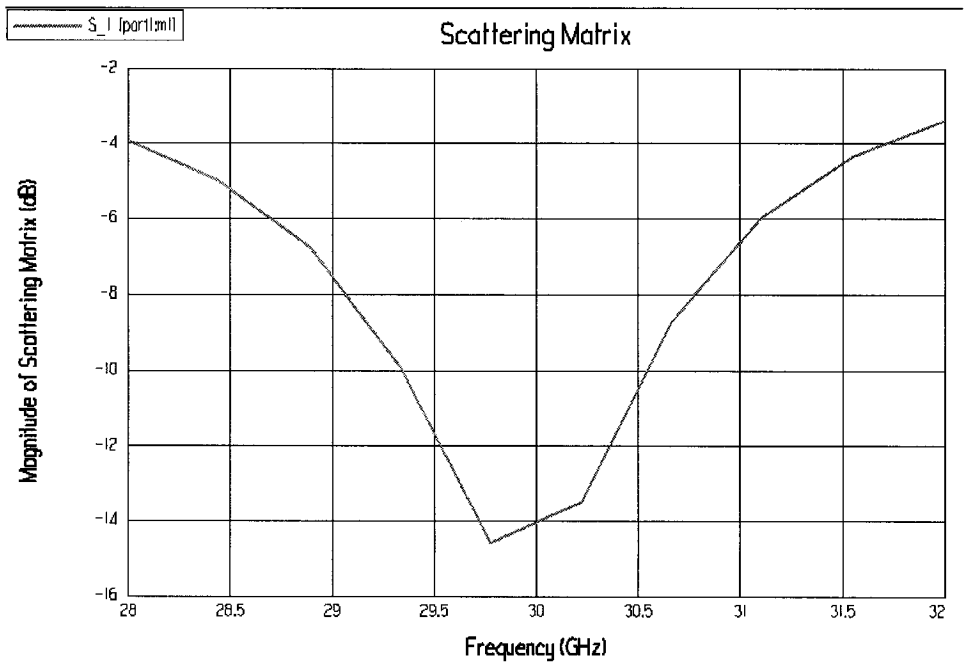

Figure 4.4: Simulated return loss for single surface fed patch

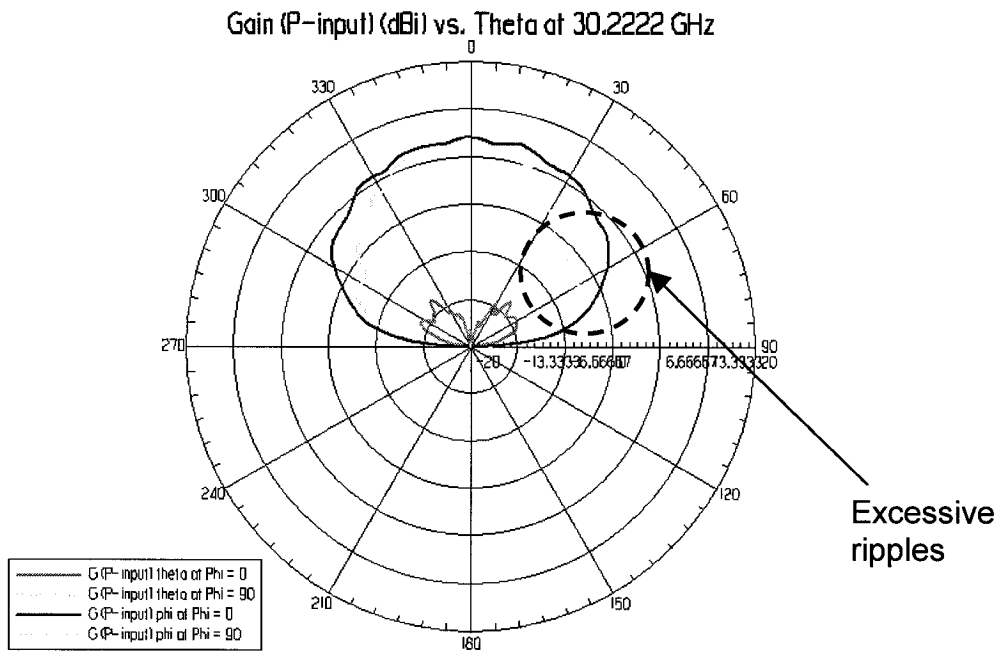

Figure 4.5 Gain for single surface fed patch

The single patch appears to be within specifications. The return loss is -14 dB for the center frequency of 30 GHz with a bandwidth of 1.2 GHz and the gain is 7dB with the H-plane and E-plane patterns as expected theoretically. However, an area of concern remains in the patterns obtained from simulation. Observing

Figure 4.5, it can be seen that the pattern is not as smooth as expected by theory. In the E-plane, between angles of 30^0 to 60^0, the ripples are much larger than expected, requiring further investigation.

One might fabricate just a single patch and measure its performance, or proceed with the full 16-element array design and see whether the excessive ripples still remain. The latter option is followed given that the H-plane ripples should easily be eliminated by the array multiplication factor and that the E-plane pattern could be affected either way.

4.1.2 16 Element Surface Fed Array – Simulated Results

The sixteen-element array with complete feed network on a board size of 150 mm by 150 mm is shown in Figure 4.6.

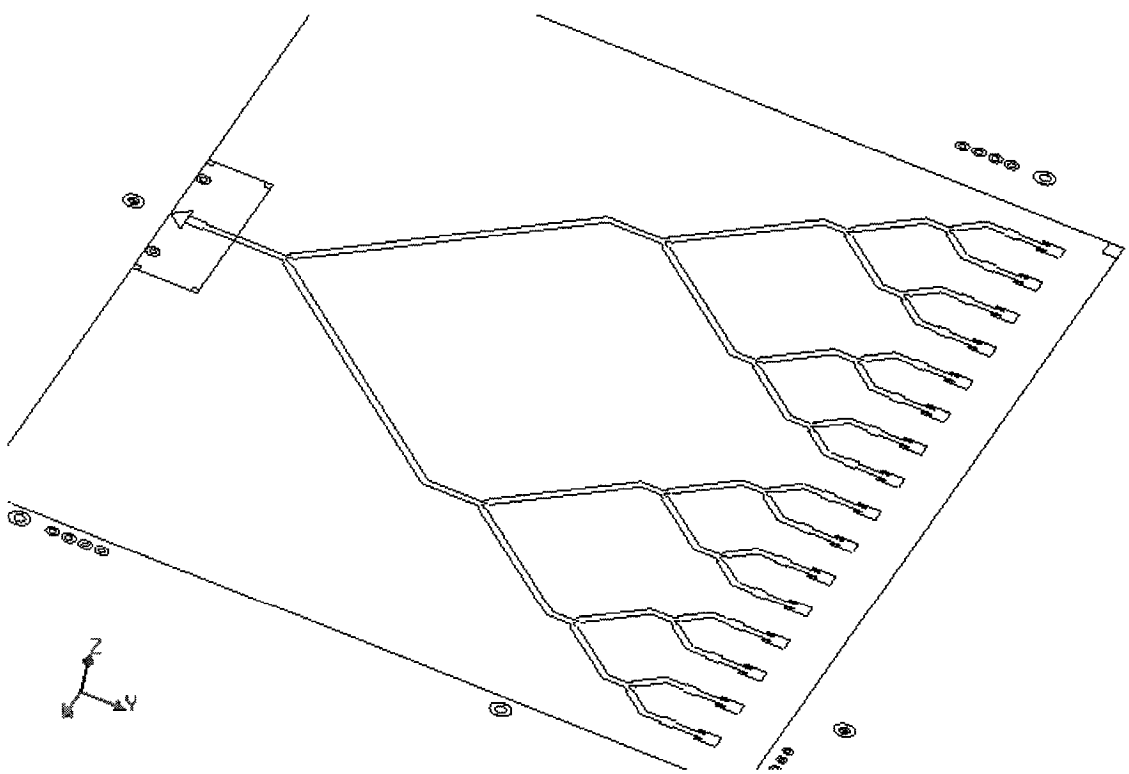

Figure 4.6: Simulation model for 16-element surface fed patch array

The power division is done with simple 3-dB Y-splits so that each element has equal amplitude and phase weighting. From Ensemble the simulated return loss and radiation patterns are shown in Figures 4.7 and 4.8 respectively.

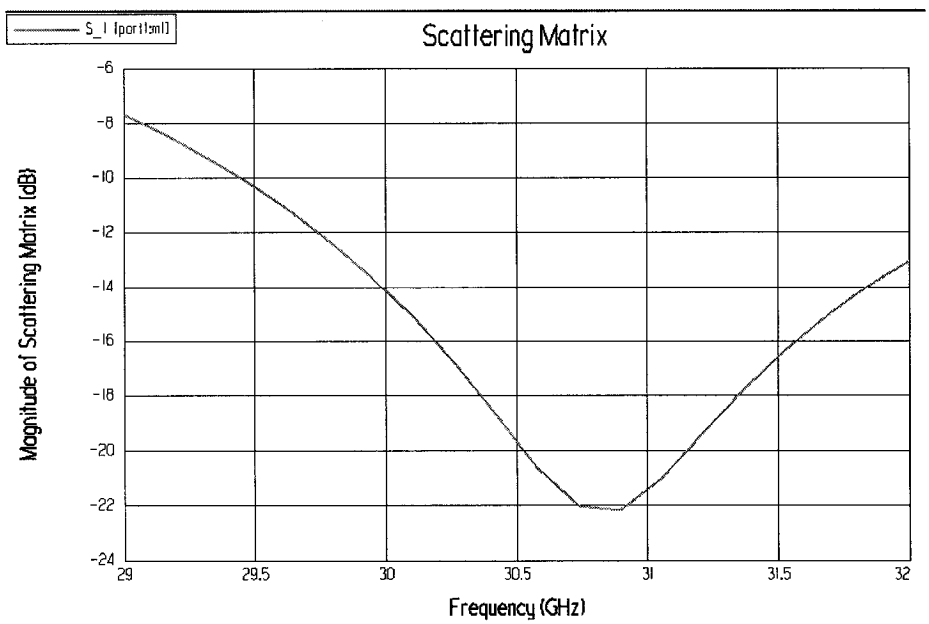

Figure 4.7: Return loss for 16-element surface fed patch array

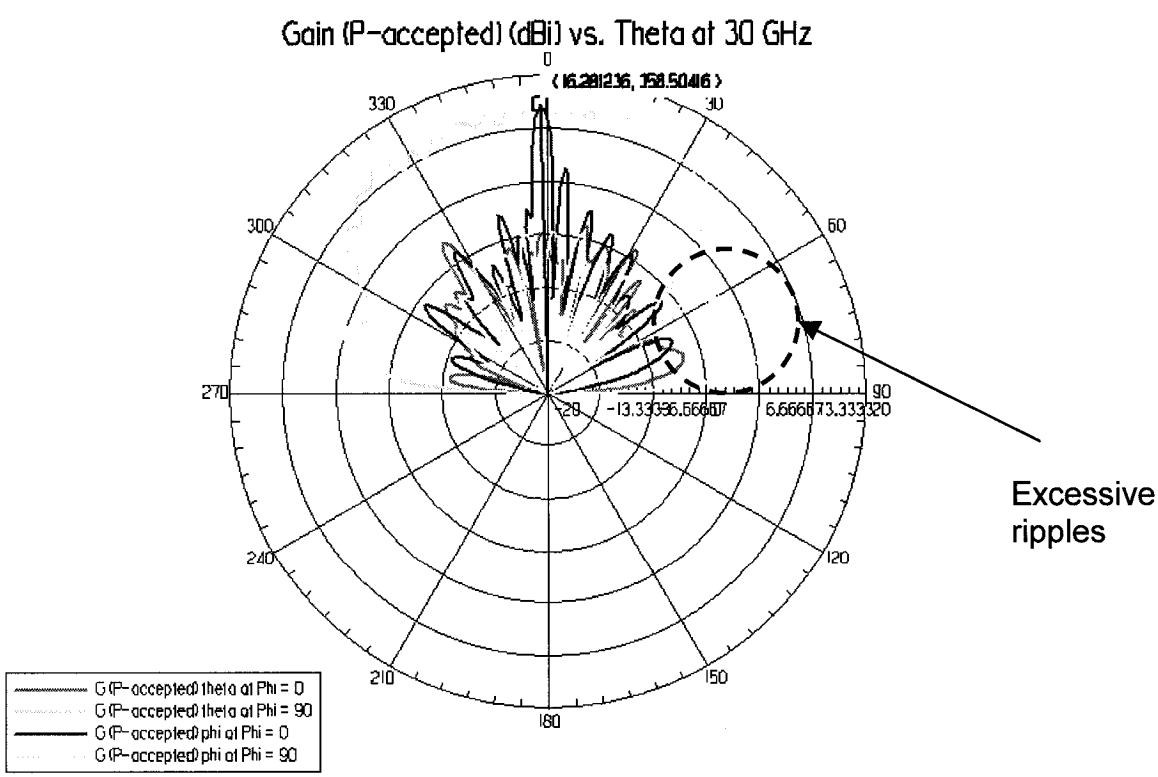

Figure 4.8: Gain for 16-element surface fed patch array

While the return loss of -14.0 dB at 30 GHz with a bandwidth greater than 1 GHz is acceptable, the radiation characteristics exhibit several deficiencies. The gain is 16.28 dB, as expected, but at an offset of 2^0 from boresight (from Equation 2.18 the directivity of a 16 element array is 16.34 dB). The E-plane pattern has the broad element pattern expected but with significant ripples of around 3 dB height, which is unacceptable. Over the E-plane angles of 30^0 to 60^0, the notch in the pattern that existed in the single patch pattern is still present in the array.

Given the complexities associated with EM simulation of such a large structure, and in order to verify the veracity of simulated results, an experimental verification is appropriate. The 16-element array is thus fabricated and tested.

4.1.3 16 Element Surface Fed Array – Measured Results

The prototype antenna fabricated is shown in Figure 4.9. The fabricated array is within manufacturing tolerances. The line widths are well above the minimum etchable tolerance width of 0.2 mm. Although not visible in the picture a K-connector block is present at the input of the array. This will affect the results somewhat by contributing to mismatch and thus reduce measured gain to less than that simulated.

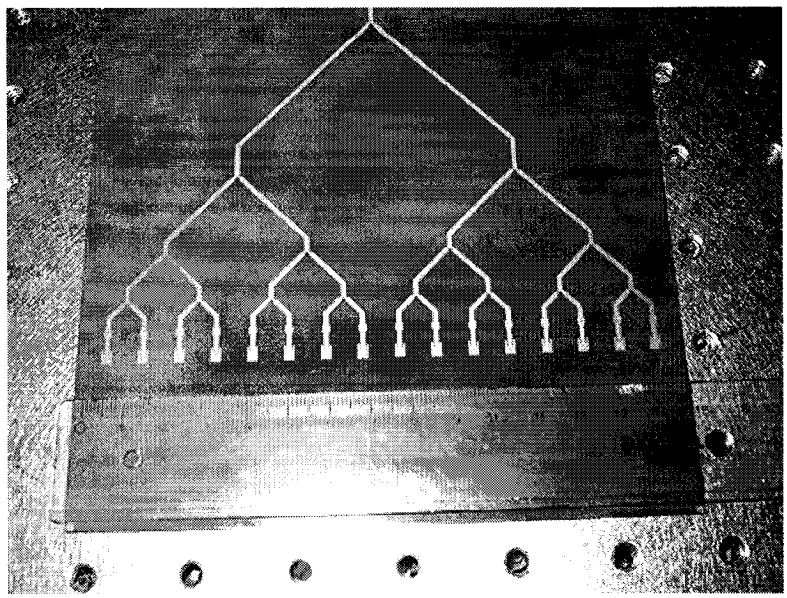

Figure 4.9: Fabricated 16 element surface fed patch array

The measured radiation patterns are shown in Figure 4.10 and the measured return loss is given in Figure 4.11.

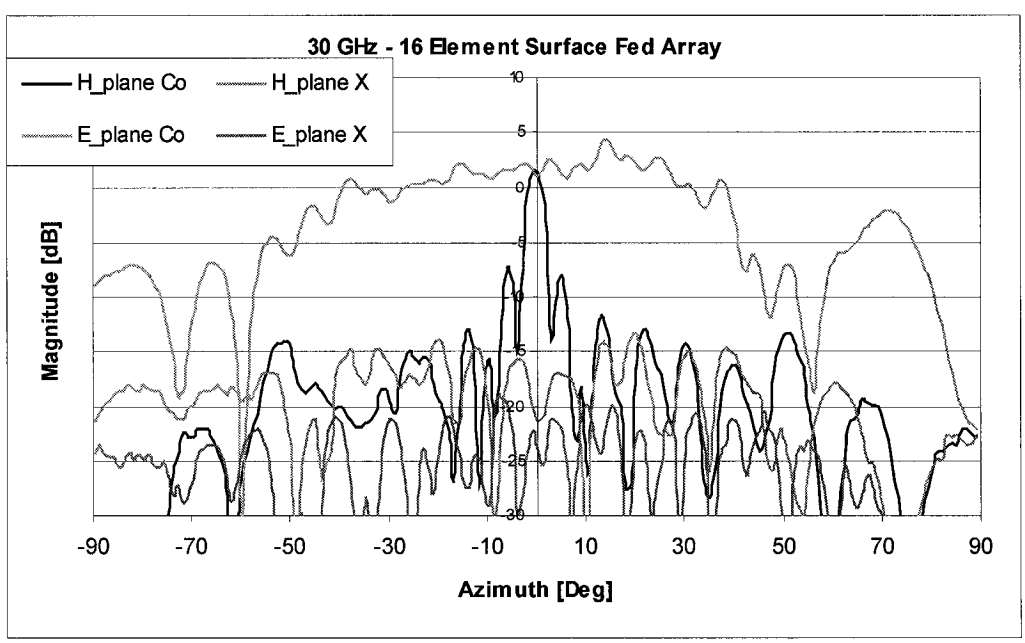

Figure 4.10: Surface fed array gain measurements

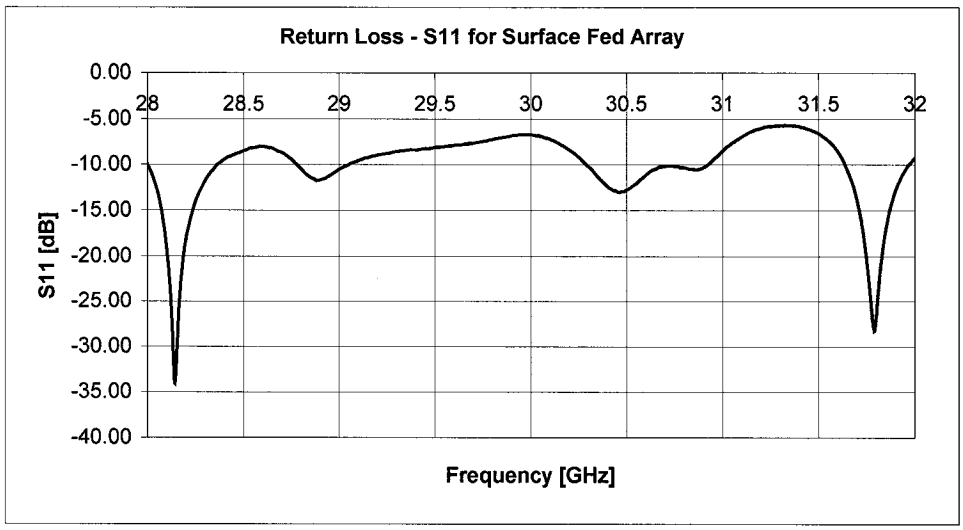

Figure 4.11: Measured return loss for 16-element surface fed patch array

The measured gain from Figure 4.10 is 1.04 dB, which is well below the simulated gain of 16 dB. The H-plane cross-pol levels are within specification but not the E-plane cross-pol levels. Referring to Figure 4.11, a return loss of -7 dB is obtained for the center frequency of 30 GHz while the best match is obtained at frequencies of 28.2 and 31.7 GHz with a bandwidth of less than 500 MHz. This shows that the fabricated patch is resonating at very different frequencies than desired. The narrow bandwidth of the array is also well below the minimum bandwidth required. This points to the fact that the matching transformers between the patch and the array are not working as designed. Table 4.1 compares the simulated and measured results at boresight for the 16-element surface fed array.

Table 4.1: Comparison of simulated and measured results for 16 element array

	Simulated	Measured	Δ
Gain	16.28 dB	1.04 dB	15.24 dB
E-plane Cross	-13.33 dB	-13.75 dB	0.42 dB
H-plane Cross	-10.23 dB	-19.96 dB	9.73 dB
Return Loss	-14 dB	-7dB	7 dB
-10 dB Bandwidth	2.5 GHz	300MHz	2.2 GHz

It is seen that the surface fed patch offers far from ideal performance. Both simulation and measurement show very similar results in that the H-plane pencil beam is skewed and the E-plane ripples are excessive. There is significant spurious radiation from the feed network, which interferes with the patch array radiation pattern. This leads to the skew in the main beam, the appearance of large and excessive ripples and finally an increase in the cross-pol levels in both the H and E-plane.

4.2 Aperture Fed Array

Aperture-coupled patches and arrays are typically fabricated using high frequency substrate boards, which are bonded together as shown in Figure 4.12. On the lower board resides the feed network and on the top board the radiating elements. These two boards sandwich a copper ground plane into which are cut slots to allow the energy to couple from the feed into the patch and from thereon radiated into free space *[Garg01]*.

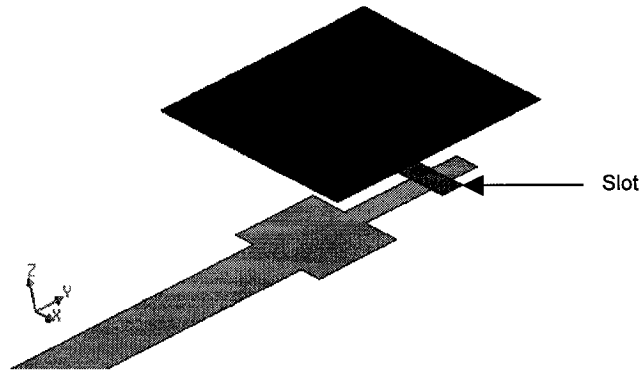

Figure 4.12: Aperture fed patch a) Layout and b) Cross section

Due to the spurious feed radiation encountered in the surface fed linear array, an aperture fed design appears to be a better choice. Separating the feed and patches onto two different boards gives greater isolation and any spurious feed radiation that exists will not directly interfere with the microstrip array, due to the enclosed ground plane. Furthermore, the material parameters of each substrate board can be independently chosen to optimize performance. For the feed network, the substrate parameters are selected to minimize radiation, while for the board on the radiating side, parameters are chosen to maximize radiation efficiency.

As before a single element is designed to ensure that the patch resonates at the correct frequency and exhibits low return loss. From here the feed network is added to the patches to complete the array.

4.2.1 Single Element Aperture Fed Patch

Unlike a surface fed patch, the design of an aperture fed patch is not as straightforward and simple. There exist no simple equations to design the

aperture fed patch. The equations that exist to determine patch width and length can still be used for sizing the patch but other important factors also play a significant role in the design. These can be seen in Figures 4.13 and 4.14.

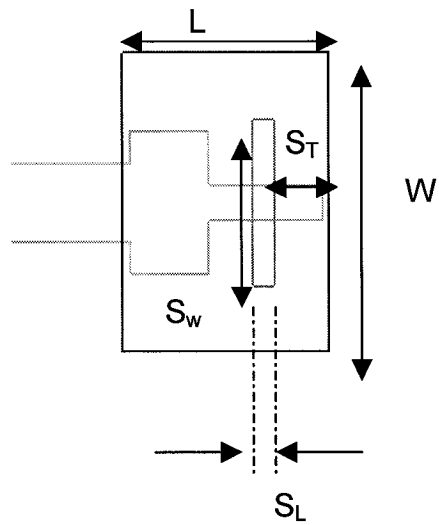

Figure 4.13: Critical horizontal dimensions aperture fed patch

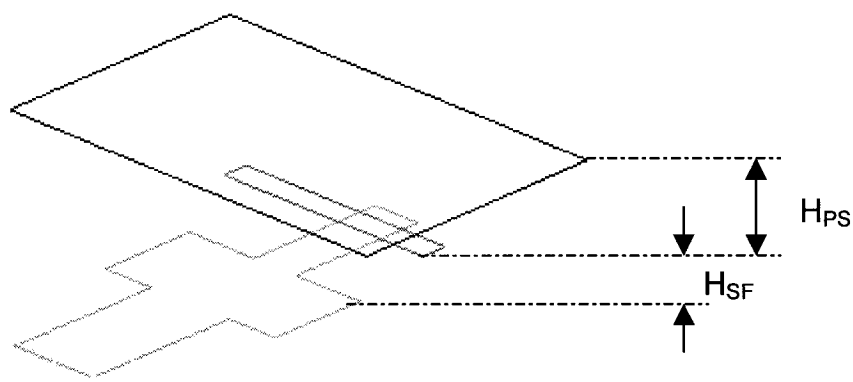

Figure 4.14 Critical vertical dimensions aperture fed patch

- L – The length of the patch sets the resonant frequency
- W – The width of the patch is useful in setting the input impedance of the patch
- S_W and S_L – Slot width and length. The slot is a cut in the ground plane through which the energy couples from the feed to the patch. It affects

both the input impedance and to an extent the resonant frequency of the patch.

- S_T – Often when designing an aperture-coupled patch a portion of the feed line is left to overlap the slot. The length of this stub is adjusted to cancel the reactance of the slot.
- H_{PS} – The height of the substrate between the patch and the slot. A thicker value is desired as it reduces the capacitance of the patch i.e. it allows for both an easier matching and also ensures that most of the fed power is radiated into free space and not stored in the substrate.
- H_{SF} – The height of the substrate between the slot and the feed. A thinner value is desired here, as it will allow for a larger range of line widths that can be etched for the feed lines, and also reduces spurious radiation from the feed lines.
- ε_{r1} and ε_{r2} – The dielectric constant of the two boards can be chosen independently thus allowing a wider range of width and lengths of microstrip to be fabricated if required. In this design however they are both chosen to be the same for simplicity.

Since so many factors influence the design of an aperture fed patch it is even more essential to use the EM simulator. Multiple iterations involving the variation of the above factors, within achievable fabrication limits, led to the design shown in Figure 4.15 and summarized in Table 4.2.

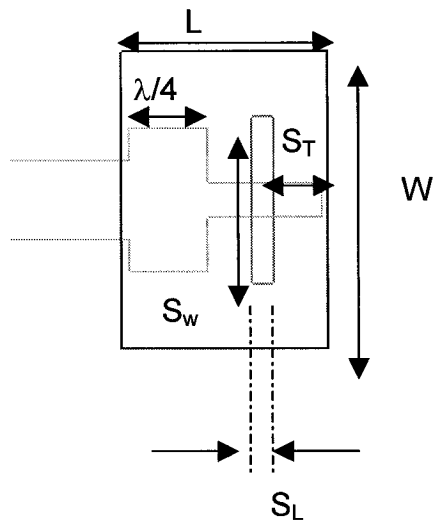

Figure 4.15: Simulated model for aperture fed patch

Table 4.2: Aperture fed patch dimensions

Parameter	Dimensions
L	3.6 mm
W	2.5 mm
S_W	0.25 mm
S_L	2 mm
S_T	0.593 mm
H_{PS}	0.762 mm
H_{SF}	0.254 mm
ε_{r1}	2.2
ε_{r2}	2.2

The simulated return loss and gain for the single aperture fed patch are shown in Figures 4.16 and 4.17 respectively.

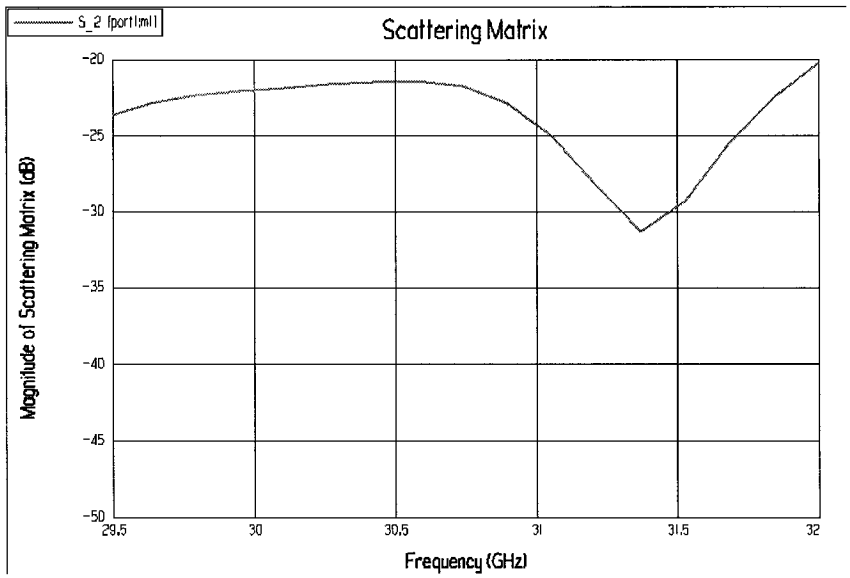

Figure 4.16: Return loss for single aperture fed patch

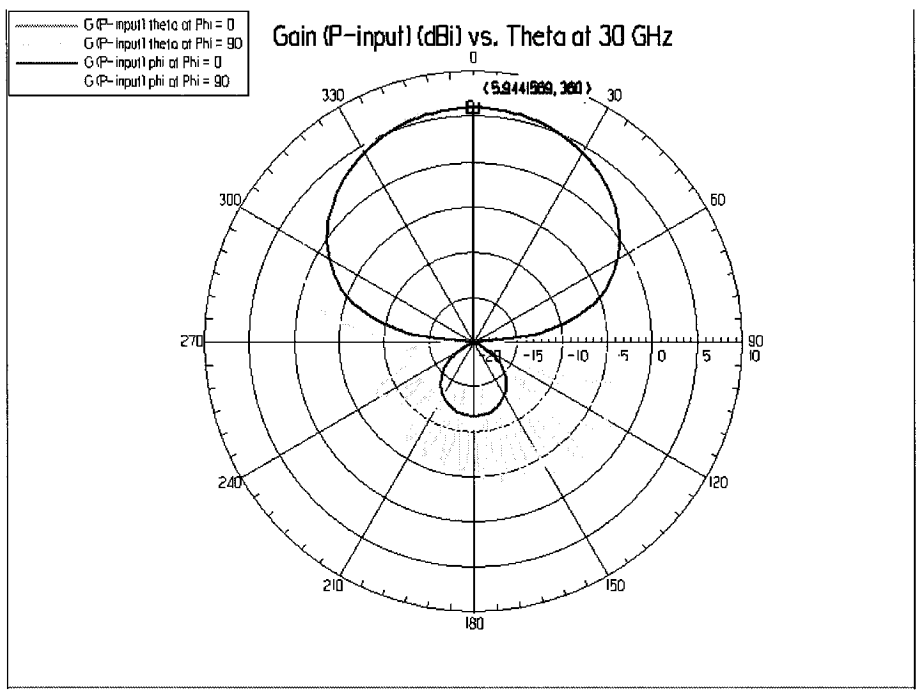

Figure 4.17: Gain for single aperture fed patch

The results are summarized in Table 4.3.

Table 4.3: Simulated results for aperture fed patch

Simulated Boresight Gain	[dB]
Gain	5.94
E-plane Cross	-43.0
H-plane Cross	-42.0
Back lobe level	-10.75

The simulated results for the single aperture-fed patch look very promising. A return loss of near -22 dB for the center frequency of 30 GHz was obtained, with the patch resonating at a frequency of 31.4 GHz. This is not a major concern as previous experience had shown that Ensemble often predicts a higher resonant frequency than is measured physically (see measured results in the next section). The return loss is less than -10dB over the entire simulated bandwidth of 29 GHz to 32 GHz. A gain of 5.94 dB at boresight can be seen. The H-plane and E-plane patterns have a shape exactly as predicted by theory. No ripples at all occur in the principal beams. The cross-pol levels are extremely low. The back lobe level is -10.75dB which is less than the rule of thumb minimum of -10 dB. Some spurious feed radiation is still present as can be seen by the pattern ripples for angle of 90^0 through 270^0, but since this is physically separated from the main beam, no interference with the radiating elements occurs.

Based on the simulated results fabrication a single patch is the next logical step. The measured results can then be compared with those simulated. Photographs of the prototype are shown in Figures 4.18 and 4.19.

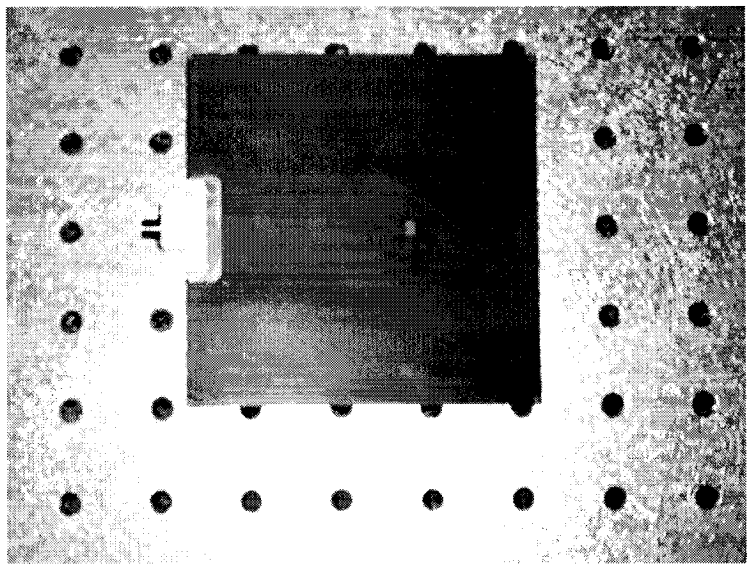

Figure 4.18: Fabricated single aperture fed patch – Top view

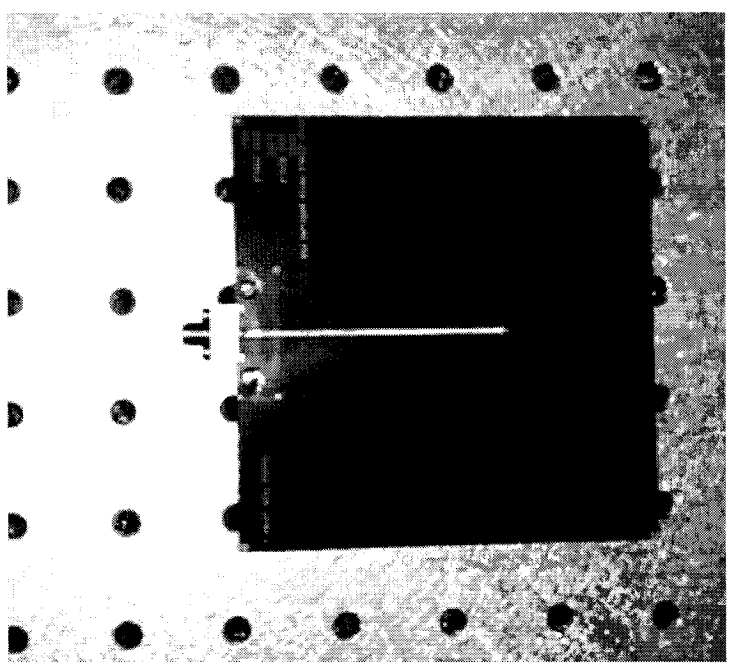

Figure 4.19: Fabricated single aperture fed patch – Bottom view

Since the fabrication of this design utilizes two separate boards alignment of the patch with the inset aperture and feed lines becomes critical. Alignment markers are added to the basic design to aid in the correct orientation of the two boards. As before the tolerance on line widths is strictly respected and a K-connector block is also added as is visible in the pictures.

Figure 4.20 shows the measured radiation patterns while Figure 4.21 shows the measured return loss.

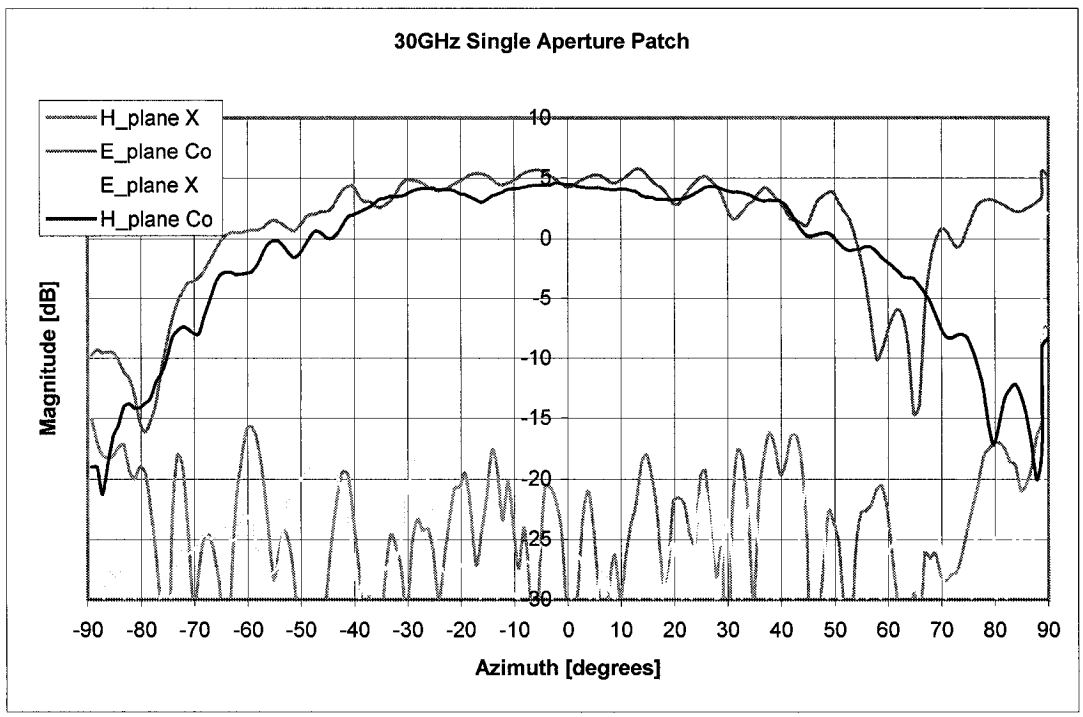

Figure 4.20: Single Aperture Patch Gain Measurements at 30 GHz

The gain was measured to be 4.87 dB with very low cross-pol levels below -30 dB. The back lobe level could not be measured due to the test setup.

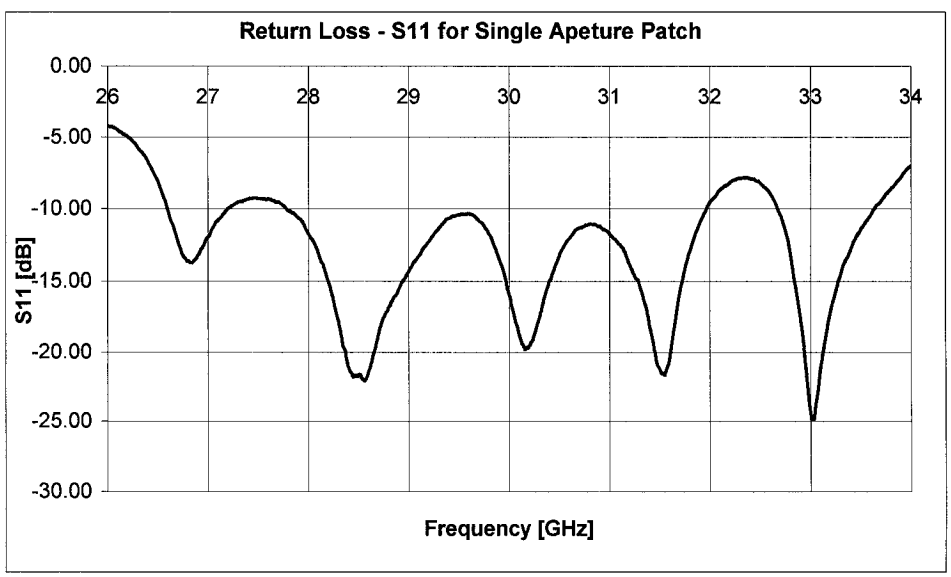

Figure 4.21: Return loss for single aperture fed patch

The return loss measured was -16dB for the center frequency with a -10dB return loss bandwidth of 4GHz.

The results for the single aperture fed patch show a substantial improvement to that displayed by a surfaced-fed patch array. However there are still some ripples in the E-plane co-pol pattern, which are not acceptable. These ripples are caused by the effect of a finite ground plane. Closely examining the distance between the ripples it can be seen that they occur regularly at intervals of 10^0. In order to characterize the effect of the finite ground plane it is necessary to model the edge of the board where scattering is occurring as a virtual source. Thus the structure tested can be viewed hypothetically as a two-element pseudo-array. Array theory predicts that the nulls in an array pattern occur at regular intervals given by the equation:

$$\theta_n = \cos^{-1}\left(\frac{n\lambda}{Nd}\right) \qquad \textbf{[4.1]}$$

Where n is an integer, N is the number of elements, d is the spacing between elements and θ_n is the angle between nulls

Plugging in the relevant parameters into equation 4.1 and rearranging to solve for d, the distance from the center patch to the edge of the board one obtains:

$$d = \left(\frac{n\lambda}{N \cos\theta_n} \right)$$
$$d = \left(\frac{1(10mm)}{2\cos 10^0{}_n} \right) \qquad [4.2]$$
$$d = 5.077mm$$

This is in fact the exact distance between the center of the patch and the edge of the board. This confirms the patch pattern is definitely being affected by the effect of a finite ground plane. Before using the aperture fed patch as designed, in a full 16-element array, the effect of the finite ground plane must be rectified or the patterns will be unacceptable. The obvious solution is to use a larger ground plane however a much more elegant solution to this problem is discussed in Section 4.2.3.

A comparison of simulated and measured results for the single aperture fed patch is given in Table 4.4.

Table 4.4: Comparison of simulated and measured results – Aperture fed patch

	Simulated	Measured	Δ
Boresight gain	5.94 dB	4.87 dB	1.07dB
E-plane Cross	-43.0 dB	-36.85 dB	6.15dB
H-plane Cross	-42.0 dB	-30.76 dB	11.24dB
Back lobe level	-10.75 dB	Not measured	N/A
Return Loss	-22 dB	-16 dB	6 dB
-10 dB Bandwidth	At least 3GHz	4.1 GHz	N/A

The measured and simulated results agreed with each other very well (A little over 1dB in terms of principal beam gains). There was a significant difference in the cross-pol levels but both simulation and measurement show that they are low enough. Simulation predicted that the aperture patch would have a large -10dB bandwidth. Due to computer and time constraints, simulations were

not carried out to determine exactly how wide a band the antenna would perform over.

4.2.2 16 Element Aperture Fed Array – Simulated Results

Once the single element design was validated it was decided to move to the full 16-element array as had been done previously with the surface fed array. One of the major concerns before designing the array is the inter-element spacing. This spacing is very important in that it sets the sidelobe levels, the beam scanning range and the cross coupling between elements. This spacing must be minimized to avoid grating lobes and to have a large beam scan range but at the same time a compromise is required in that placing the elements too close to each other significantly increases mutual coupling thereby degrading gain. (See equations 2.16 and 2.17 for scan range).

The effects of element spacing on the array pattern for the 16-element array were simulated using Ensemble. Keeping every other parameter equal, i.e. 16 elements on ε_r = 2.2 substrate the distance d above was varied over four different values as shown in Figure 4.22. The radiation characteristics are plotted as in Figure 4.23 to see the sidelobe levels while the coupling between elements is obtained by evaluating the S_{21} and S_{31} between the patches.

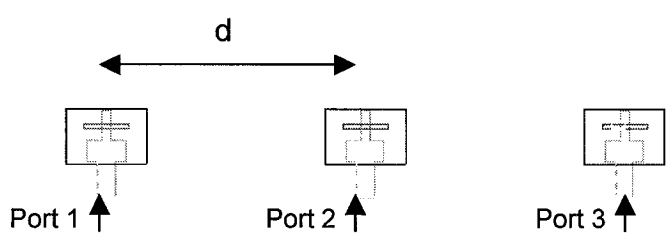

Figure 4.22: Spacing between elements

The results are summarized in Table 4.5. For detailed plots for all cases refer to appendix A1.

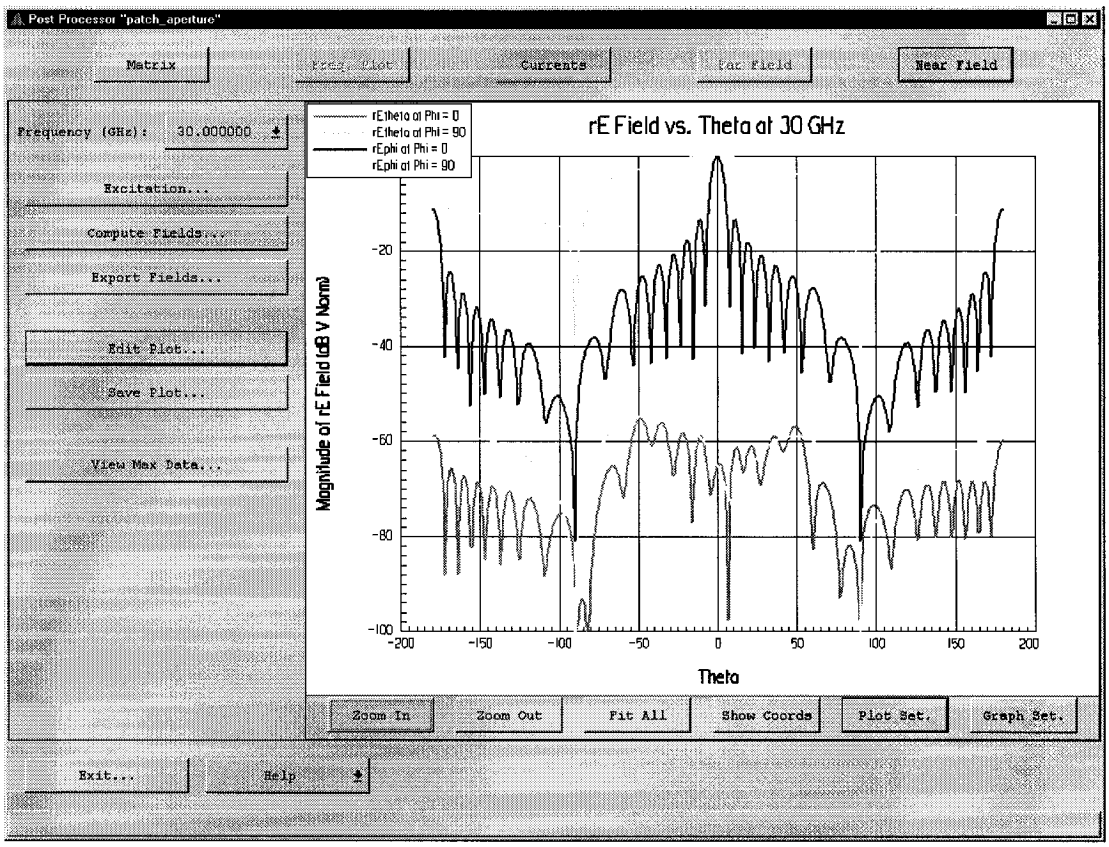

Figure 4.23: Simulated results for inter-element spacing of 4.6mm

Table 4.5: Effect of element spacing on array performance

Case	Edge to edge spacing [mm]	Center to center spacing – d [mm]	Center to center spacing – λ's	# of sidelobes	Coupling [dB]	Back lobe level [dB]
1	1	4.6	0.46	14	-13	-9
2	2	5.35	0.54	16	-16	-12
3	3	6.65	0.66	20	-24	-13.5
4	8	11.1	1.1	14	-26	-12

From the study done in the simulations above it is seen that the only case where the expected number of sidelobes occur is for an inter-patch spacing of 1mm. This is advantageous in that minimum power is wasted in the sidelobes. The down side of this spacing is that the back lobe level is significantly higher

giving a back lobe level of -9 dB which is unacceptable for the design. (Need <-10dB).

There seems to be a direct relationship with the spacing and the back lobe levels with higher spacing yielding better back lobe levels. This only occurs up to a certain spacing before the grating lobes appear in the visible portion of the pattern as is seen in case 4. When it is quite evident that grating lobes occur there is significant degradation of the front- to-back ratio.

Although the larger inter-element spacing yields more than expected sidelobes the front-to-back ratio is significantly better than for smaller spacing. As well the coupling between the patches is significantly lower for larger spacing. The potential downsides for a larger spacing however include a smaller beam scan and greater loss of power to the extra sidelobes.

Based on these conclusion it was obvious that a spacing in between 0.4λ to 0.6λ, is optimum in terms of sidelobe levels and back lobe levels. This information plus the results already known for the single element patch now made it possible to finalize the array design.

4.2.3 16-Element Aperture Fed E-Plane Array

The design of the single patch as well as the study done on inter-element spacing between the patches showed that the ground plane plays a significant effect on the pattern of the patch. In order to minimize this effect the layout of the array was changed from an H-plane array to an E-plane array as seen in Figure 4.24.

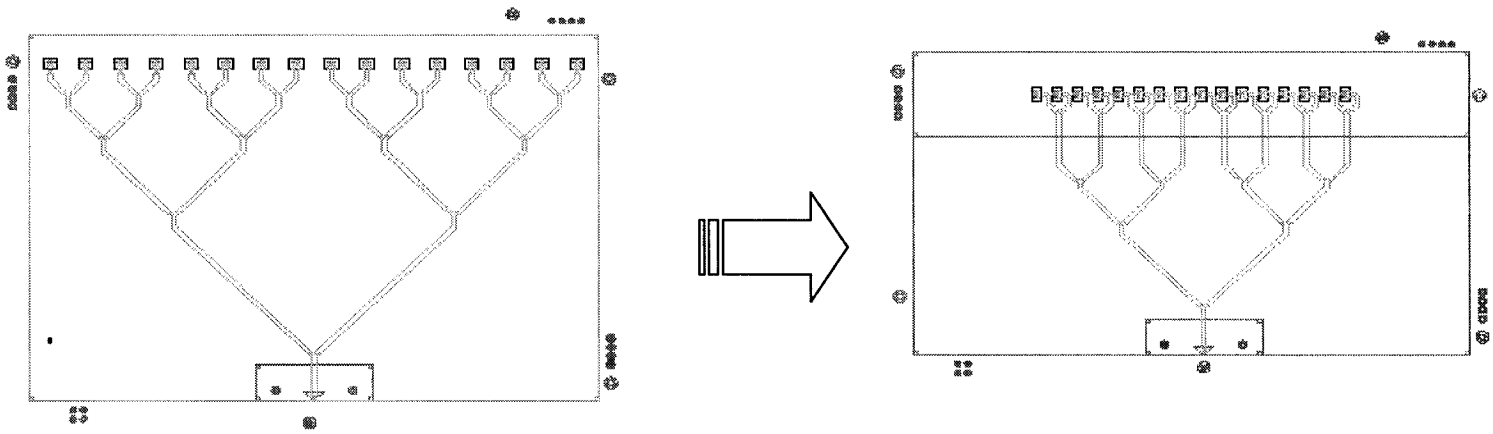

Figure 4.24: Evolution of aperture fed array

To understand the reasoning behind this change it is essential to re-examine the theory of a patch. The theoretic pattern for a single patch on an infinite ground plane is shown in Figure 4.25.

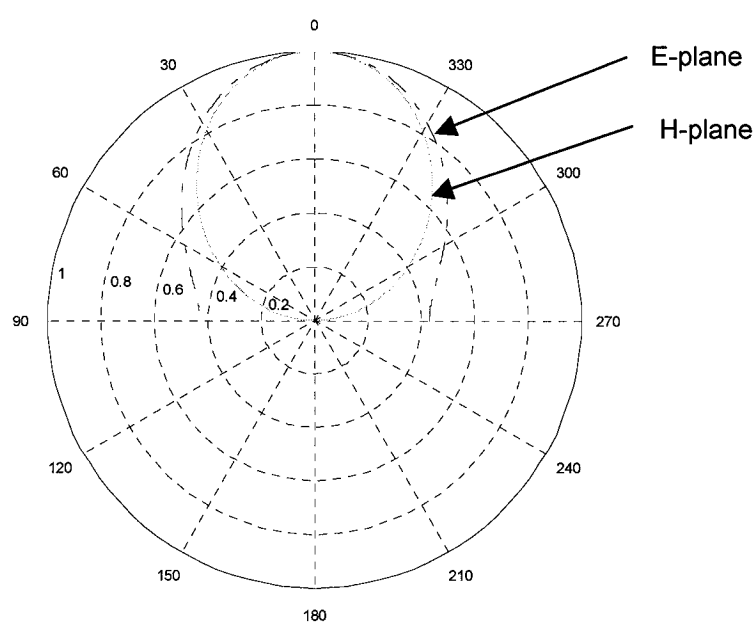

Figure 4.25: Theoretical gain patterns for single patch

The H-plane pattern has nulls at the horizon ($\theta = 90^0$ and $\theta = 270^0$), while the E-plane pattern, still shows fairly significant radiation at the horizon. There will therefore be a greater amount of scattering from the edge of a finite ground

plane in the E-plane than in the H-plane. By orienting the patches in the linear array, so that their E-fields are aligned (an E-plane array), the amount of scattering due to the finite ground plane will be considerably reduced. In the plane of the array, the array factor will have little radiation at the horizon since it is a pencil beam, while in the orthogonal element plane, the element pattern has a null at the horizon, so the overall amount of scattering should be greatly reduced.

In addition to this change the spacing between the array elements is now tightened to 0.54λ, which is the optimum spacing as found in the study done in section 4.2.2. Changing the spacing will prevent grating lobes from occurring and it will also allow a large beam scan range (See section 2.4.1 for beam scan range equations)

$$\cos\theta_{\max} = \frac{\lambda}{d_{\max}} - 1$$
$$\theta_{\max} = \cos^{-1}\left(\frac{10mm}{5.4mm} - 1\right) \qquad \textbf{[4.3]}$$
$$\theta_{\max} = 31.58^0$$

The spacing now allows for a beam scan of up to 90^0 - θmax = 60^0. The simulated patterns and return loss are shown in Figures 4.26 and 4.27.

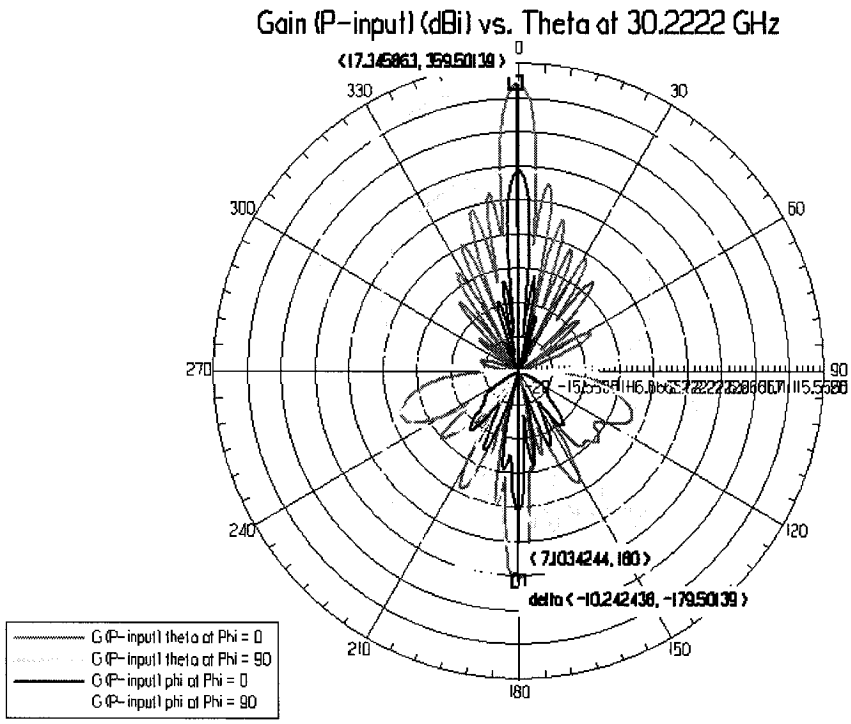

Figure 4.26: Simulated gain for E-plane array – Polar plot

The simulated radiation patterns look quite promising. The gain of the array is 17.3 dB with E and H-plane cross-pol levels at 5.89 dB and -6.03dB respectively. This is still at least -15dB below the main lobe thus meeting specifications. The back lobe level simulated is -10.24dB.

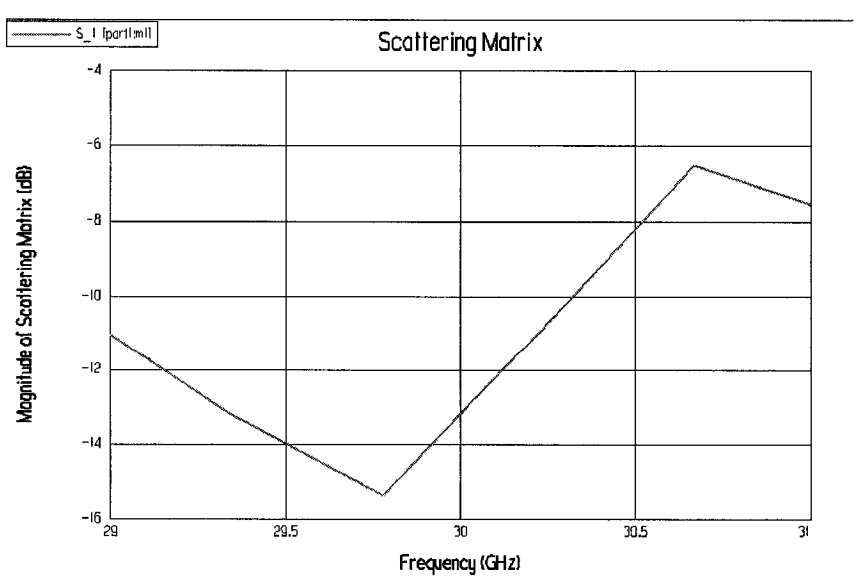

Figure 4.27: Simulated return loss for E-plane array

The return loss predicted by the simulator is -13dB for the center frequency with a -10dB return loss bandwidth of 1.3GHz. Once again even though the return loss isn't centered exactly around 30GHz previous experience indicates that there will be a frequency shift from the simulated to the measured results so these results are adequate at present.

4.2.4 E-Plane Array – Measured Results

The fabricated 16-element E-plane, aperture fed array is shown in Figures 4.28 and 4.29.

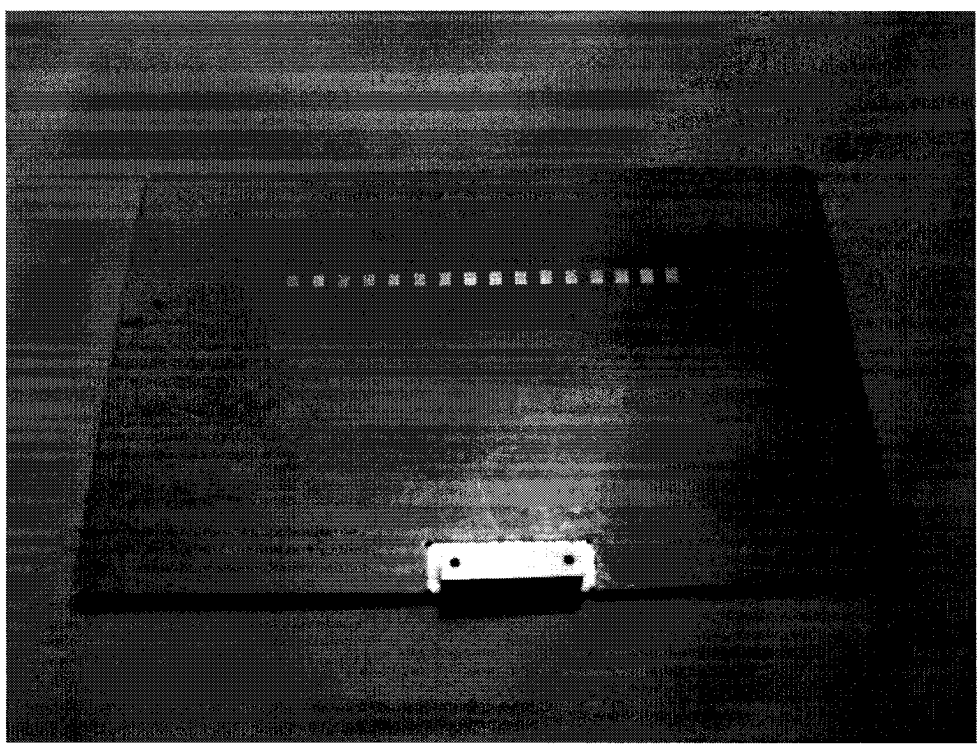

Figure 4.28: Fabricated E-plane array- Top view

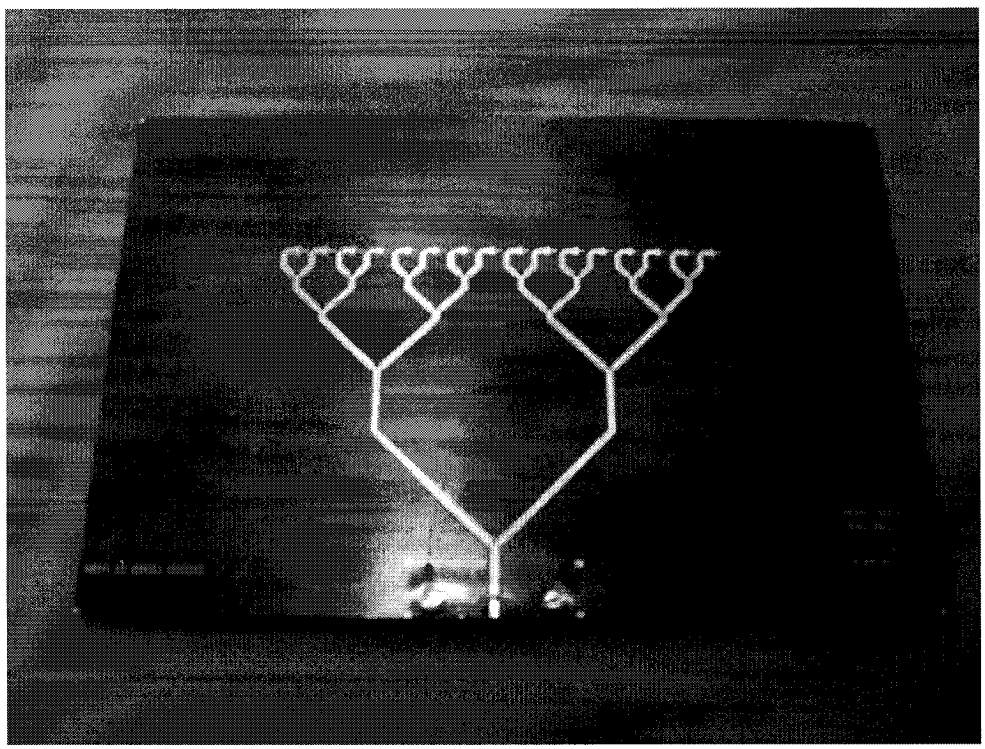

Figure 4.29: Fabricated E-plane array – Feed view

Fabrication of this array is more complex as the spacing between the feed lines was quite small as seen in Figure 4.29. However it is just above the minimum acceptable distance. As per the single patch alignment markers were required and a K-connector block is also present.

Measured patterns and return loss are shown in Figures 4.30 and 4.31.

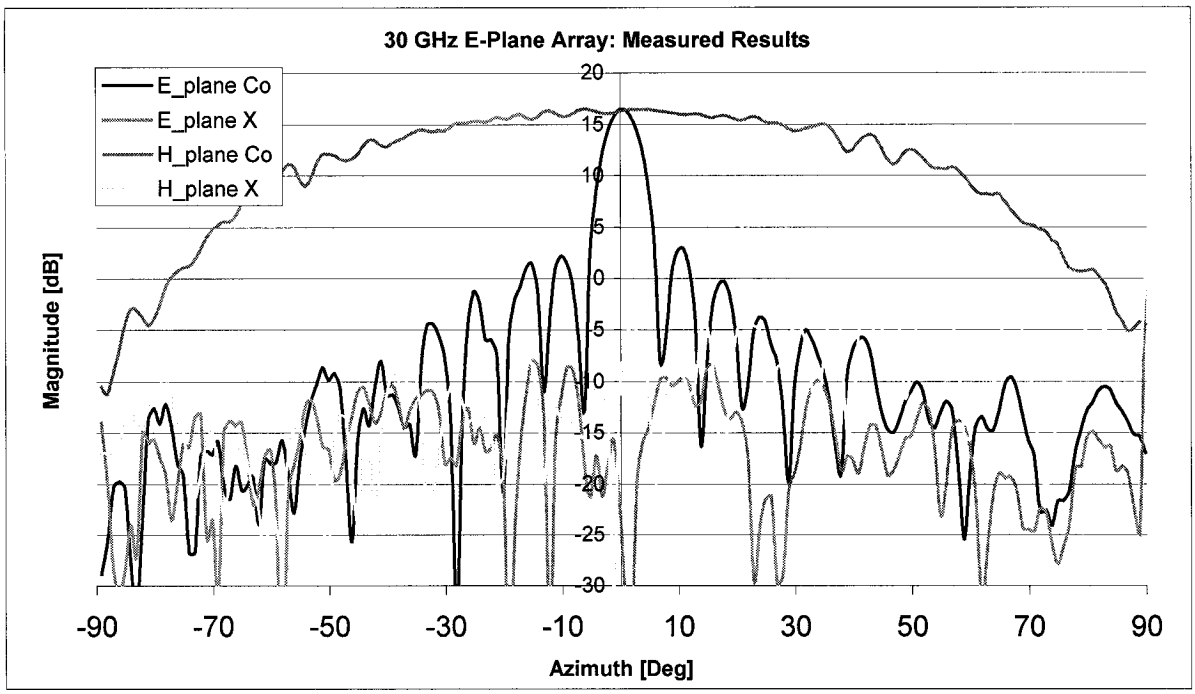

Figure 4.30: Measured gain for E-plane array

The results for the aperture fed E-plane array are markedly improved from the surface fed array. The lack of feed interference sees the gain increase significantly to 16.45 dB, which is much closer to that expected. The cross-pole levels are also much lower than the specifications.

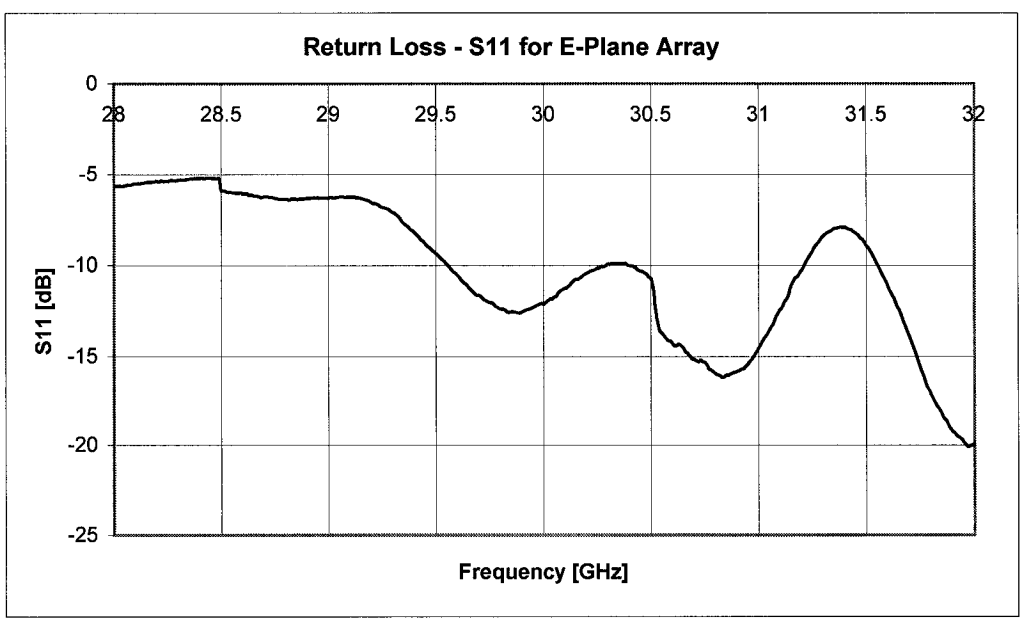

Figure 4.31: Measured return loss for E-plane array

The return loss measured is -13dB for the center frequency with a -10dB return loss bandwidth of 1.75GHz. This is also much better than specifications. A comparison of simulated and measured results for E-plane array can be seen in Table 4.6.

Table 4.6: Comparison of measured and simulated results for E-plane array

	Simulated	Measured	Δ
Boresight gain	17.3 dB	16.45 dB	0.85 dB
E-plane Cross	5.89 dB	-31.52 dB	-25.63 dB
H-plane Cross	-6.03 dB	-6.18 dB	0.15 dB
Back lobe level	-10.24 dB	Not measured	N/A
Return Loss	-13 db	-13 dB	0
-10 dB Bandwidth	1.3 GHz	1.75GHz	0.45 GHz

The measured and simulated results agree very well. The measured gain of the principal beam is less than 1dB different than that simulated. The E-plane cross pol level was not so close in agreement but this can easily be explained by the way the nulls of the cross-pol aligned with the angles. Taking the cross-pol level just a few degrees away from boresight yields a value that is much closer to that simulated.

In conclusion the final E-plane array design is seen to rectify many of the shortcomings of the surface fed array and that of a potential aperture fed H-plane array. Not only is feed interference removed but as well the pattern is smoothed, so that it is ripple free. The gain of 16.45dB and the bandwidth 1.8GHz displayed by the E-plane array are more than satisfactory. The evolution of this design not only validates patch and array theory but also reinforces the use of Ensemble as a design tool for high frequency arrays.

4.3 Bent Array

The linear array is designed to incorporate active elements i.e. high power amplifiers in order to boost the EIRP of the antenna. Due to the heat generated by the amplifiers, a heat sink is required to remove the excess heat. As will be further discussed in Chapter 5, the heat sink will be placed on the radiating side of the board. The problem with this scenario is that the heat sinks metallic fins will potentially interfere with the radiation pattern of the array as shown in Figure 4.32.

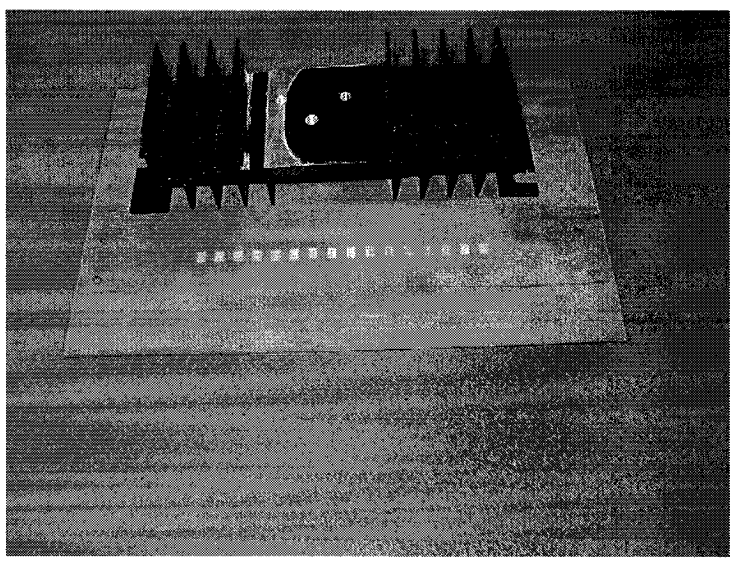

Figure 4.32: Unbent array with heat sink

To mitigate the effects of the heat sink on the radiation pattern a novel solution can be implemented whereby the Duroid board is mechanically bent to make the antenna elements orthogonal to the fins of the heat sink. The following sections describe some of the methods used to validate the use of mechanical shaping of the antenna array board to improve the electrical performance of the active array.

4.3.1 Comparison of Array with and without Heat Sink

To fully characterize the extent of interference cause by the heat sink fins, array patterns were measured with and without the heat sink. In both cases only the 30 GHz passive E-Plane array was measured. Figure 4.33 shows the radiation patterns of the E-plane array without the heat sink.

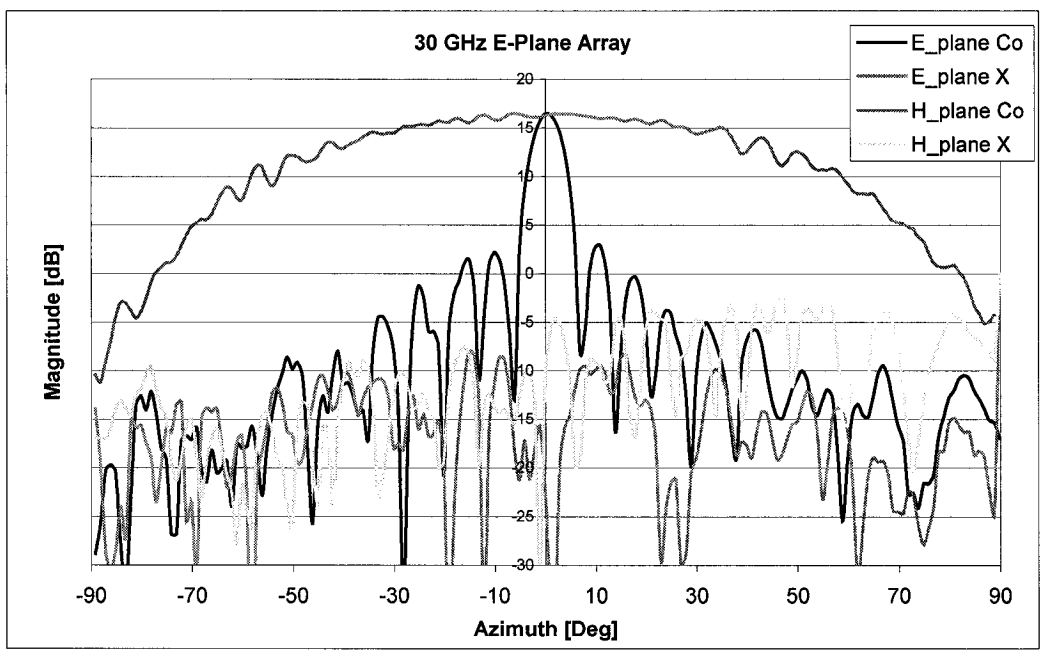

Figure 4.33: Pattern for Array without Heatsink

Summarizing the key performance characteristics of the array we can see that the gain of the array is 16.45 dB with maximum E-plane and H-plane cross-pol levels at -10dB and 3 dB respectively. Also the principle beams have 2 dB ripples.

Figure 4.34 depicts a simulation model of a passive array with heat sink fins. It can be clearly seen that the fins of the heat sink are electrically visible to the array and will cause some interference in the radiation pattern.

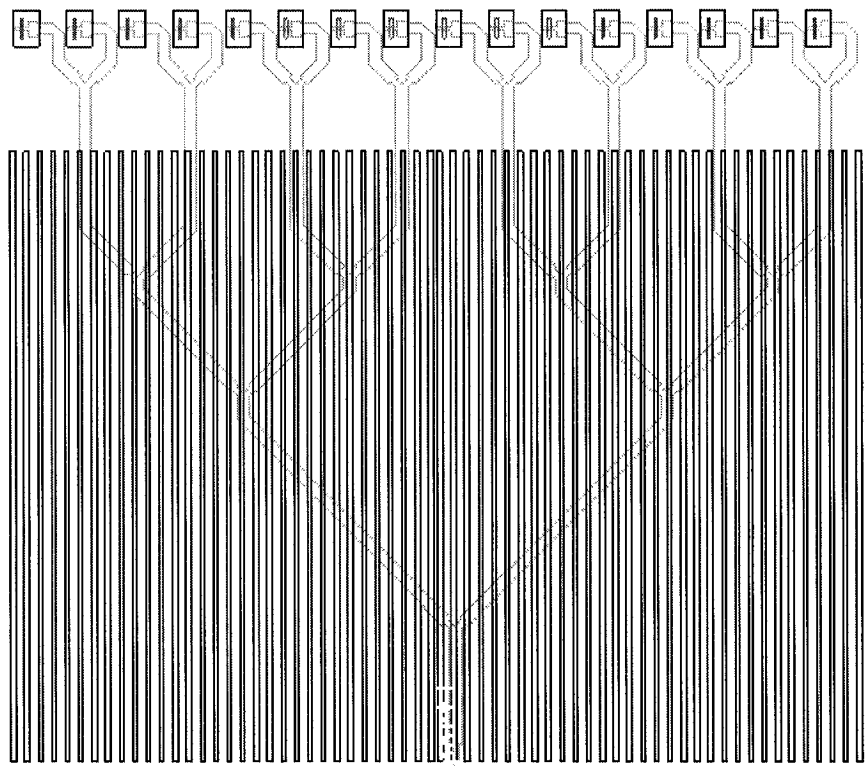

Figure 4.34: Simulate array with heat sink

It was hoped to study the effect of the fins using Ensemble. However the complexity of the structure made it a very time-consuming simulation with results that would often not converge. This theoretical/simulation method could not be pursued and a manufactured array with an integral heat sink was studied instead to more clearly understand the performance loss that would occur.

Figure 4.32 depicts the manufactured array measured. The radiation patterns of the antenna with the heat sink are shown in Figure 4.35.

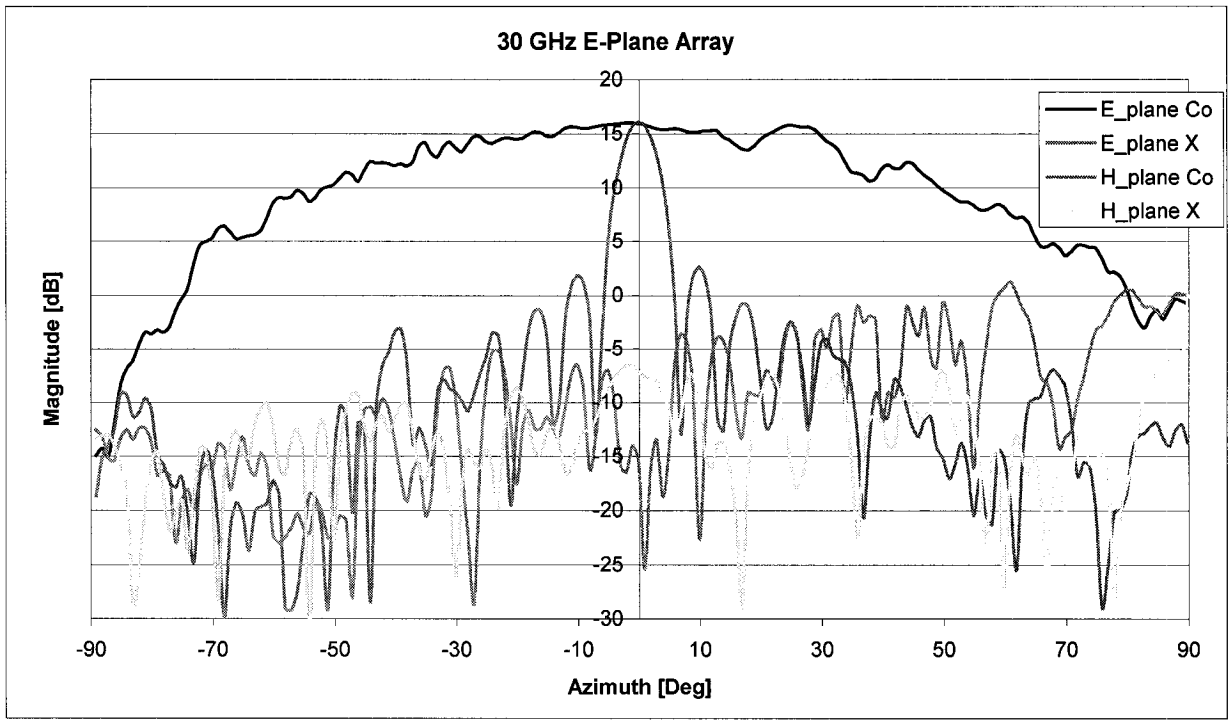

Figure 4.35: Pattern for Array with heatsink

Comparing the pattern to those in Figure 4.33, the addition of the heat sink increases the ripples in the E-plane to a height of 4 dB. There is also a significant increases the cross-pol levels to a 2 dB and -6dB for the E and H-plane respectively. Of most concern however is that the gain drops to 16 dB.

4.3.2 Solutions to Interference

In order to reduce the effect of the heat sink on the radiation pattern of the array, it is necessary to somehow make the heat sink invisible to the patches of the array. A novel idea of doing this was to bend the Duroid substrate so that the heat sink was at 90^0 to the array itself.

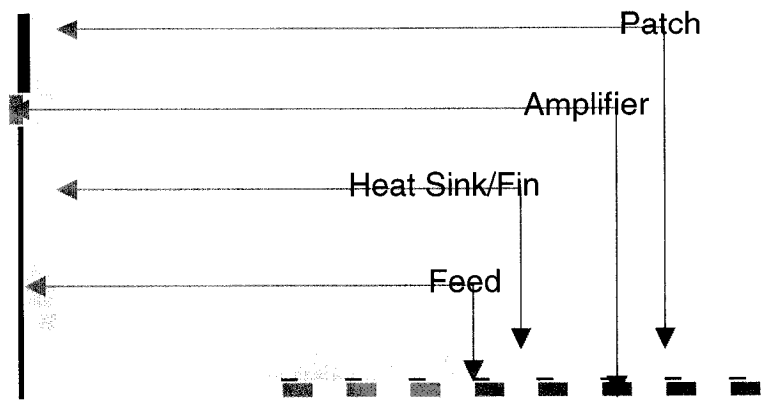

Figure 4.36: Unbent array

The flat array as shown in Figure 4.36 is bent through an angle of 90^0. Making the heat sink orthogonal to the patches should make the fins of the heat sink invisible to the patches and therefore the interference source to the radiation pattern should be removed. This is better illustrated in Figure 4.37.

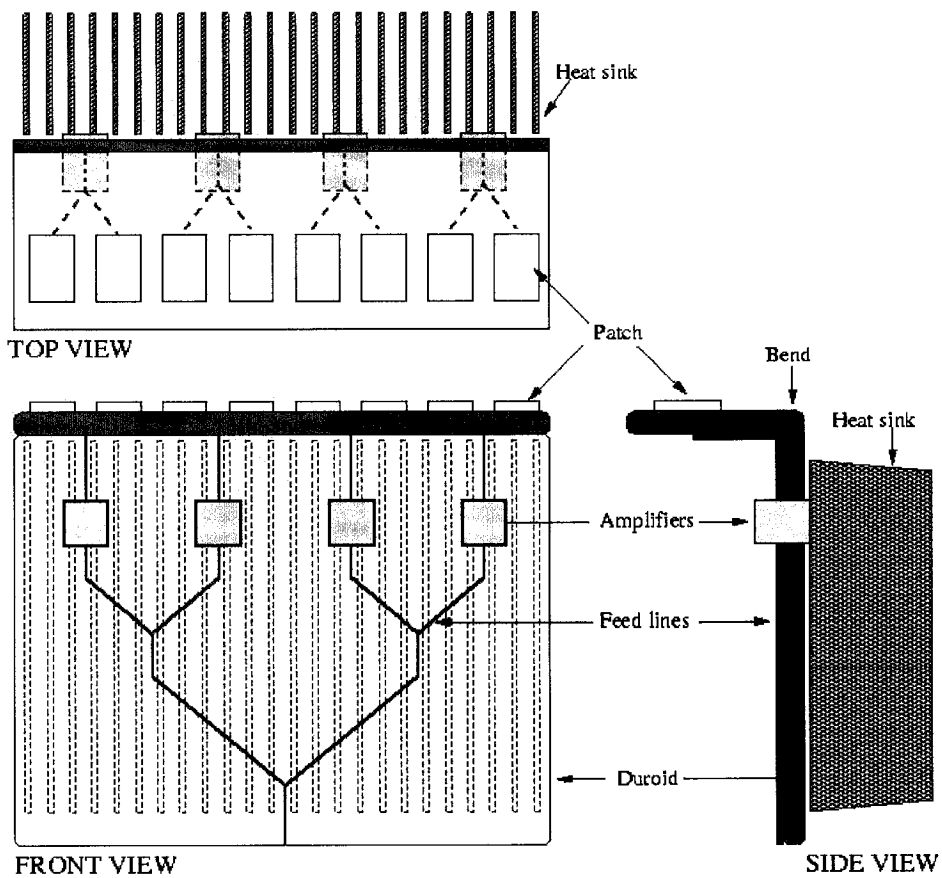

Figure 4.37: Conceptual drawing of bent array with heat sink

However the effect of bending on the electrical and mechanical properties of the Duroid remained unknown. Bending might physically lead to cracking of microstrip lines or it might electrically alter the performance of the microstrip line by increasing the capacitance of the line and thus modifying the characteristic impedance as compared to an unbent line.

4.3.3 Microstrip Characterization on Bent Substrates

To measure the effect of bending, six 50 Ω, microstrip lines were fabricated using the same substrate as that of the array. The six lines were bent through various diameters and their S-parameters measured to quantify the effect of bending.

Six boards were etched on 5880 Duroid - ε_r = 2.2 with a thickness of 0.254 mm which is the same as the board thickness of the feed lines for the 16 element array. Each of the boards is etched with a straight 50 Ω microstrip line. These microstrip boards were bent around various diameter rods. The rods utilized are of diameters of 0.5", 0.75", 1.0", 1.5", 2", and 2.5". To prevent cracking the boards are first heated with a heat gun and then made to conform to the rods. The boards are taped overnight to the stock diameter rods in order to retain the curvature and to reduce spring-back as much as possible. Once the boards retain the required curvature they are connected to a network analyzer using K connectors and the S-Parameters measured. Figures 4.38 and 4.39 show the stock diameter rods around which the boards are bent.

Figure 4.38: 0.5 thru 1.5 inch rods used for bending

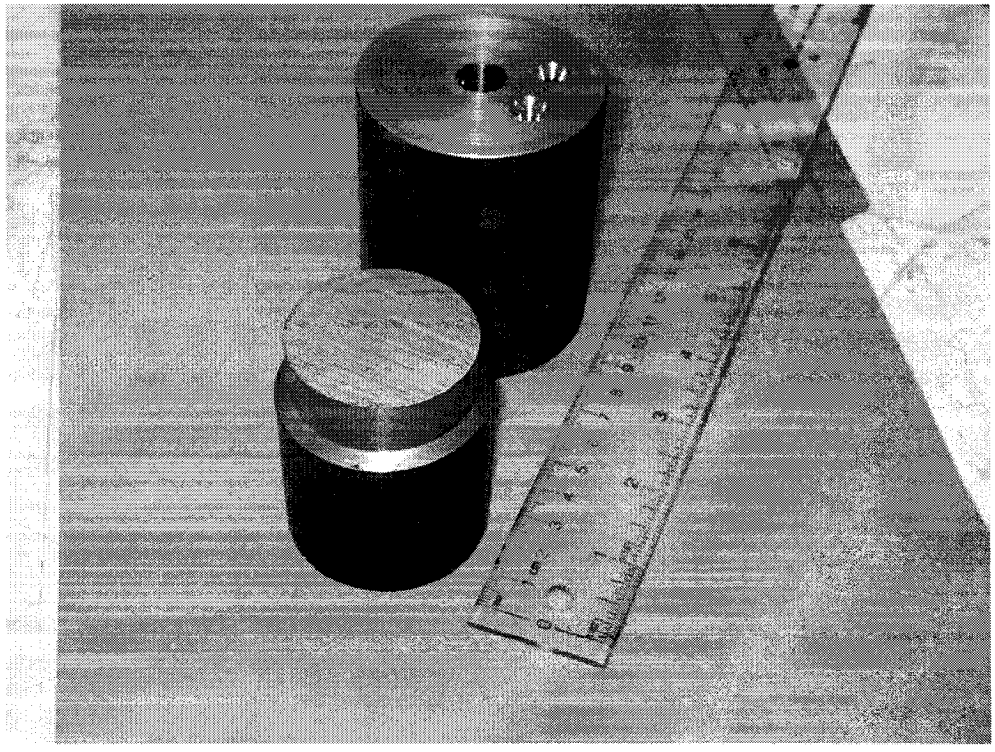

Figure 4.39: 2 and 2.5 inch rods used for bending

The flat Duroid board shown in Figure 4.40 is bent to conform to the stock diameter rods. The results of the bending process can be seen in Figures 4.41 through 4.44.

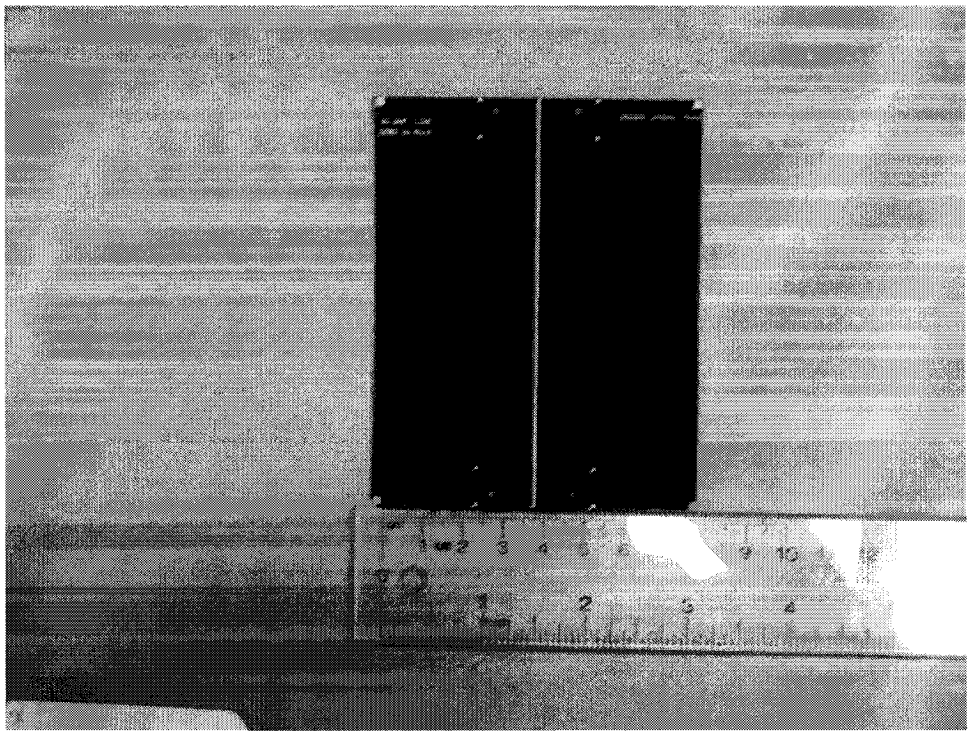

Figure 4.40: Unbent 50 Ohm line on 5880 Duroid

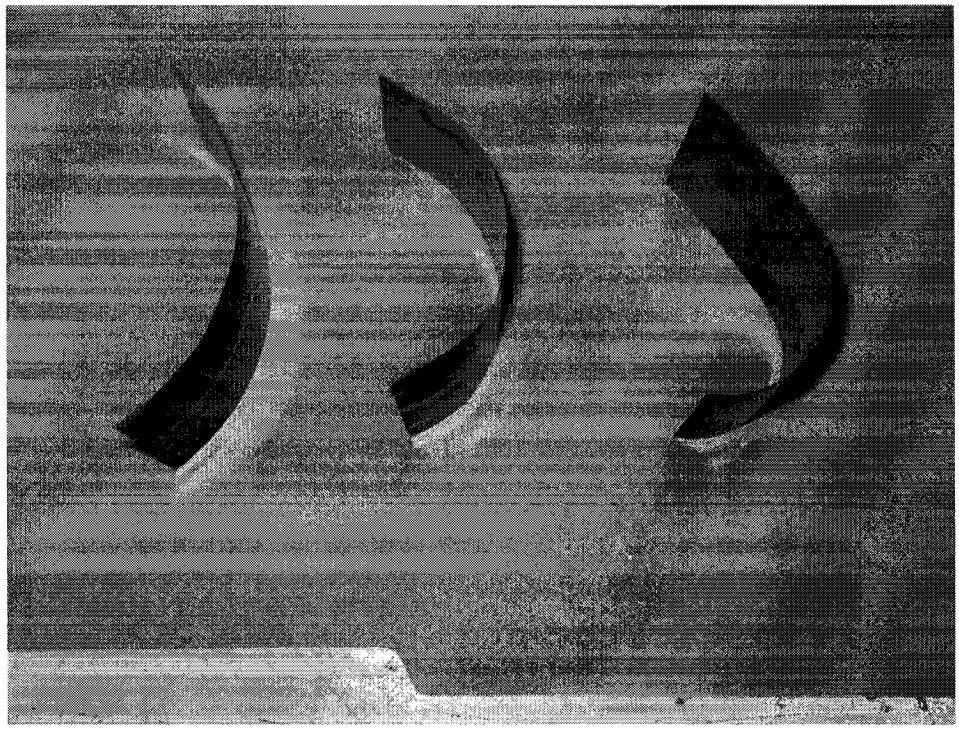

Figure 4.41: Bent lines 1.5 thru 2.5 inches – Top View

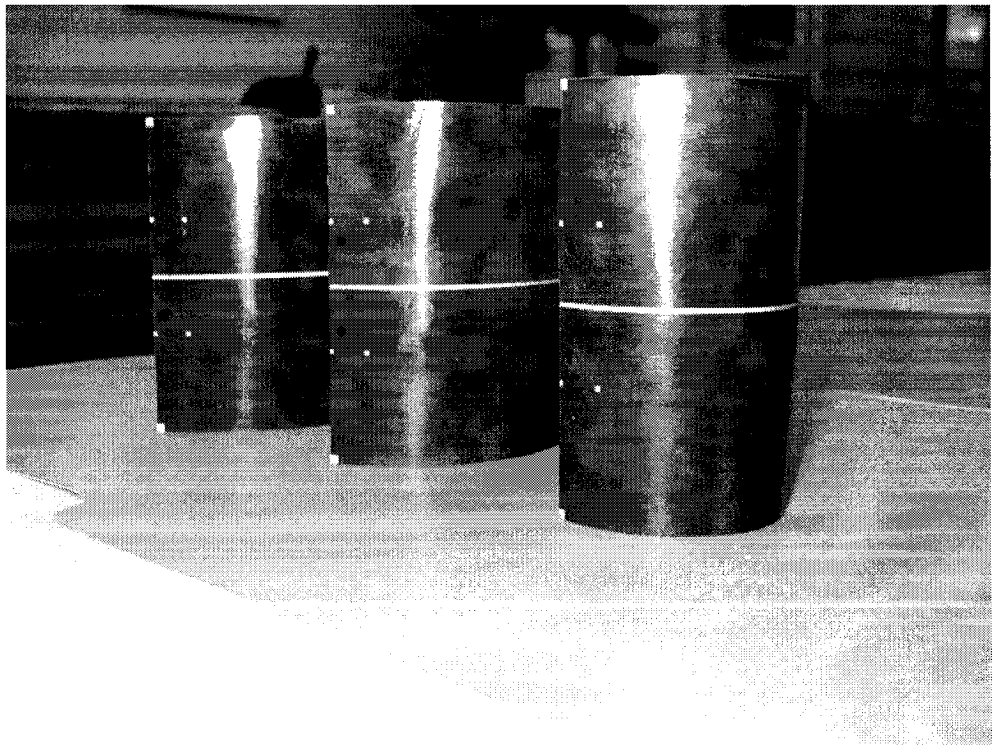

Figure 4.42: Bent lines 1.5 thru 2.5 inches – Isometric View

Figure 4.43: Bent lines 0.5 thru 1.0 inch – Top View

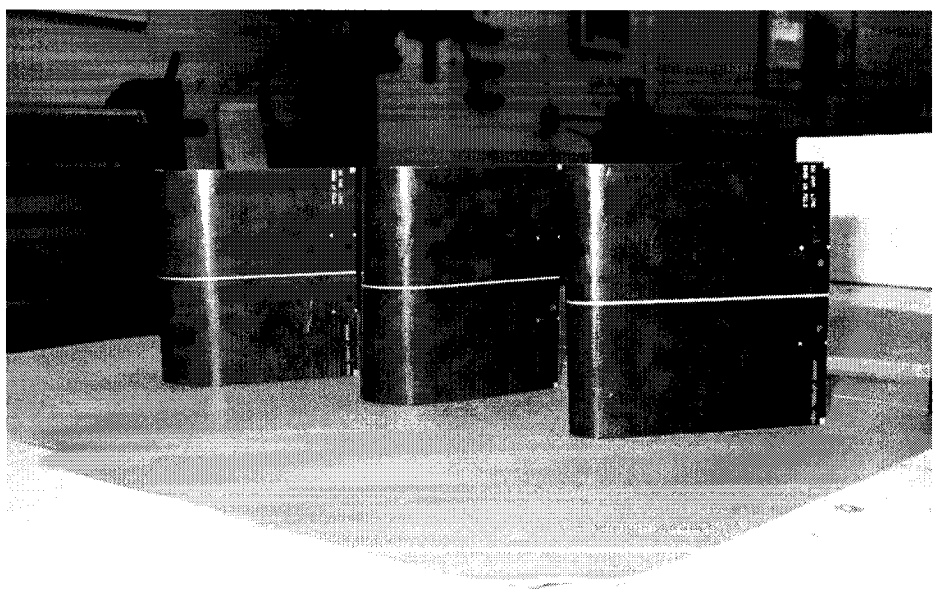

Figure 4.44: Bent lines 0.5 thru 1.0 inch – Isometric View

The S-parameters of the flat boards were measured and compared with those of the original unbent boards. This is done in order to determine the tightest radii through which the board could be bent without significantly degrading the electrical performance of the microstrip line. The measurements of S-parameters were only carried out in the range of 27 to 32GHz as it is felt that if the boards work at a higher frequency band, operation at the lower frequency band around 20 GHz should not be a problem.

To simplify the comparison the S-parameters for both the unbent and the bent lines are graphed and overlaid as in Figure 4.45. This represents the tightest bend radii tested. See Appendix A for the S-parameters for all other bend radii.

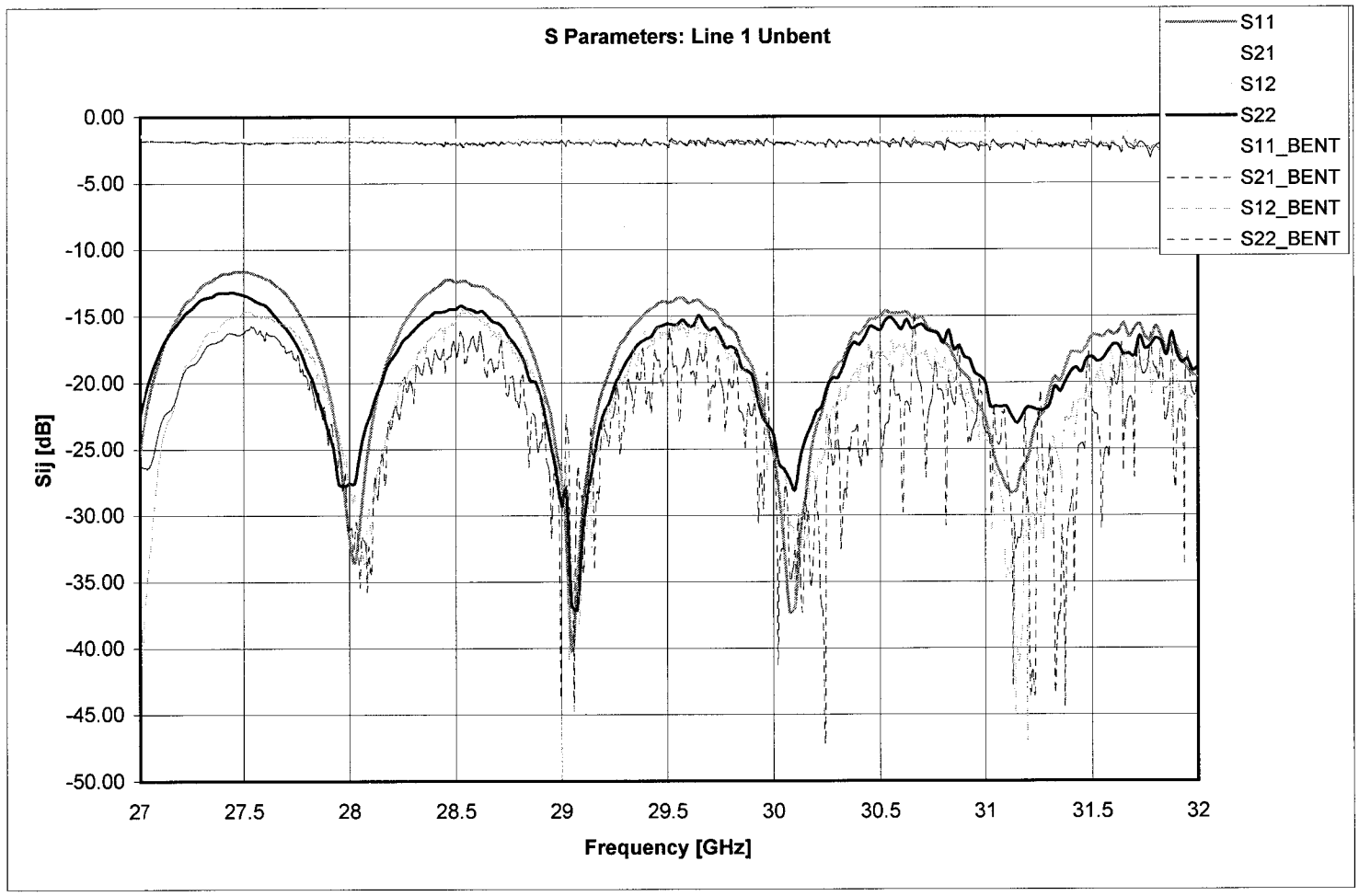

Figure 4.45: S-parameters for 0.5 inch bent line

4.3.4 Bent Array Implementation

Characterizing the six different bend radii, shows that even the tightest bend of 0.5" does not significantly degrade the performance of the microstrip line. In the final array implementation a 0.5" radius was therefore chosen. The array was bent using the same procedure as that used for the single 50 Ω line Duroid boards. The array after bending is shown in Figure 4.46.

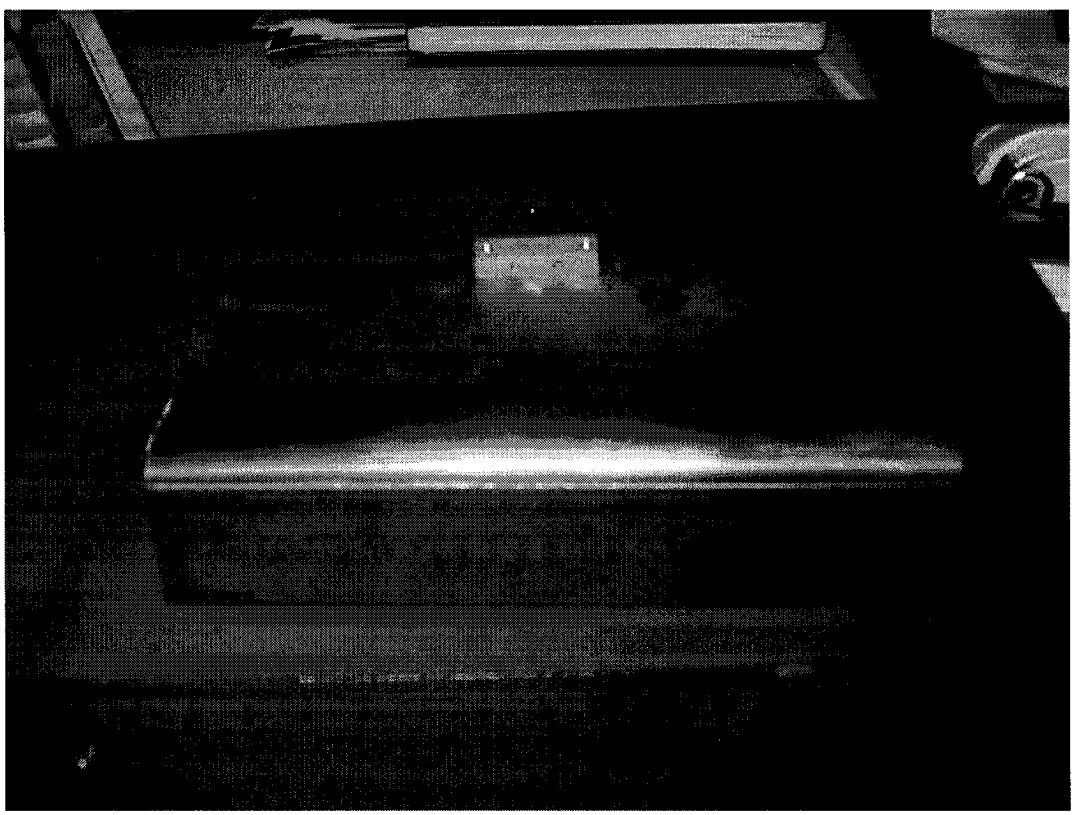

Figure 4.46: Bent array shown without attached heat sink

The bent array radiation patterns were re-measured and can be seen in the Figure 4.47.

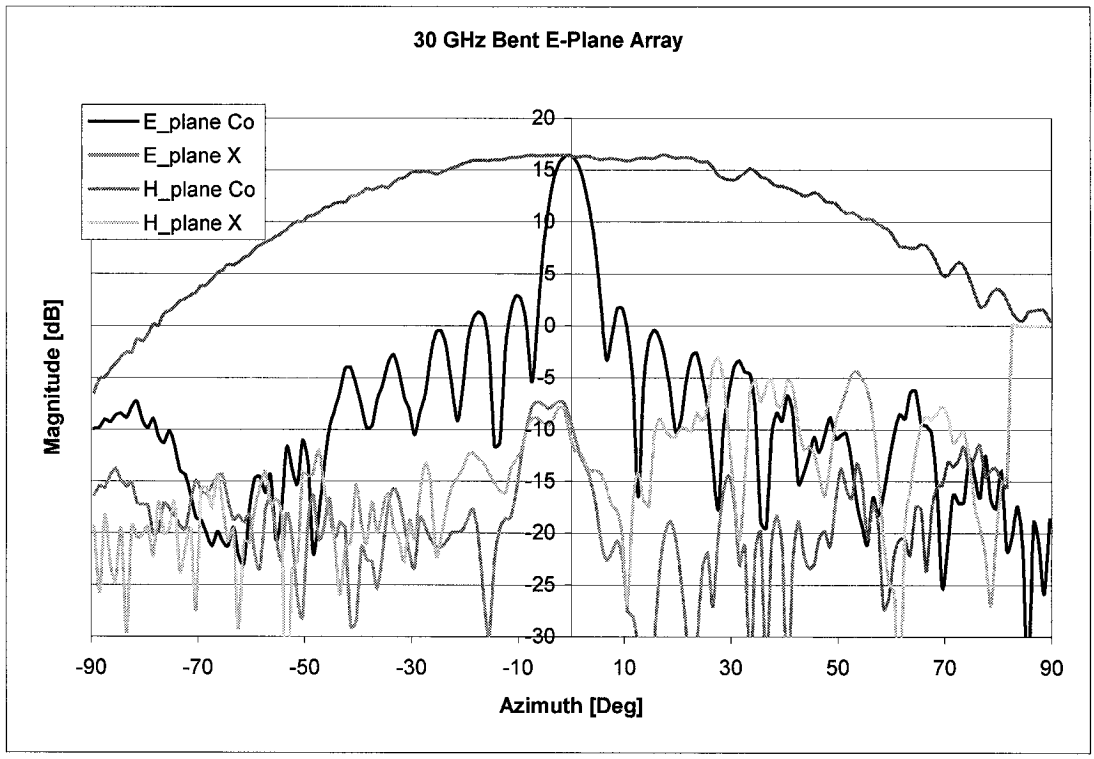

Figure 4.47: Measured gain for bent E-plane array

The gain of the bent array is 16.3dB with a maximum E-plane cross-pol of -8dB and an H-plane cross-pol of -2dB. The maximum ripple height is less than 1 dB.

4.3.5 Summary of Results from the Three Arrays

A comparison of the results obtained from the three different arrays can be seen in Table 4.7.

Table 4.7: Comparison of unbent and bent arrays

	Unbent Array [dB]	Unbent Array with Heat Sink [dB]	Bent Array with Heat Sink [dB]
Boresight gain	16.45	15.85	16.3
Average E-Plane Cross-pol levels	-17.57	-10.53	-19.35
Average H-Plane Cross-pol levels	-11.96	-13.94	-15.22
Maximum ripple height	2	4	<1

From the table above it is quite readily apparent that there is significant degradation of gain in the unbent array with a heat sink. This is obviously not desired. Bending the array while not completely restoring the gain of the array to the original levels brings back up to with in 0.45 dB to 16.3 dB.

According to the observations made it became quite apparent that the novel idea of bending the array is a very viable option. The initial step of checking the effect of bending on single 50Ω lines very quickly showed that for the radii checked there would be little if any effect on the characteristic impedance of the microstip line. This is essential as any change in the characteristic impedance could have an adverse effect on the power distribution over the array elements (Recall that impedance impacts the power splitters). Once an acceptable bend radius was found the array could be bent and the patterns for the array re-measured.

Comparison between the original array, the unbent array with a heat sink and the bent array with a heat sink showed quite promising results. The gain lost through interference by the heat sink is regained by bending. This in itself is of major importance to the array design especially when the gain is increased through the use of active elements. The second advantage of bending is that bending improves the cross-pol performance of the array as compared to the unbent case. This can be seen when comparing the average cross-pol levels in Table 4.7. Once again this is of major importance as high cross-pol levels result in wasted power and in the worst case can also result in unwanted feed back to the amplifiers thus causing oscillation. Finally the advantage of bending can be

seen in that the array pattern is smoothed out with the ripples reduced from 4 dB to less than 1dB

All in all the idea of mechanically shaping the array has reaped tremendous advantages for the design. A simple bending procedure ensures that the active elements of the array can be easily cooled using a heat sink, with little or no sacrifice to the electrical performance of the array. This simple method can potentially aid many active array designs where complex, cooling methods must be utilized to preserve the performance of an antenna.

4.4 Dual Frequency Arrays

EHF SATCOM terminals employ two frequencies one for the uplink (transmit) and another for downlink (receive). For commercial terminals, the two frequencies are 30 GHz and 20 GHz respectively. Up to this point the design has focused solely on the transmit 30GHz case as designs at higher frequencies are inherently more difficult. To realize an antenna array capable of working at both frequencies several options may be followed. The three most relevant to this work and considered in this section are the design a single patch that is dual frequency capable *[Maci97]*, the design a two element stacked patch structure *[Jame88]* and the design an interleaved array

Dual Frequency Capable Patches

This method relies on the use of a single aperture coupled patch with two orthogonal feeds, as shown in Figure 4.48. The design must carefully balance length and width of one patch as this reverses to become the width and length of the second patch (Conceptually as there is only patch). It offers significant

advantages in that it results in a compact antenna solution without the need for a frequency diplexer.

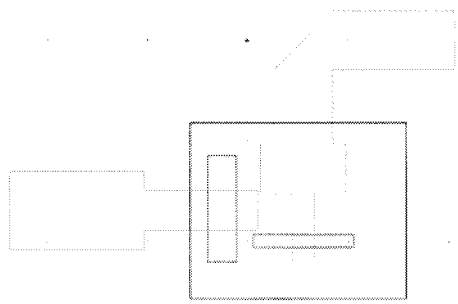

Figure 4.48: Dual frequency patch

The drawback of this approach however is that it is quite difficult to design due to the tight tolerance requirements. There is also significant cross-coupling between the feeds leading to poor transmit-receive isolation. The greatest drawback of this approach, for the application at hand, however is the fact that there is no easy way to make both patches radiate a circularly polarized wave. Circular polarization (CP) is essential as virtually all SATCOM application utilize CP waves.

Stacked Patch Structure

A stacked patch structure is one in which two patches are separated vertically as shown in Figure 4.49. One patch resonated at frequency f_1 while the other is sized to resonate at f_2.

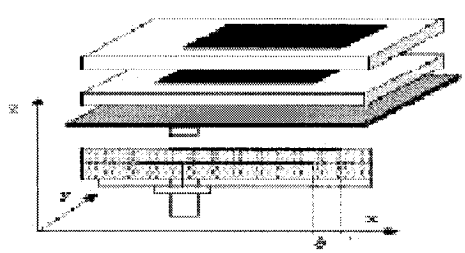

Figure 4.49: Stacked patches *[Jame88]*

The advantages of this approach are that it will result in a compact antenna and that circular polarization is possible. The disadvantages of this approach are that the frequency separation of the two patches must be large on the order of a factor of 10 making it ill-suited for the 20/30GHz frequency separation required.

Interleaved Arrays

Instead of stacking the patches vertically, the interleaved technique involves the separation of two patches horizontally as shown in Figure 4.50. The smaller patches operate at 30 GHz and the larger ones at 20 GHz.

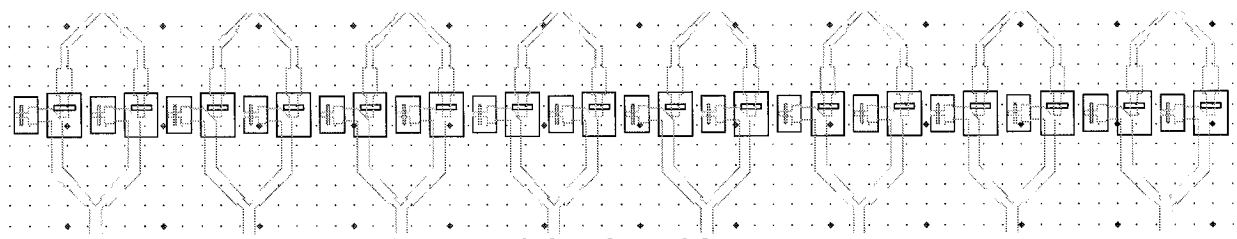

Figure 4.50: Interleaved Array

Some advantages of this approach are that circular polarization is possible as the individual elements operate at a single frequency, independent beam steering is possible, manufacturing tolerance requirements are not as stringent and any combination of frequencies can be accommodated.

The disadvantages of this approach are that a larger area is required for the antenna and the spacing between the elements of an individual array have to be made larger, reducing the maximum beam scan angle. To improve isolation one of the arrays is oriented so that it is an E-plane array and the other an H-plane array.

After considering the three dual frequency array options the interleaved array emerges as the best candidate and its design is pursued further. The array

is designed using linear polarized elements initially, and subsequently converted to circular polarization by suitably modifying the patch elements.

4.4.1 Interleaved Array

An interleaved array was designed and simulated using Ensemble. The main area of concern is the minimum spacing achievable between the elements of the two arrays. This is important, as a tight spacing is desired to maximize the scan range of the antenna. At the same time this, must be balanced against the increase in mutual coupling that would occur with the reduced spacing. In order to reduce simulation and design time for the structure (the full structure would contain 32 elements with 2 feeds) it was decided to halve the array to 8 elements each for transmit and receive. The half array would still give accurate enough performance metrics to ascertain the feasibility of the design. The simulated structure is shown in Figure 4.51.

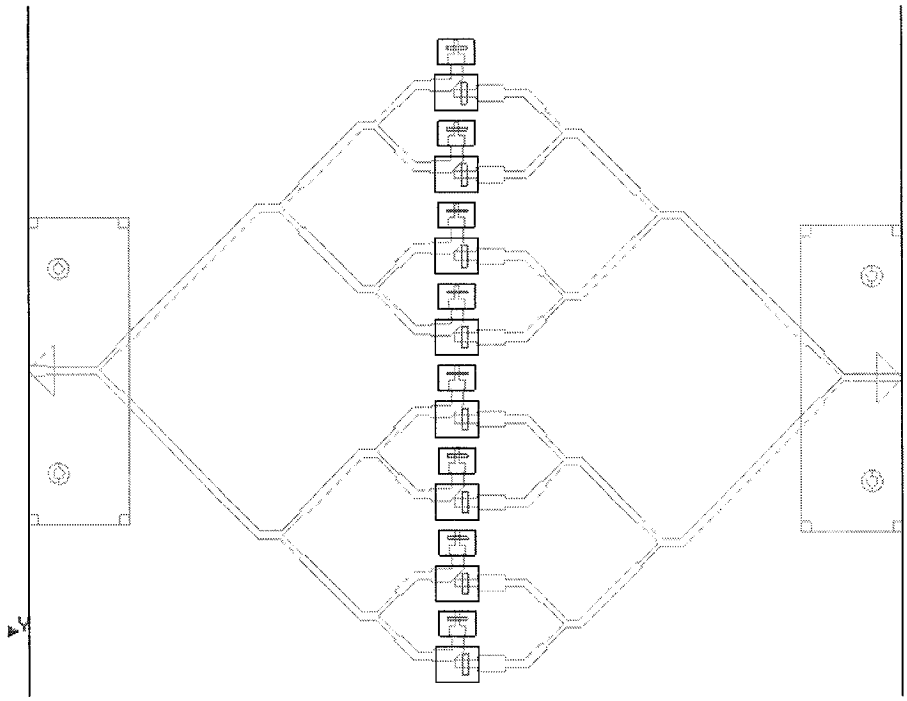

Figure 4.51: Simulated dual frequency array.

For the 30 GHz elements the patches were reused as designed in section 4.2. The same is the case for the equal division power splitters. The feed itself is redone to account for the new element spacing. The edge-to-edge spacing between adjacent patches is now 1 mm. This is the optimum spacing in terms of good isolation while maintaining a large scan range.

Figure 4.52, 4.53 and 4.54 are the results obtained from simulating the structure above. It is a combined sweep from 18 to 32 GHz. The optimum return loss is obtained for the two desired center frequencies of 20GHz and 30GHz. As well the cross coupling S21 between the two feeds is low enough to not be a major concern.

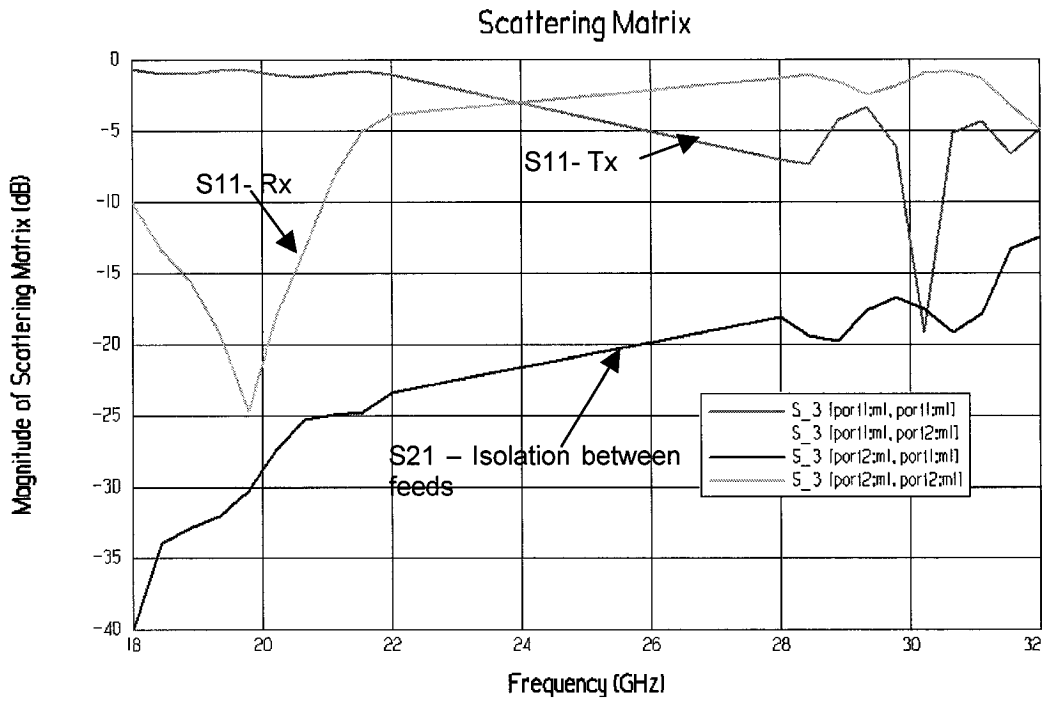

Figure 4.52: Return loss for both ports of interlaced array

Figures 4.53 and 4.54 show the gain obtained at each of the center frequencies.

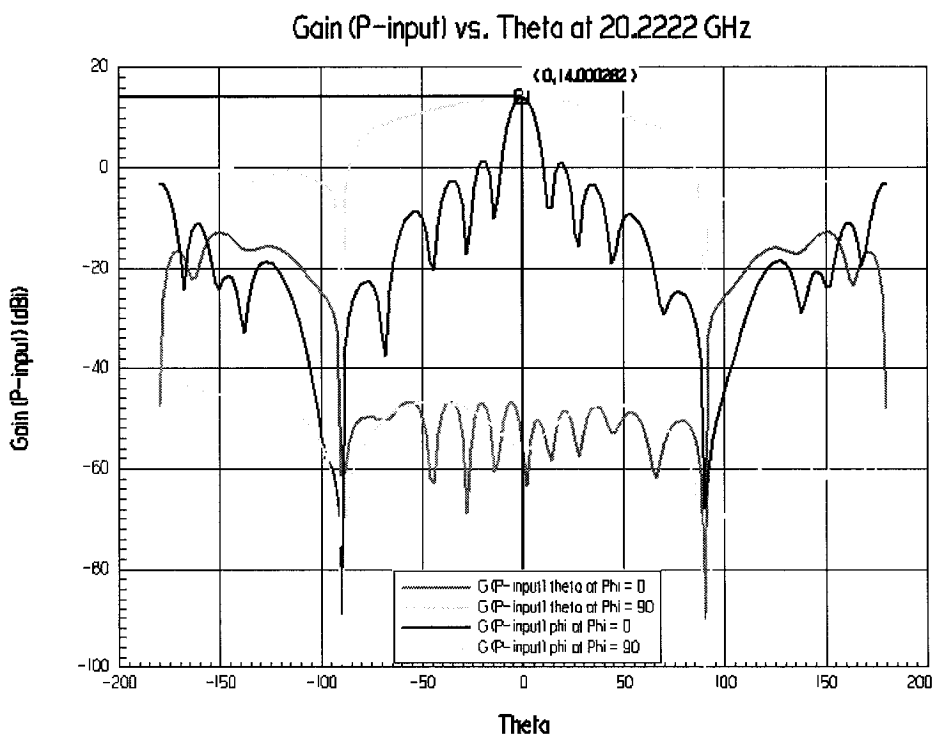

Figure 4.53: Gain of interleaved Array at 20GHz - Simulated

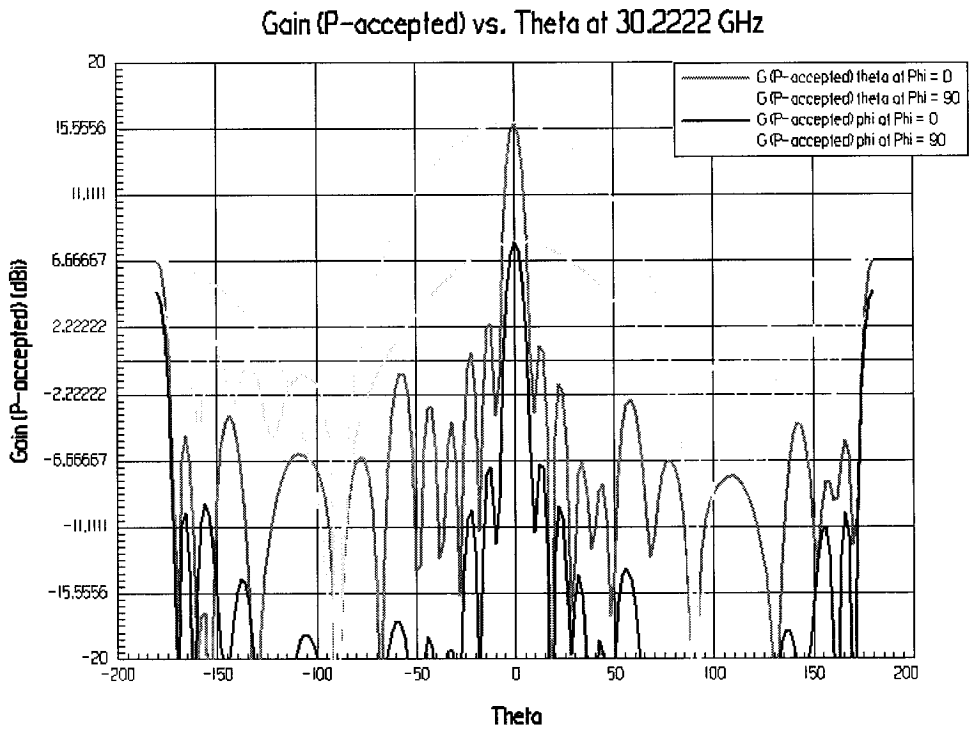

Figure 4.54: Gain of interleaved Array at 30GHz – Simulated

The simulated results look good. The array has a gain of 14 dB for the 20 GHz side and 15.55dB for the transmit side. This is as expected for an 8 element array. As indicated by Figure 4.52 the patches seem to resonate at the correct center frequencies. The return loss is -25 dB and -18 dB for the 20 and 30 GHz arrays respectively. As well for the spacing selected the isolation between arrays is below -15 dB for the entire band of operation.

4.4.2 Interleaved Array – Measured Results

The interleaved array that was fabricated is pictured in Figures 4.55 and 4.56.

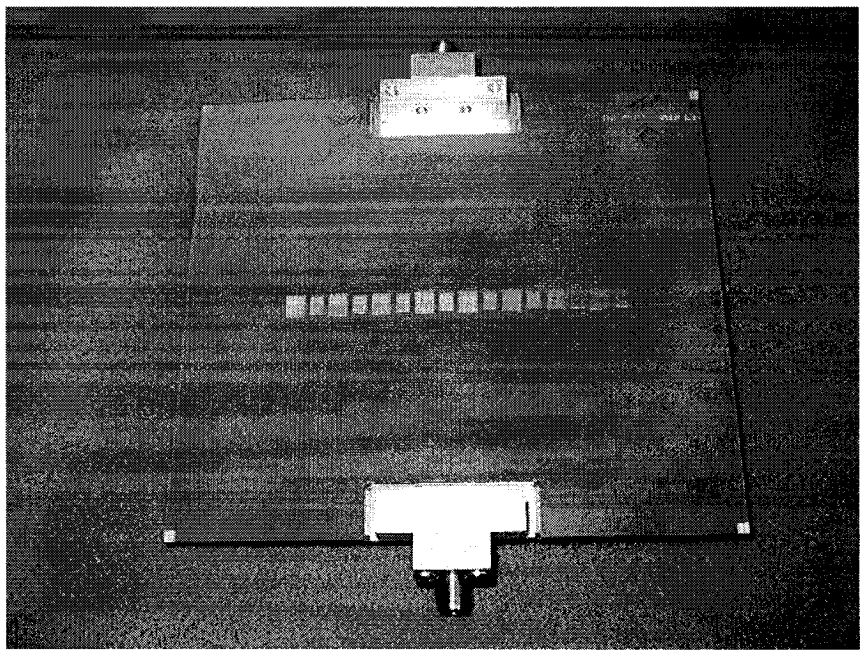

Figure 4.55: Interleaved array – Patch side view

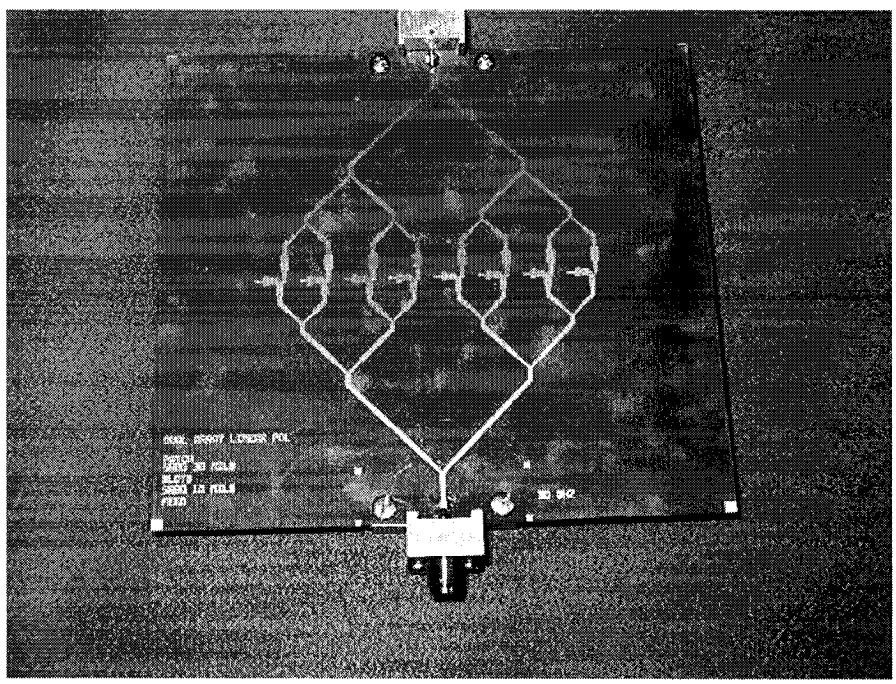

Figure 4.56: Interleaved array – Feed side view

The fabrication did not present an untoward difficulty. The feeds were quite close to each other but the minimum etchable distanced was maintained to prevent the feeds from fusing. As usual K-connectors were added to either side

Measured return loss and patterns for the interleaved array can be seen in Figures 4.57, 4.58 and 4.59.

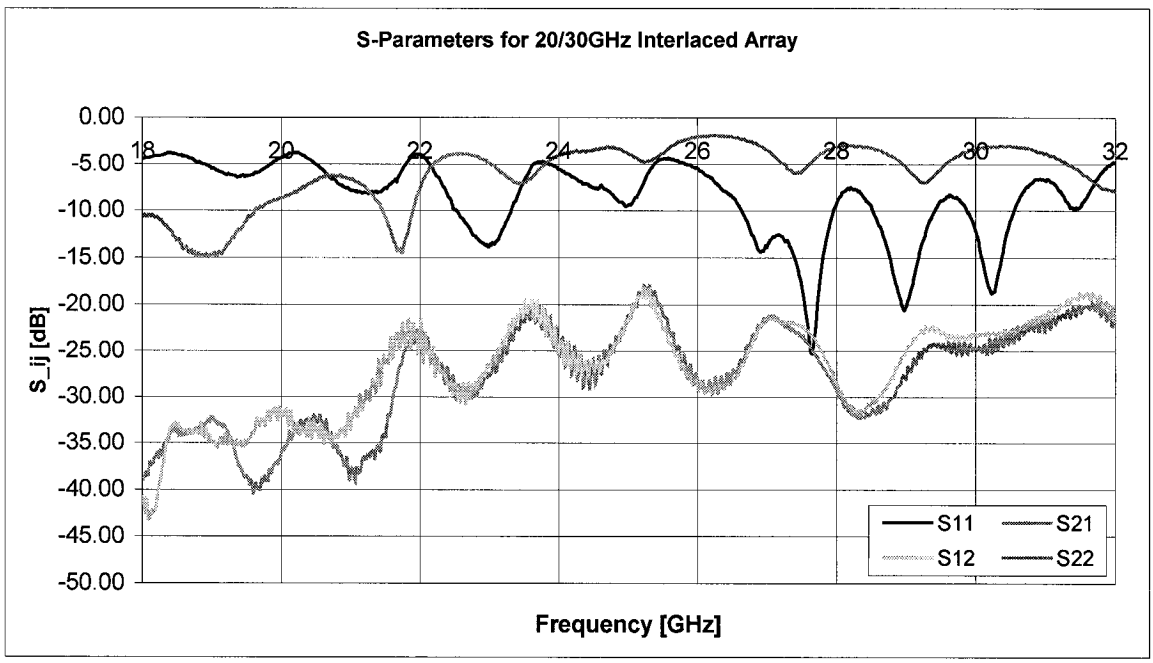

Figure 4.57: Return loss and isolation for interleaved array – Measured

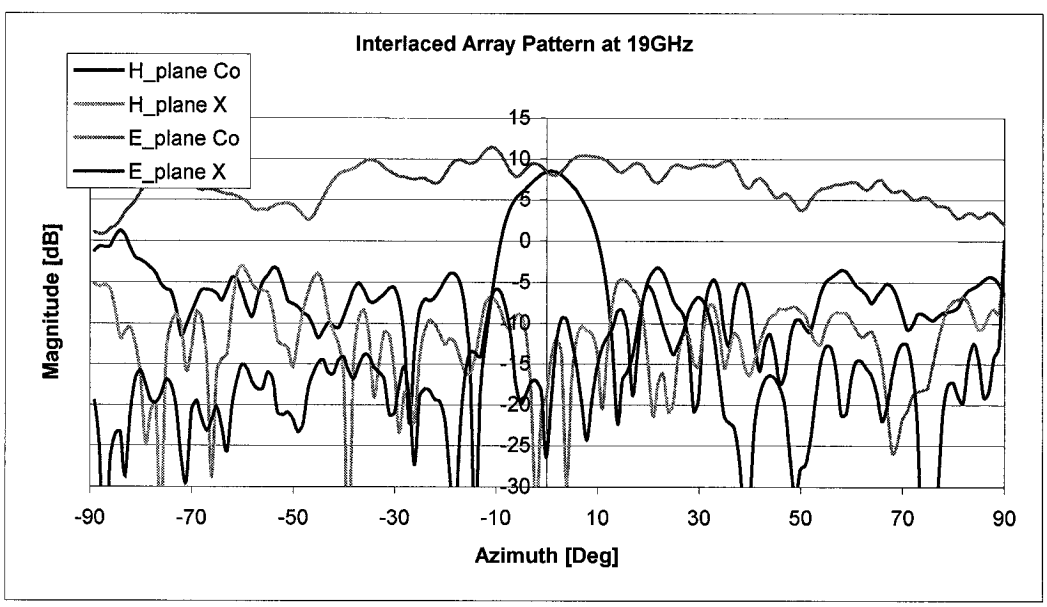

Figure 4.58: Gain for interleaved array, receive section – Measured

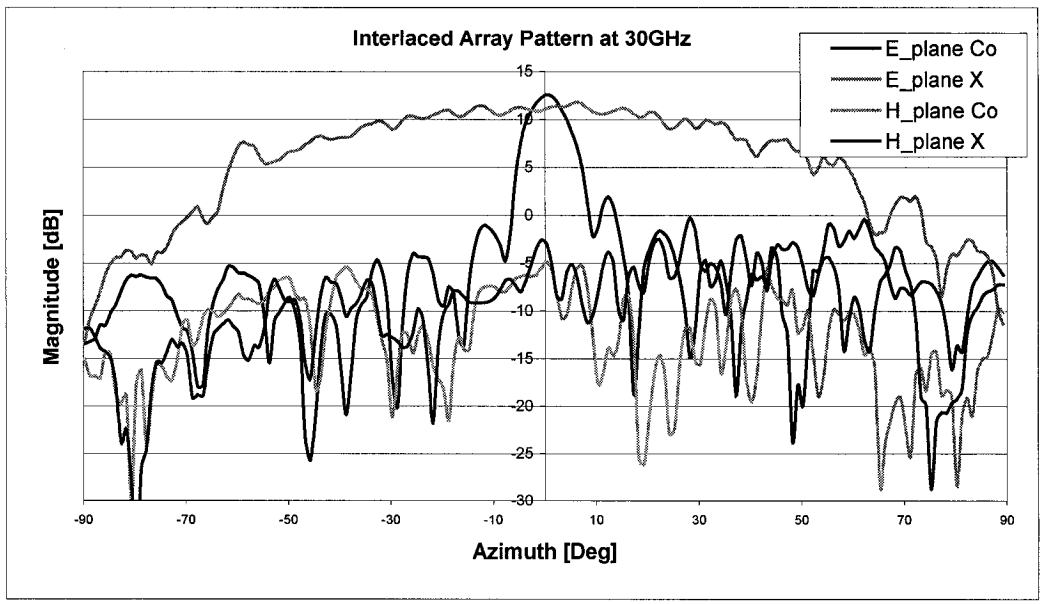

Figure 4.59: Gain for interleaved array, transmit section – Measured

The measured results were quite close to simulated values. The gain of the 30 GHz array is 12.46 dB while that of the 20 GHz array is 8.48 dB. The maximum cross pol levels are -4.89 dB and -4.02 dB for the 30 and 20 GHz arrays respectively

In conclusion, the half size interleaved array shows very promising results. The patch elements worked as expected i.e. appropriate gain was observed over the desired frequency bands. The 20 GHz array did not display best results at 20 GHz but instead at 19 GHz. This points to a flaw in some aspect of the feed network however is close enough to the frequency band of interest to show the promise of using such an array. The 20 GHz array has less gain than the 30GHz array because the elements of both arrays have the same physical (not electrical) spacing, as given by equation 2.18. The number of side lobes is 6, which is also consistent with array theory. The side lobe levels are at least 10dB below the main lobe, which is also a good result. All in all this approach to the design of the transmit and receive array for a SATCOM terminal is very viable.

4.5 Circularly Polarized Patch Antennas

Another important parameter for SATCOM applications is the polarization of the wave. In general SATCOM applications employ circular polarization (CP) as this enables the ground terminal to still receive some fraction of a signal even if the transmitted wave undergoes polarization transformation as it travels through the atmosphere. Due to this requirement the radiators used in any SATCOM application must be capable of supporting CP waves.

Microstrip antennas are primarily linear radiators. In order to obtain circular polarization it is necessary to excite the patch with two orthogonal modes with a 90^0 phase difference *[Bala82].* There are a number of methods to do this for a square microstrip patch *[Garg01].* One of the more common methods is to cut off two opposite corners of the patch, as seen in Figure 4.60 The truncated corner length is the parameter that must be adjusted in order to obtain a good axial ratio (AR) i.e. AR < 3dB.

Two individual CP patches are designed, one for 20 GHz and the second one for 30 GHz. As usual the designs were simulated first using Ensemble and then fabricated and measured. In addition to the basic parameters of return loss and gain there is also the added design goal of good axial ratio.

4.5.1 Circularly Polarized Patch Antennas – Simulated Results

Figure 4.60 presents the structures simulated. The dimensions of the CP patches are summarized in Table 4.8. From the simulation it was readily observed that the frequency for which best AR performance was obtained was

not the frequency at which the optimum return loss was observed. A tradeoff was therefore necessary and is shown by the results in Figures 4.61 to 4.64.

Table 4.8: CP patch dimensions

Patch Dimensions	L [mm]	W [mm]	Truncated corner length [mm]
20 GHz patch	4.47	4.47	1.414
30 GHz patch	3	3	1.131

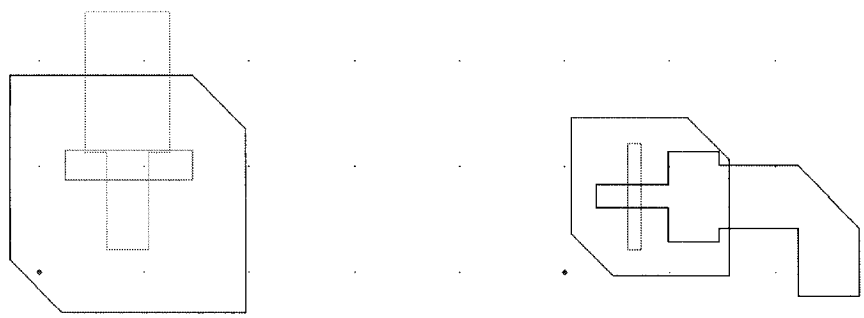

Figure 4.60: CP patches 20GHz and 30GHz

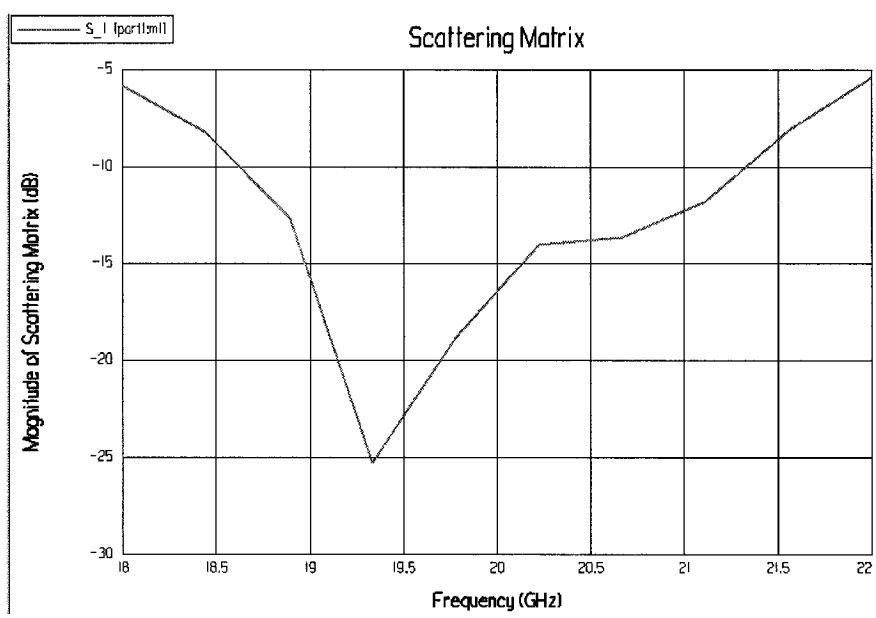

Figure 4.61: Return loss 20GHz CP patch – Simulated

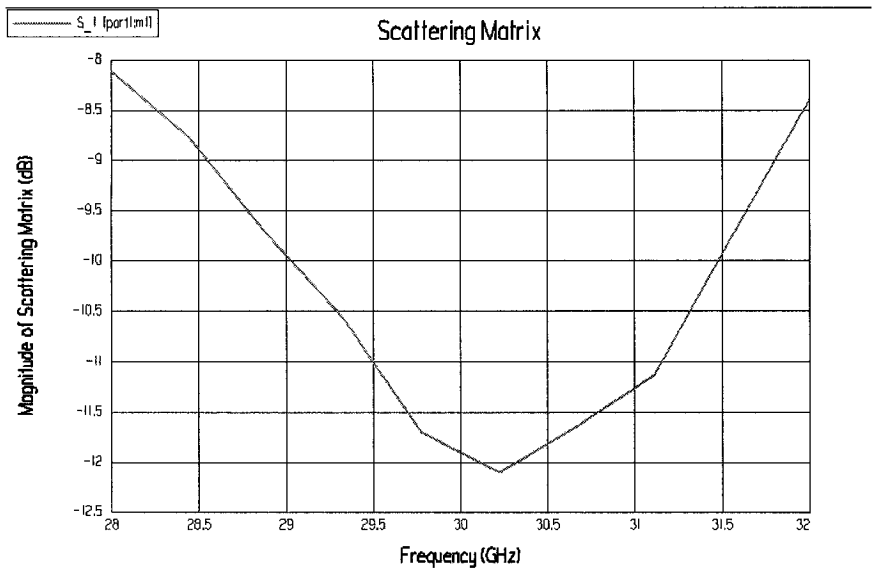

Figure 4.62: Return loss 30GHz CP patch - Simulated

The return loss observed for the two patches though not centered exactly at the required frequencies are enough to meet the matching requirements. The 20 GHz CP patch has a return loss of -17dB and the 30 GHz patch -11 dB. These high return loss values are part of the trade off that is required to center the best axial ratio around 20 and 30 GHz.

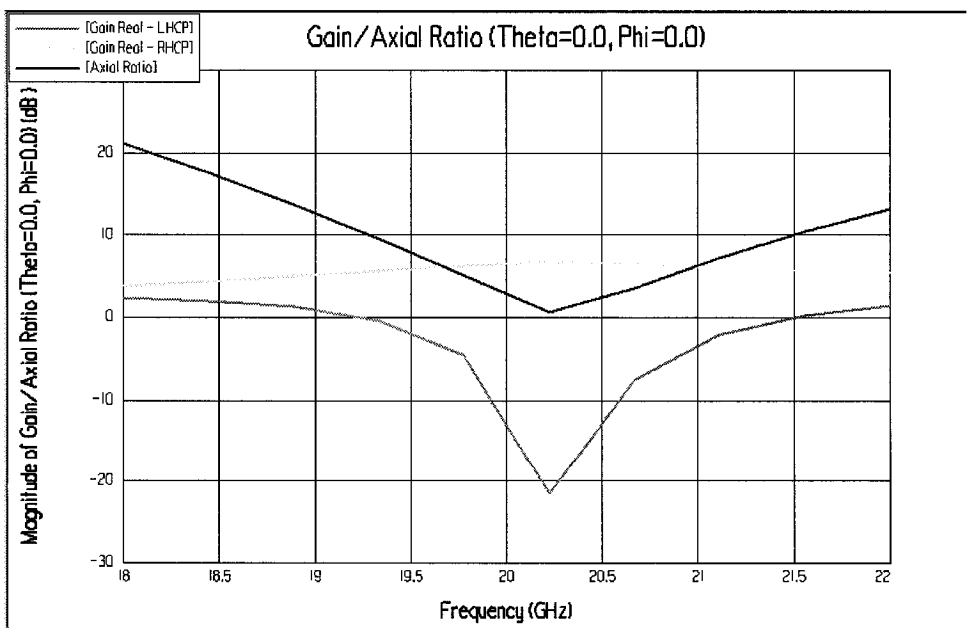

Figure 4.63: Gain and Axial ratio 20GHz CP patch - Simulated

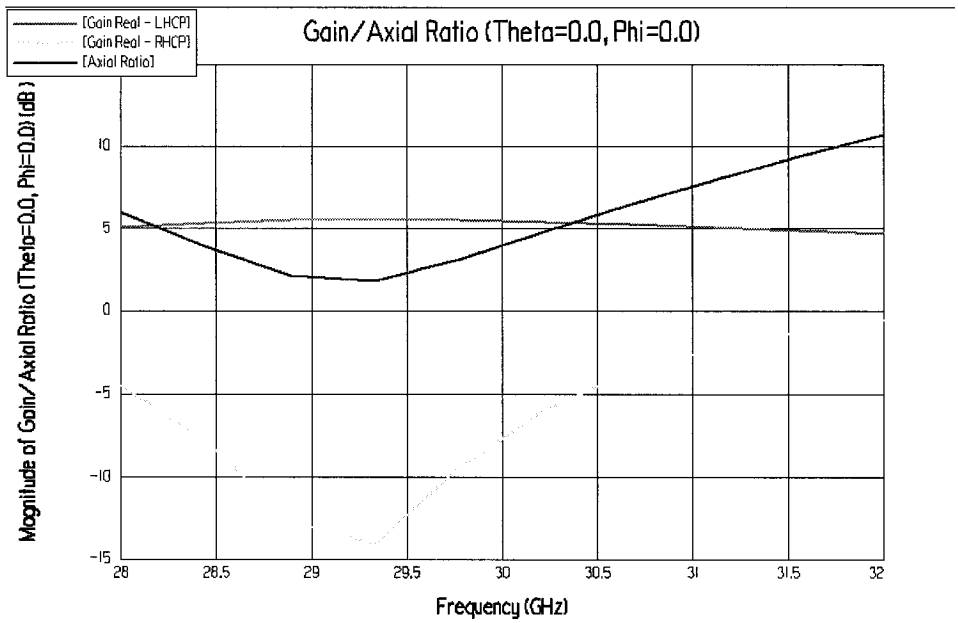

Figure 4.64: Gain and Axial ratio 30GHz CP patch - Simulated

The axial ratio simulated for the two structures is below the 3 dB required over a band of 0.5 GHz. This points to good circular polarization. Once again the best AR could not be centered exactly on the frequencies of operation. However as discussed before a compromise had to be made.

The simulations very clearly show the sense of polarization of the patches with the 20 GHz patch being LHCP and the 30 GHz one RHCP. This was purposely done in order to improve isolation when the patches are used for an interleaved array as discussed in section 4.5.3.

4.5.2 Circularly Polarized Patch Antennas – Measured Results

Fabrication of the patches was straightforward as there was no extensive feed network. The truncated corner length were also close to the desired values. Figures 4.65 and 4.66 show the two CP patches fabricated.

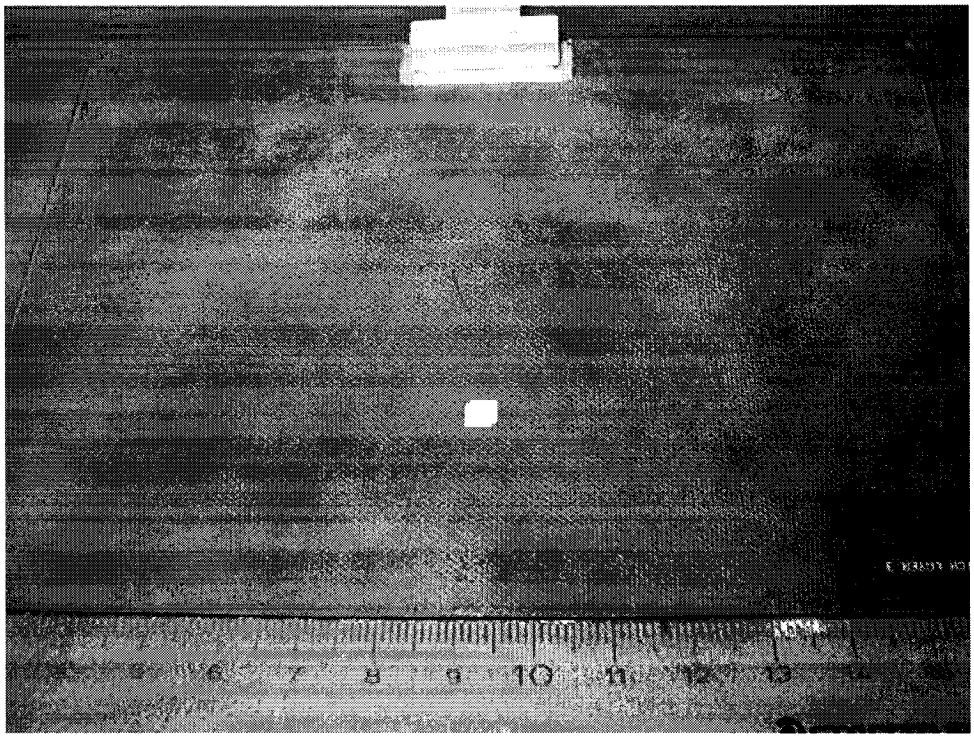

Figure 4.65: 20GHz CP patch

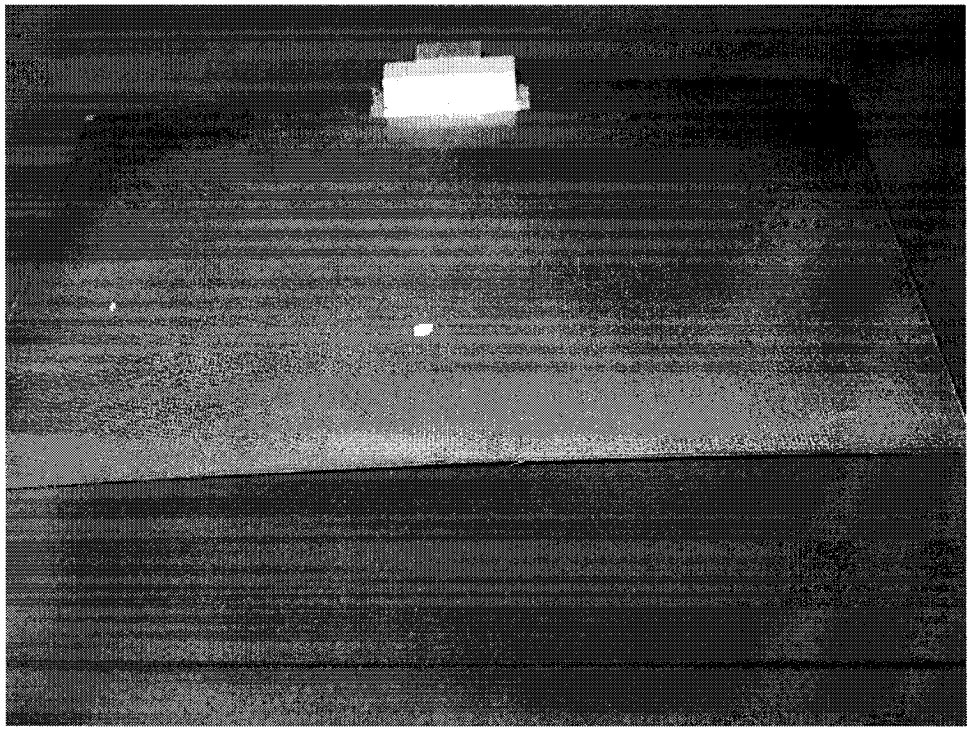

Figure 4.66: 30GHz CP patch

In order to measure the AR and gain of the CP patches a spinning linear test setup was used. Pattern measurements were made at 0^0,45^0 and 90^0

degrees of rotation to certify that the AR was constant over all planes. The return loss observed is shown in Figure 4.67 and 4.68 while the patterns are shown in Figures 4.69 and 4.70.

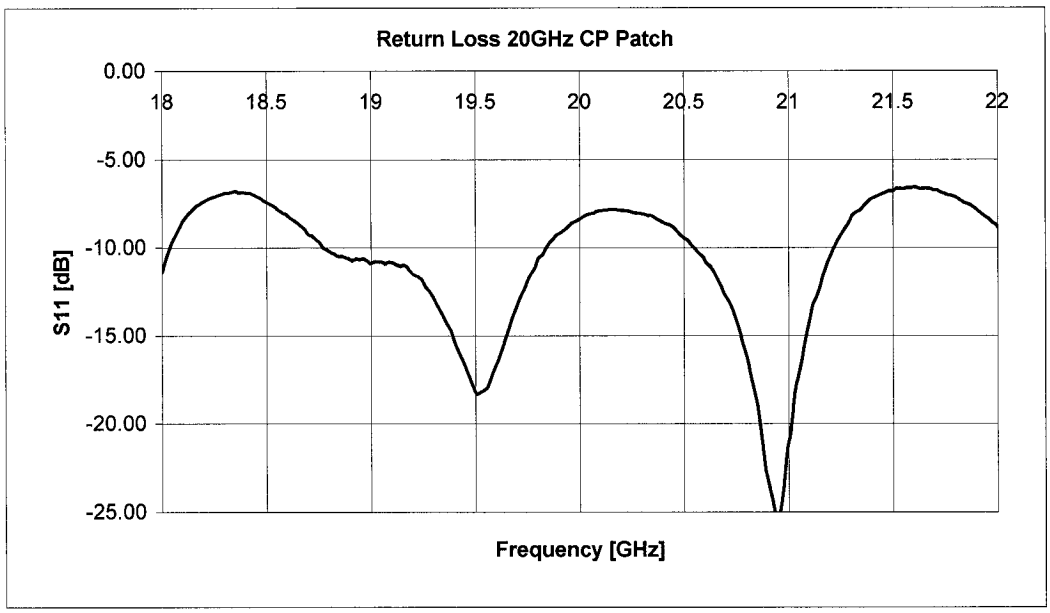

Figure 4.67:Return loss 30GHz CP patch - Measured

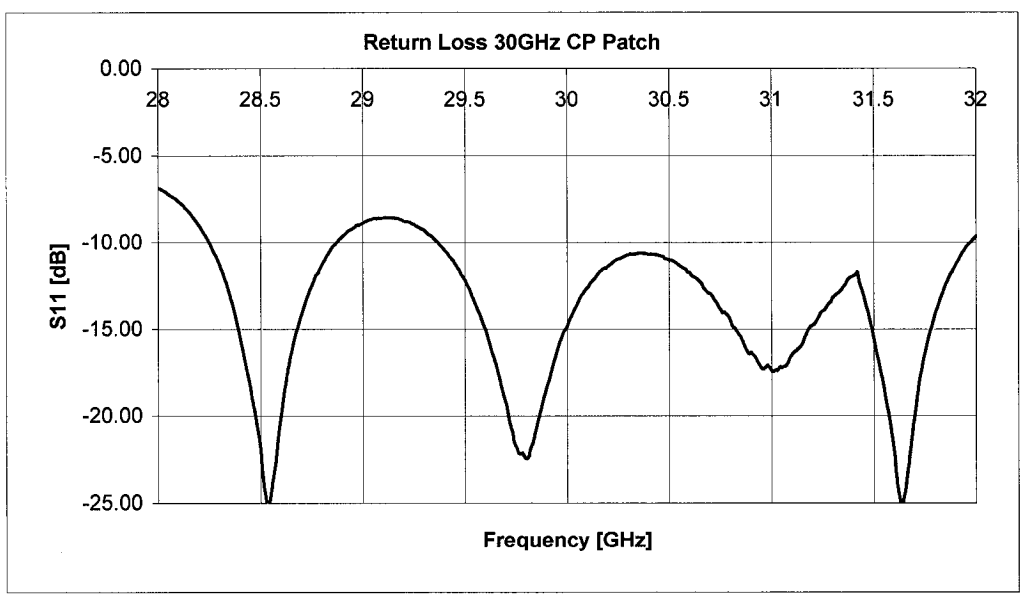

Figure 4.68: Return loss 30GHz CP patch - Measured

As was expected the patches resonated slightly off the center frequencies required. This it is hoped would be offset by the improved AR performance.

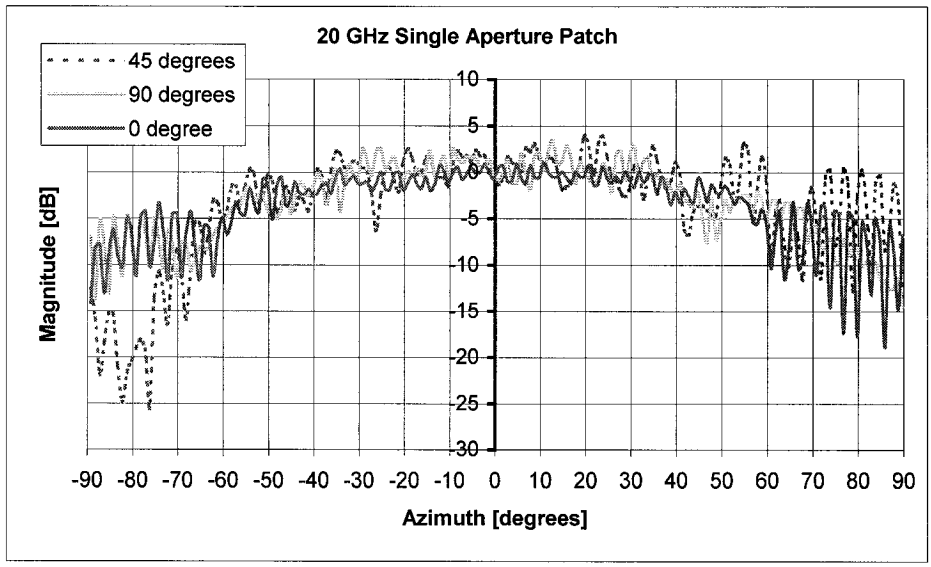

Figure 4.69: Gain and Axial ratio 20GHz CP patch - Measured

The axial ratio for the 20 GHz CP patch is 1.58dB which is better than the desired 3dB for angles $-10^0<\theta<10^0$(AR is measured by the depths of the ripples in the pattern. These ripples are caused by the fact that a linear transmit antenna that is being spun is utilized for testing as opposed to a circularly polarized standard antenna). The axial ratio is also consistent for the three planes measured.

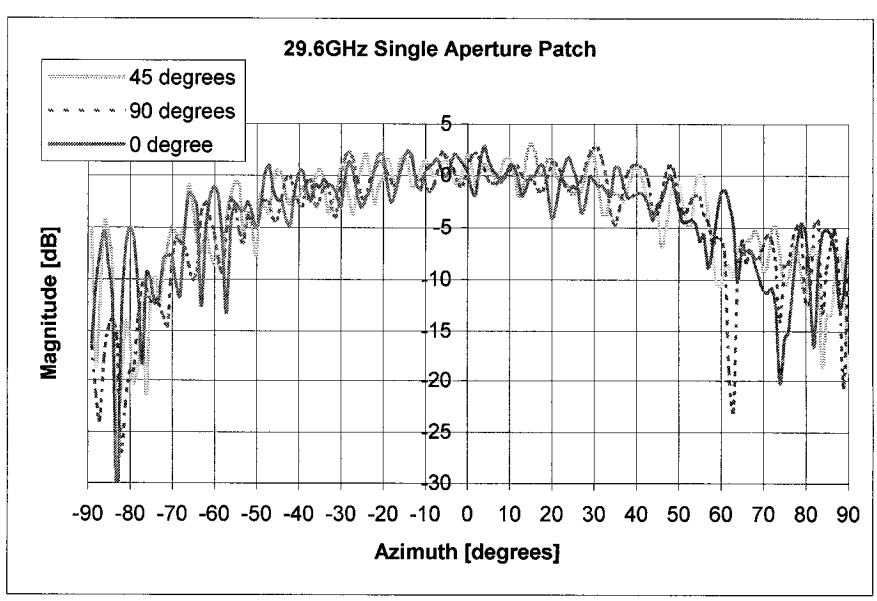

Figure 4.70: Gain and Axial ratio 30GHz CP patch - Measured

The axial ratio for the 30 GHz CP patch is measured to be 2.65dB which is better than the desired 3dB for angles $-10^0<\theta<10^0$. The axial ratio is consistent for the three planes measured.

There is one problem with the measured results. The patch seems to provide best AR performance not at the target frequency of 30GHz but at 29.6GHz. Although this is far from ideal the results are within the desired band of 500MHz offset from the center frequency. This issue was expected from simulations where it was observed that it was extremely difficult to obtain best AR at the same frequency as that where the best return loss was obtained

In order to correctly compare the simulated and measured values the gain of the CP patches must be corrected. This is mainly because a spinning linear test methodology was used as opposed to a true CP measurement *[Stou00]*. The corrected gain G_A for the two patches and the correction factor G_C are:

$$G_C = 20\log\left(\frac{1}{2}\left[1+10^{-AR/20}\right]\right)dB$$
$$G_A = G_0 + G_C + 3dBic \qquad \textbf{[4.4]}$$

Where G_0 is gain as measured from the spinning linear test, G_C is the gain correction factor and G_A is the gain of the CP patch

As an example for the 20GHz patch from the measured results the gain can be calculated to be:

$$G_C = 20\log\left(\frac{1}{2}\left[1+10^{-1.58/20}\right]\right)dB$$
$$G_A = 1.35dB + -0.75 + 3dBic \qquad \textbf{[4.5]}$$
$$G_A = 3.6dB$$

Similarly for the 30GHz patch G_A = 4.738dB

A comparison of simulated and measured Results for CP Patches can be seen in Tables 4.9 and 4.10.

Table 4.9: Simulated vs. measured results for 20GHz CP patch

	Simulated	Measured	Δ
0^0 cut	5.72dB	3.6dB	2.12dB
Return Loss	-17dB	-18dB	1dB
AR <3dB bandwidth	0.9GHz	0.4	0.5GHz

Table 4.10: Simulated vs. measured results for 30GHz CP patch

	Simulated	Measured	Δ
0^0 cut	5.4dB	4.738 dB	0.662dB
Return Loss	-11.8dB	-15dB	4dB
AR <3dB bandwidth	1.5GHz	0.6GHz	0.9 GHz

The simulated results agree satisfactorily with the measured results. There is some discrepancy but it is well within expected values.

4.5.3 Circularly Polarized – Dual Frequency Array

With the basic elements designed all that remains is to mate the dual frequency linear array with the CP patch elements designed. This will result in a design that would be capable of receiving at 20 GHz and transmitting at 30 GHz simultaneously while supporting CP waves. However a paucity of high frequency material, as well as time meant that this aspect of the design was not completed. This work can easily be carried out in any future design iterations as all the basic building blocks i.e. the CP radiating elements at both frequencies as well as appropriate feed networks exist. The design work that remains is the mating of the CP radiating elements to the interleaved feed with appropriate matching. The important thing to note is that by using all the ideas presented above a fully capable passive array for a SATCOM terminal can be built.

4.6 Conclusion – Passive Design

Multiple linear array configurations are investigated over the course of this chapter, in an aim to satisfy the requirements for a SATCOM terminal. In summary the evolution of the design from a planar array to a linear array and lens configuration is examined. The refinement of this concept is aimed at eliminating the reflector and duplicating its beam pattern, using alternate means.

To satisfy the beam requirements a surface fed linear array is initially examined. A single element is first characterized followed by a 16-element array. It is seen that the surface fed array displays significant distortion in it principal beams. To eliminate distortion an aperture fed patch is then developed. After characterizing a single aperture fed patch, the patch is used in a 16 -element array. In order to further smooth out the pattern an E-plane array is used instead of an H-plane array.

The next sequence of the design involves the characterization of the effects of bending Duroid board. This is done to eliminate distortion that can occur due to the use of heat sinks for cooling the active elements that are further discussed in Chapter 5.

Finally the passive design switches focus from designing solely at the transmit frequency of 30 GHz, to designs at the receive frequency of 20 GHz as well. Additionally circular polarization capable patch elements are also examined in an effort to convert the linear polarized array to a CP array.

In conclusion the linear array passive design has been well characterized and is now suitable for integration with active elements.

CHAPTER 5

LINEAR ARRAY ARCHITECTURE – ACTIVE DESIGN

Active elements such as phase shifters and amplifiers may be integrated with antennas to increase the functionality of the array. As a final objective of this design, MMIC amplifiers are integrated with the passive array discussed in the previous chapter, in order to increase the EIRP and gain of the antenna. For the array under consideration, power amplifiers are added to the transmit section only whereas the integration of LNA's into the receive section is left as further work. This is mainly done to help demonstrate the validity of spatial power combining techniques without unduly complicating the design.

This chapter presents the selection of the MMIC amplifier and the number and location of the active devices in the array. Measurements of the integrated array are also presented. The measurements shown are first with the active array only and then with the subsequent addition of the linear 1-D lens for beam shaping.

5.1 Amplifier Selection and Performance Characterization

Several factors must be taken into account in order to select the correct amplifier for the application at hand including gain, bandwidth, DC power consumption, efficiency, input and output return losses, area and cost. Seven EHF band amplifiers were analyzed to determine the most suitable amplifier and Table 5.1 summarizes these key characteristics.

Table 5.1: Amplifiers evaluated for the project

Part No. *	Freq [GHz]	Gain [dB]	P1dB [dBm]	DC Power [W]	S11@29GHz [dB]	S22@29GHz [dB]	Chip Dimensions LxW [mm]		Area [mm2]	Price [U$]
RMPA29200	29-31	17	33	7.5	-12	-10	4	2.98	11.92	126
TGA-1172	27-32	18	29	3.78	-12	-12	2.69	1.37	3.69	95
TGA4509-EPU	27-32	22	30	2.52	-12	-10	2.4	1.2	2.88	40
RMPA29000	27-30	23	30	3.5	-10	-10	5.2	2.95	15.34	92
TGA4501-SCC	24-31	23	34.5	12.6	-8	-12	4.3	3	12.90	110
TGA-9070-SCC	23-29	23	30	2.8	-10	-12	4.1	3	12.30	153
TGA-1073B-SCC	27-32	25	28.5	2.94	-10	-15	3.12	2.15	6.71	64
RMPA29300	27-32	22	34	8	-6	-6	4.53	4.18	18.94	N/A
RMPA29400	27-32	25	35	8			4.73	3.42	16.18	N/A
RMDA1840	18-40	22	23	2.2	-15	-10	4.67	2	9.34	55
RMDA20420	20-42	22	23	1.26	-20	-8	1.72	0.76	1.31	31
TGA1073A-SCC	26-34	19	25	1.32	-10	-12	1.95	1.15	2.24	30
TGA-1193	27-32	18	31.5	7.56	-12	-12			0.00	178
TGA9070-SCC	23-29	23	30	2.8	-5	-12	4.1	3	12.30	97
TGA4513-EPU	27-32	32	32	6.72	-14	-14	2.8	2.2	6.16	88
TGA4901-EPU	25-31	34.8	34.8	13.2	-8	-12	13.34	9.6	128.06	N/A

**Note: All part numbers with prefix R are Raytheon and T are Triquint*

A tradeoff study was carried out for the various amplifiers to determine which amplifier best suited the requirements at hand. A numerical tradeoff study was used to assign a weighting factor to the different amplifier parameters in order to better quantify the relative merits of each amplifier. The factors were ranked as follows: cost, gain, power, PAE, area, P_{1dB} and return loss. This analysis made it abundantly clear that the **TGA4509-EPU** was best-suited amplifier for this array.

5.1.1 Amplifier Measured Performance

The TGA4509-EPU amplifier was measured to ensure that its performance agreed with the manufacturers specifications. There is some degradation compared to the specifications, as the MMIC amplifier is placed in a chip carrier that is more suitable for integration with the array. The S-parameters for the TGA4509-EPU amplifier in a chip carrier are shown in Figure 5.1. Appendix D1 presents detailed chip carrier drawings.

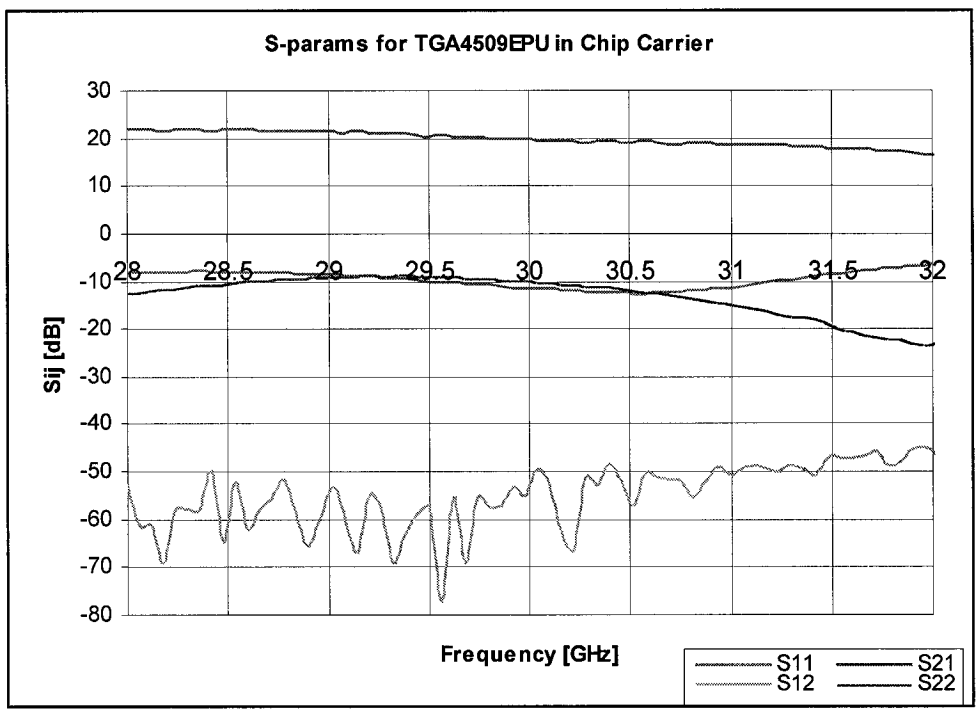

Figure 5.1: S-param for TGA4509EPU in chip carrier

5.2 Amplifier and Array Integration

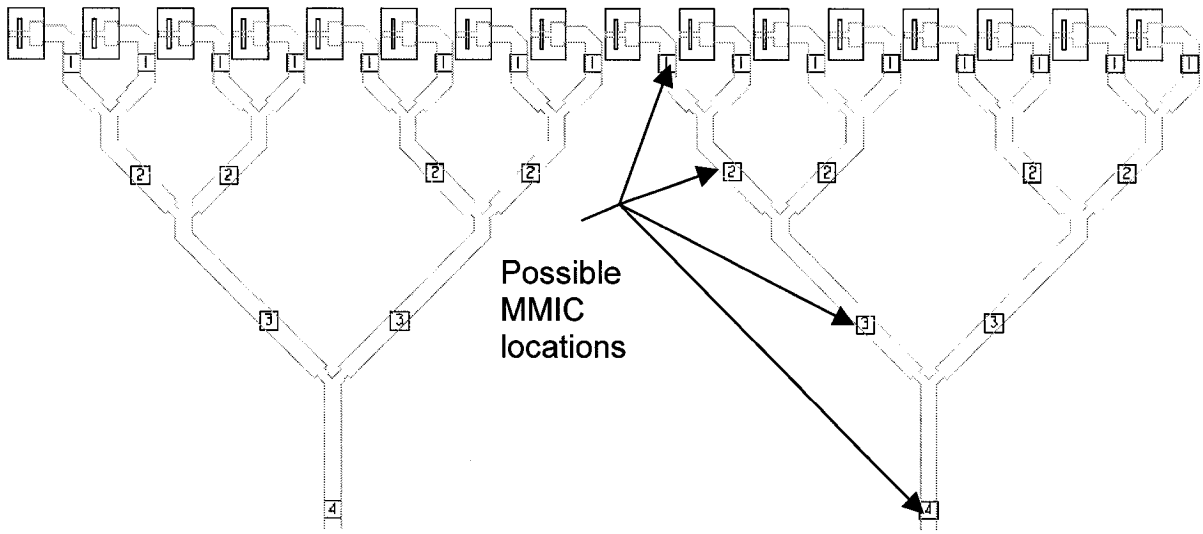

Figure 5.2: Potential amplifier locations

After deciding on the active device to be used, the number and position of the amplifiers must be determined. Figure 5.2 shows potential placement points for the active elements. Four major configurations are possible, which could also be mixed to yield other combinations. Keeping these parameters in mind, and using the amplifier selected in the previous section as the unit device, Table 5.2 presents possible results, which meet or surpass the minimum EIRP requirement of 45 dBm. This requirement is based on comparable Ka-band space combiners e.g. Lockheed Martin Ka-band array *[Harv00]*.

Table 5.2: Amplifier placement configurations

Configuration	Number of Amplifiers	Cost [U$]	Output power [dBm]	EIRP	DC Power [W]
1	16	640	42.04	58.04	40.32
2	8	320	39.03	55.04	20.16
3	4	160	36.02	52.04	10.08
4	2	80	33.01	49.04	5.04

The above calculations are done on the premise that the nominal antenna gain of the passive array is 16 dB and that the amplifiers have an output power of 30 dBm with operation at an input backoff of 1dB. However EIRP alone is not the deciding factor. Other mitigating factors that will affect amplifier selection and will have to be traded off with EIRP to set the number and location of the amplifiers include:

- Cost – The more amplifiers used the higher the cost of the array.
- Thermal issues – The amplifiers generate considerable heat. Thermal management will be an issue and the number of amplifiers employed will be limited by the effectiveness of the heat dissipation mechanism used.
- Integration – The mechanical complexity increases with increasing number of amplifiers, although this factor is difficult to quantify.
- Cross Coupling – With a large number of amplifiers in close proximity there remains a danger of the output of one amplifier coupling into the input of another, thus causing oscillation.
- Area – In most designs this would be an issue, but since the feed for the array is relatively spread out, the chip carriers can easily be accommodated. Therefore this factor is not a major concern

Based on these selection criteria, configuration 3 (4-amplifier configurations) meets the minimum required EIRP of 45 dBm. Configuration 4 (2-amplifier configuration) also works, but factoring in effects such as line and connector losses make it marginal. The four-amplifier configuration is economical

and reduces the complexity and time associated with assembling an array with a larger number of amplifiers. As well, the amplifiers have a relatively large interspacing, thus reducing the risk of feedback and oscillation.

5.3 Active Array – Two Element Prototype Design

Although the final design is to contain four-amplifiers, the active array was initially built in an intermediate configuration consisting of a prototype 2-element array with just a single amplifier. This was mainly done as a risk-mitigating step. By designing the smaller and simpler array, issues such as the design of an adequate DC bias network and correct grounding to prevent feedback and oscillation in the system could be implemented and validated. As well any manufacturing difficulties could be more easily remedied without sacrificing a large number of devices.

To correctly ground and isolate the RF and DC paths the cross section shown in Figure 5.3 is proposed. The corresponding layout is shown in Figure 5.4. The entire board is perforated extensively with vias between the metallic heat sinks and the sandwiched ground plane, thus ensuring proper grounding. Adequate spacing is also provided for the chip carrier. Decoupling capacitors are added to prevent DC leakage into the RF lines and a potentiometer is inserted to individually control the amplifier gate voltage. Finally the chip carrier is mounted on a brass pedestal to ensure proper contact with the heat sink for good thermal dissipation.

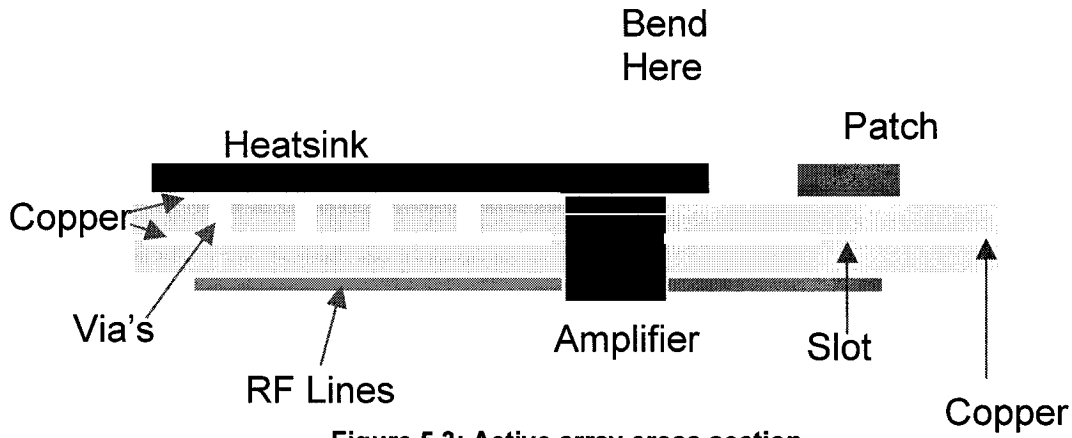

Figure 5.3: Active array cross section

In terms of the microwave design, the amplifiers S-parameters from section 5.1.1 were modeled as "black-boxes" in Ensemble and individual pieces of the feed were designed. The feeds were separately matched at the output and input of the amplifier, as can be seen by the matching stubs in the prototype layout of Figure 5.4.

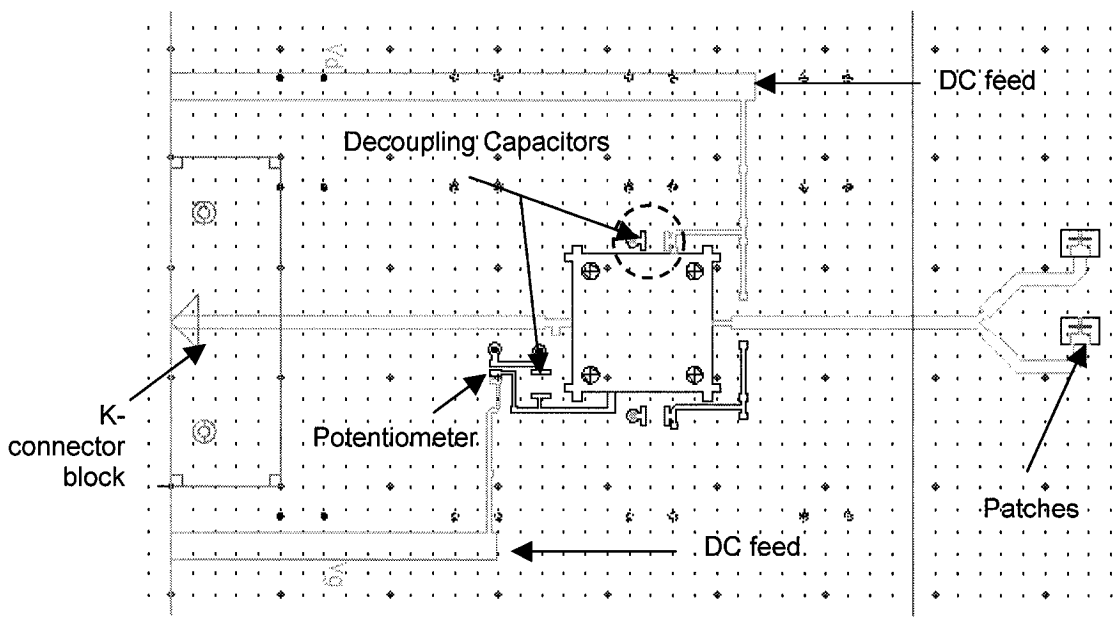

Figure 5.4: 2-Element prototype active array layout

The layout shown in Figure 5.4 above was fabricated. Figure 5.5 is a picture of the feed side of 2-element active array and Figure 5.6 of the patch

side. The chip carrier is clearly visible as well as the decoupling capacitors and potentiometer. For detailed mechanical drawings see Appendix D2

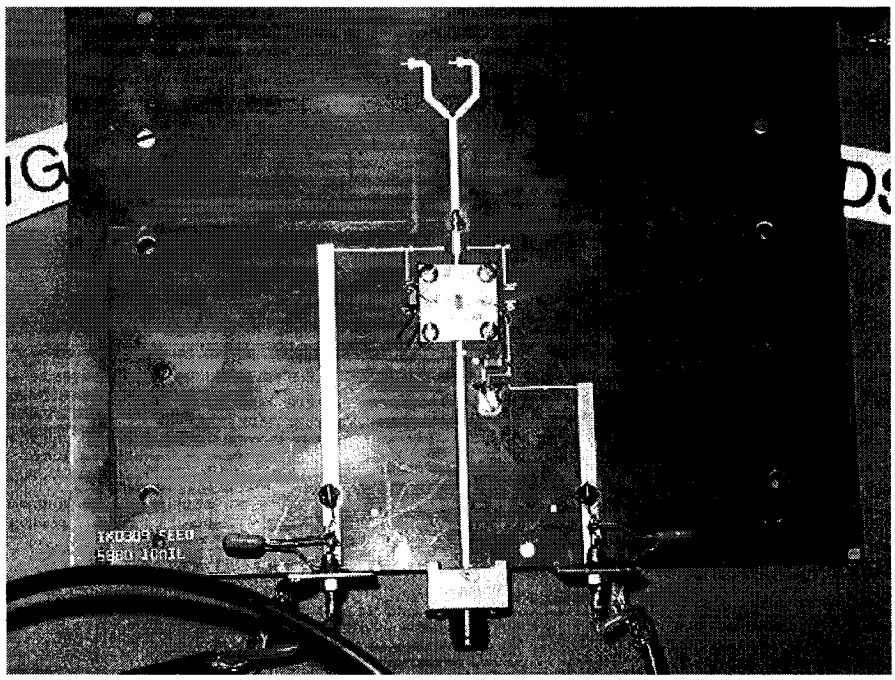

Figure 5.5: 2-Element prototype active array – Feed side

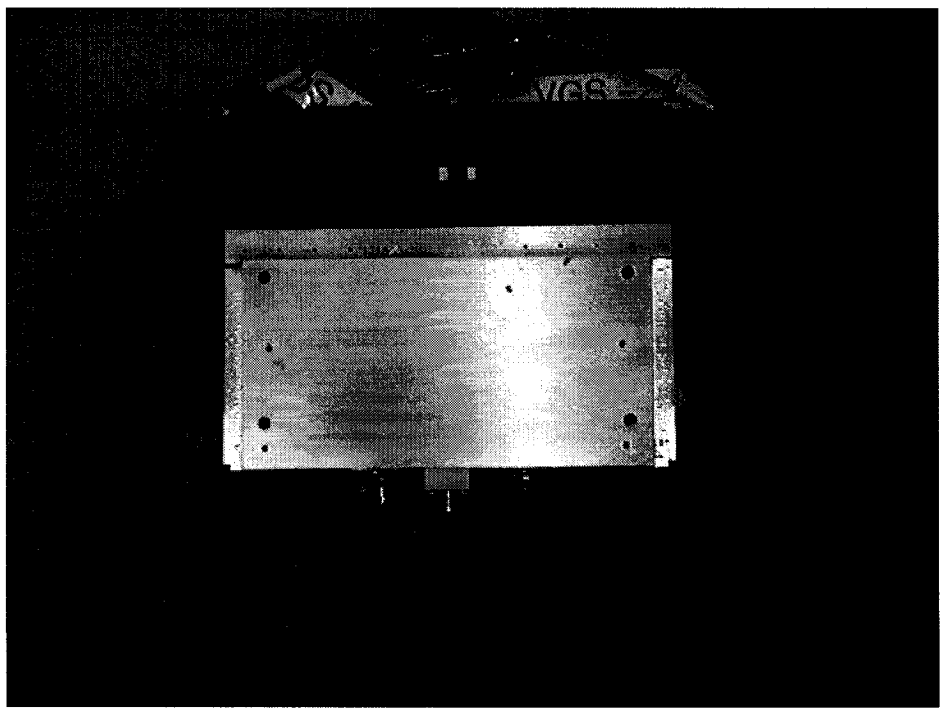

Figure 5.6: 2-Element prototype active array – Feed side

5.3.1 Gain for Two Element Active Array – Measured

The two-element prototype was tested in an anechoic chamber and the radiation pattern shown in Figure 5.7 is observed.

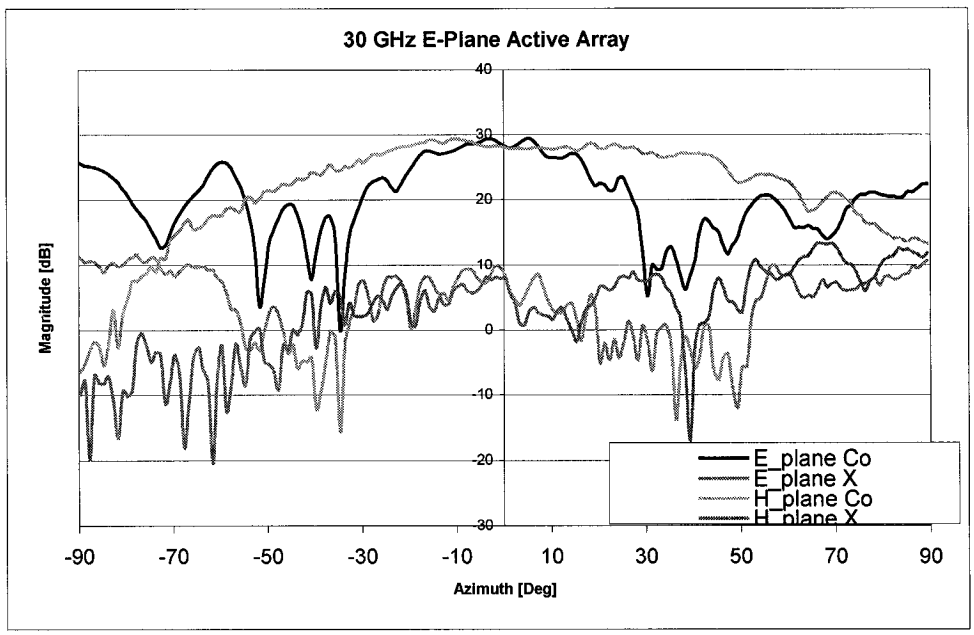

Figure 5.7: Gain of two element active array

The gain of the array was measured to be 27.85dB with cross-pol levels at 10dB and 13.29dB in the E and H-plane respectively. The two-element prototype successfully demonstrated the functionality of the active array. The gain is expected to be:

Amplifier gain (see Section 5.1.1)	20 dB
Single patch gain (see Section 4.2.1)	4.81 dB
Array factor gain (see Equation 2.18)	3dB
Expected gain	**27.81dB**

The expected gain agrees very favorably to the measured gain of 27.85dB. The patterns are as expected for a two element array with low ripples, some focusing in the E-plane and a broad pattern in the H-plane.

Overall the main aim of increasing the gain of the antenna was achieved. The antenna displayed significant gain for the number of elements present. The output power from each of the radiating elements, combined in free space as desired, to significantly boost the antenna gain. The success of this prototype is a good stepping-stone to the full 16-element design.

5.4 Active Array – 16 Element Final Design

After characterizing the performance of the two-element prototype, the design shifted to the full 16-element array. Manufacturing challenges encountered in the prototype design were rectified and the full array was fabricated. As before the cross section of the array remained similar to that seen in Figure 5.3. Figure 5.8 is the layout of the 16-element active array. For the 16-element array four amplifiers were utilized or 1 amplifier per 4 radiating elements.

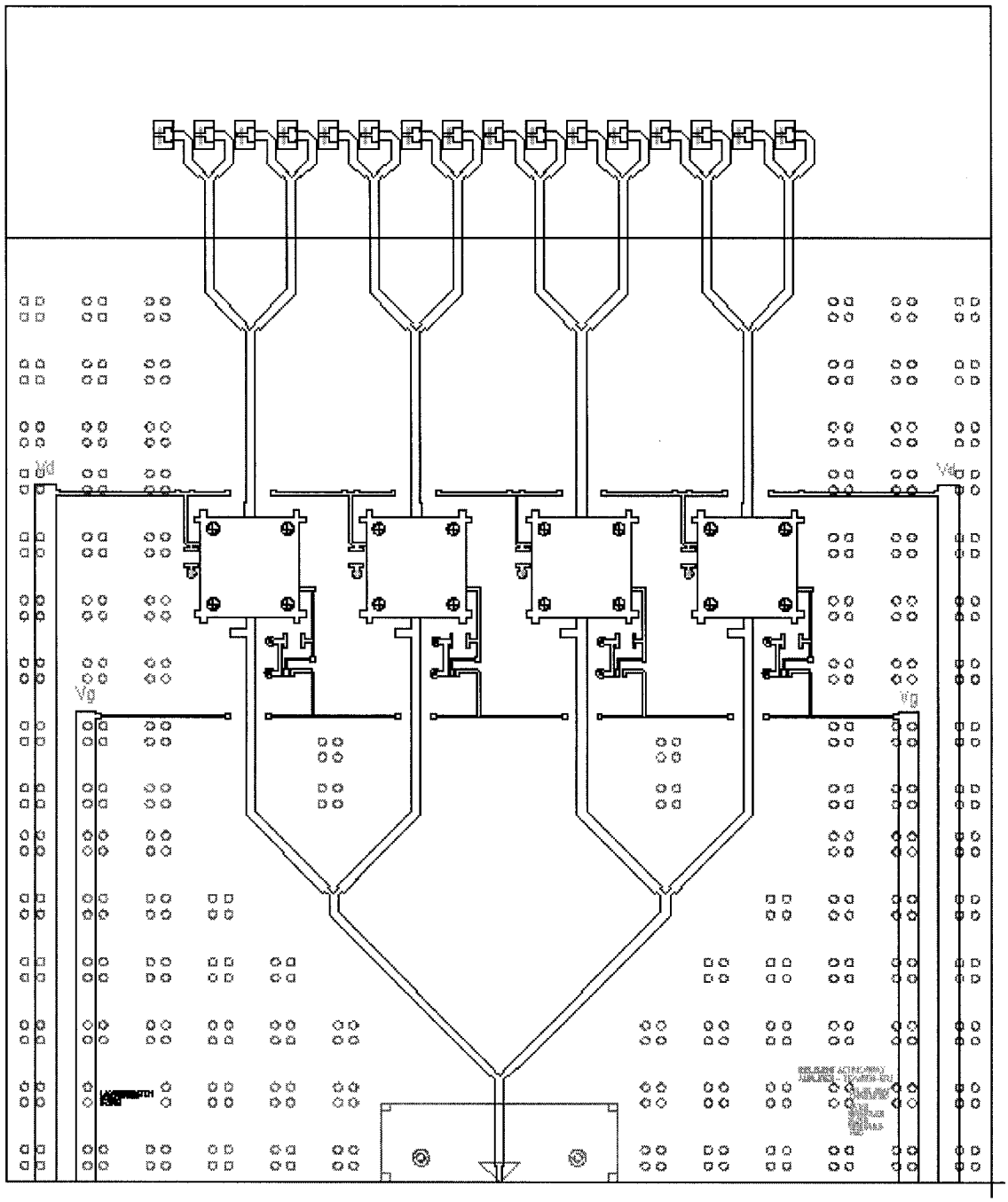

Figure 5.8: 16-Element active array layout

The layout shows all three layers of the board. As per the two-element prototype, pads were created for decoupling capacitors and potentiometers. The entire board was once again perforated with via's for grounding. A major difference between the prototype and the final design is the doubling of the number of DC feed lines with corresponding cross connection, in order not to

over-current the traces. Cross connection between the duplicate DC lines also improves redundancy should any flying leads get broken. Allowance is also made for the bend to be put in the board. The fabricated array with heat sinks and amplifiers prior to bending can be seen in Figures 5.9 and 5.10.

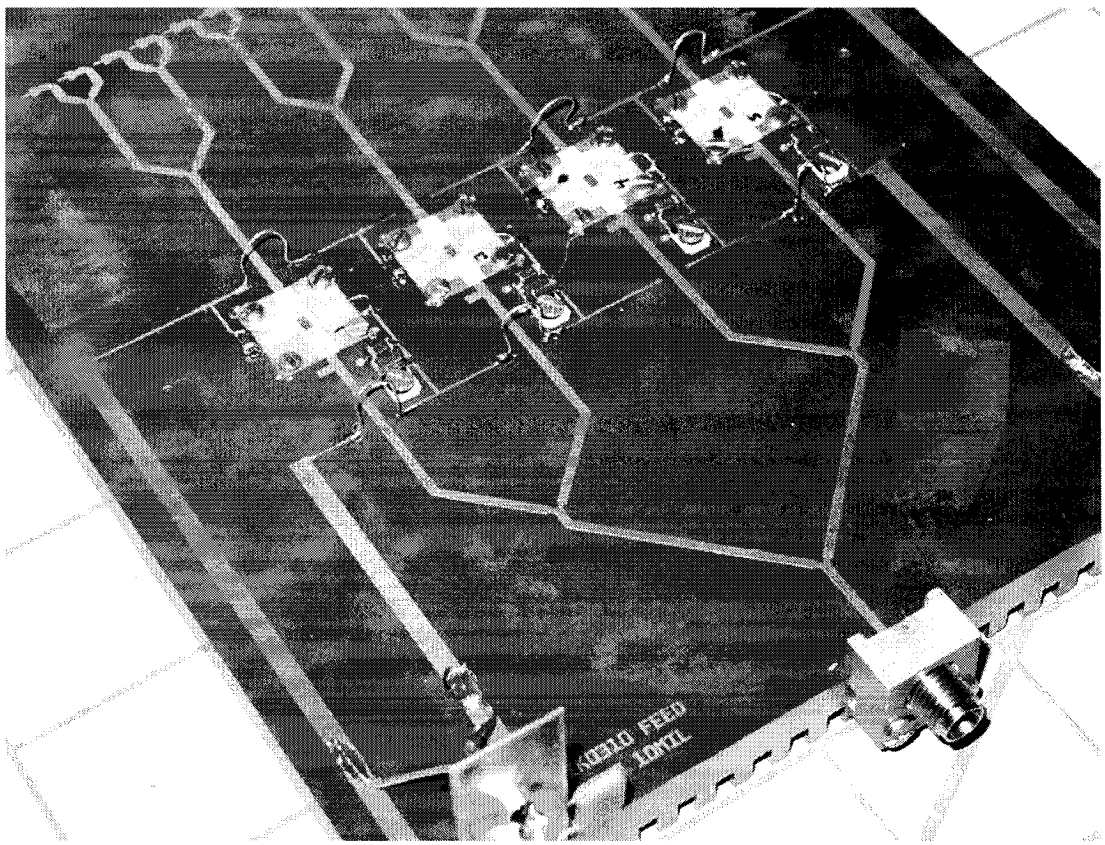

Figure 5.9: 16-Element active array – Feed side

Fabrication of the arrays was as expected. No compromises had to be made to the RF performance to ease fabrication concerns. As always line width tolerances were respected. In addition the DC line widths are carefully chosen in order to ensure they can carry the required current density. Two types of connectors were added, a K-connector for RF connectivity and two DC connectors on to which DC cables were soldered. To prevent the bending of the

bond wires during measurement, standoff white plastic blocks were added as is evident on the far left of the array in Figure 5.10.

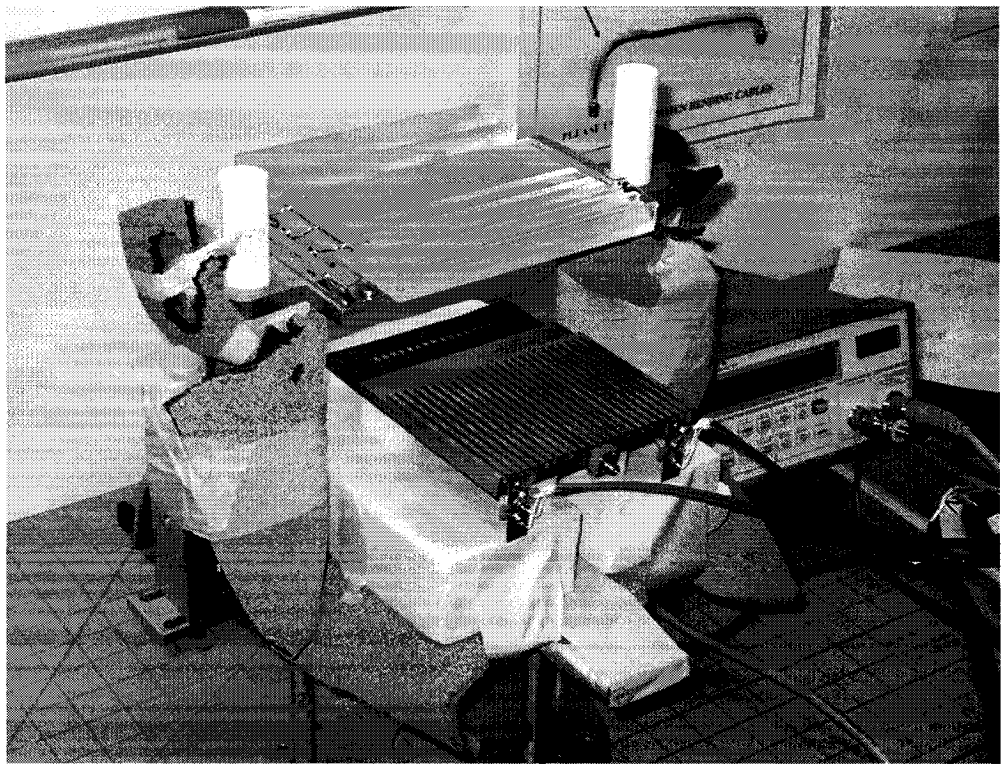

Figure 5.10: 16-Element active array – Patch side

Figures 5.11 and 5.12 show the array after bending. Bending was more difficult in this case due to the weight of the heat sink and the extra care required to avoid damage to the active components. The heat sink and active elements are clearly visible. It can also clearly be seen that the heat sink remains electrically invisible to the array due to the bending of the board.

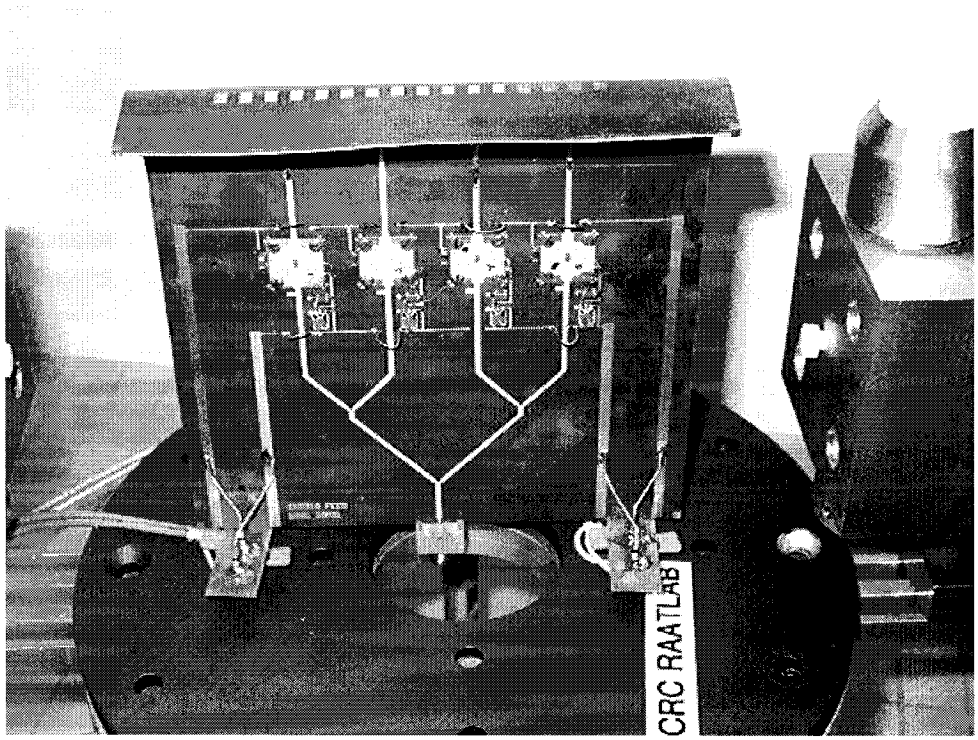

Figure 5.11: 16-Element bent active array – Feed side

Figure 5.12: 16-Element bent active array – Patch side

5.4.1 Measured Gain for 16 Element Bent Active Array without Lens

To ensure that the active array operated correctly it was tested by itself i.e. without the lens. This way the complexity of testing could be progressively incremented. Of note too is the fact that extra care had to be utilized during measurements due to the high RF output power of the antenna array. At the power levels being radiated there are significant health risks. This often meant that the array placement could not be minutely adjusted, as had previously been the case with the passive arrays.

Figure 5.13 shows the radiation patterns observed for the 16-element bent active array without a lens.

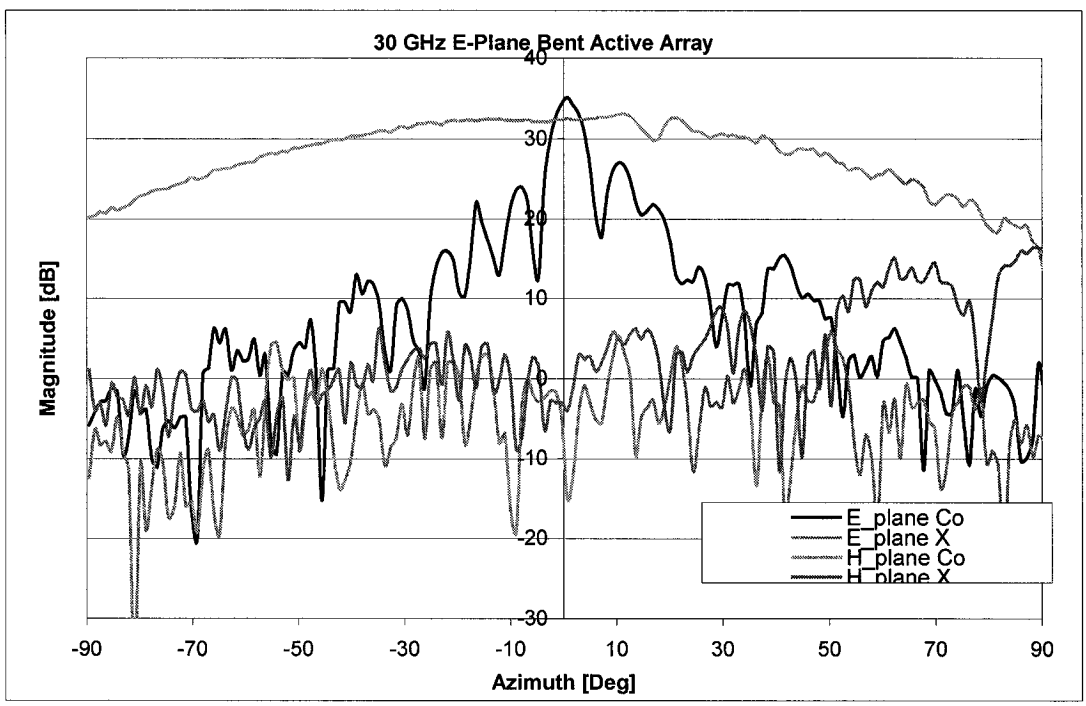

Figure 5.13: 16-element active array without lens – Measured patterns

The gain of the array was measured to be 35.11 dB. The E and H-plane patterns do not converge at boresight due to fact that the array is not at 0^0 elevation. The nature of the test stand made it difficult to accurately level the

array leading to E and H-plane pattern cuts in slightly offset planes. This is not a major issue as the results obtained were well within expected values. As was found from the passive bent array measurements the cross-pol levels are quite low with an E-plane cross-pol at -5dB and H-plane cross-pol at -5dB. For the 16-element array the gain was expected to be in the region of 36.3 dB, based on the calculation below:

Amplifier gain (see Section 5.1.1)	20 dB
Passive array gain (see Section 4.2.4)	16.3 dB
Theoretical gain	**36.3 dB**

The measured gain of 35.11 dB is very close to the expected gain of 36.3 dB with effects like bond wire and connector losses almost certainly accounting for the discrepancy. The measurements indicate that the active array is working very well. As was desired the output power from each of the amplifiers is feeding into the radiating elements and combining in free space. Clearly the initial goal of applying spatial power combining techniques has been successfully fulfilled. This allows for the next step in testing in which the beam is shaped using a lens.

5.4.2 Measured Gain for 16 Element Bent Active Array with Lens

To shape the broad element pattern as described in chapter 4 a lens is placed in front of the array. The combination of focusing achieved by the array factor and the lens should yield a narrow pencil beam over all planes. To perform this testing a 4 zone Fresnel lens was utilized (See Appendix E for further details on lens construction). The lens used can be seen in Figure 5.14.

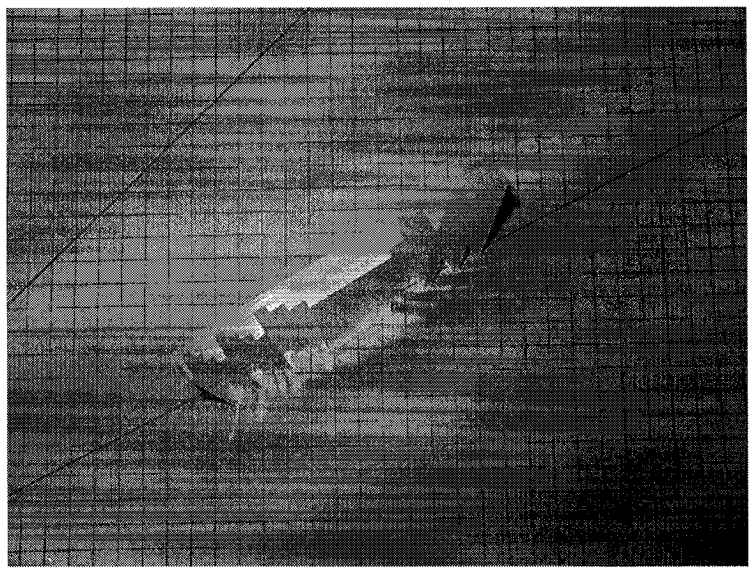

Figure 5.14: Four zone Fresnel Lens

The lens however has to be placed at the correct focal distance away from the array in order to achieve optimum focusing. The lens utilized has a nominal focal length of 75mm. To ensure correct focal distance the lens and array were placed in a test stand as shown in Figure 5.15. The focal distance was varied, by adjusting the test stand arms until optimum gain was observed. As well it was extremely important to maintain the lens and array parallel to each other to prevent the beam from skewing off boresight.

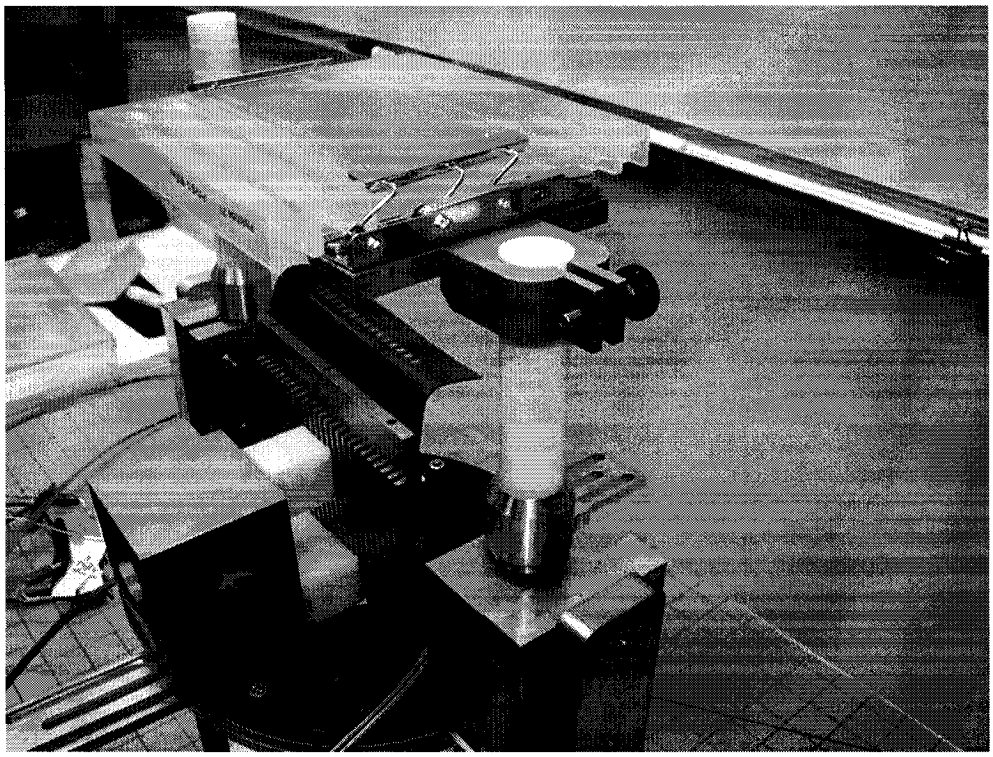

Figure 5.15: Linear active array and lens test setup

The test stand was mounted in the anechoic chamber. In order to prevent reflection of the metallic test stand all surfaces were covered with absorber sheets as is depicted in Figure 5.16.

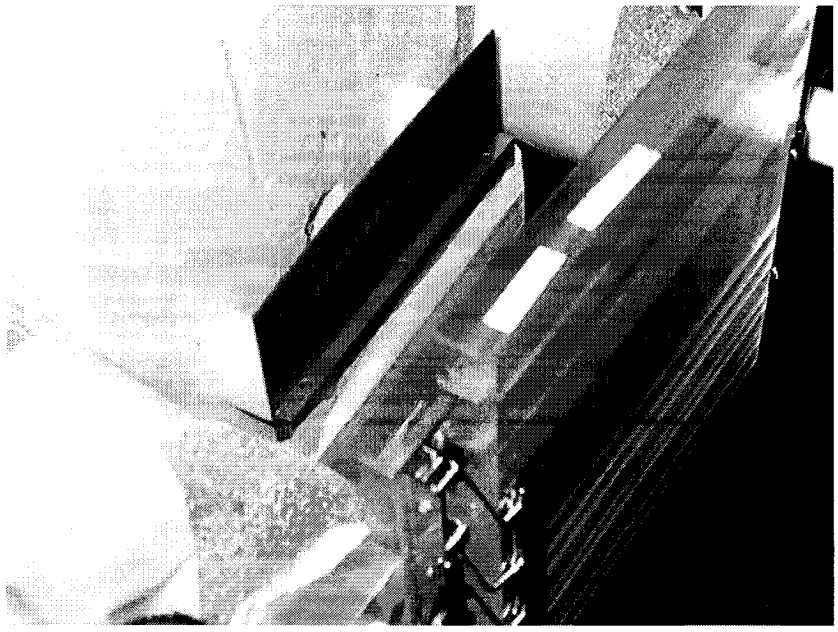

Figure 5.16: Varying the focal length of the lens

The patterns observed are depicted in Figure 5.17.

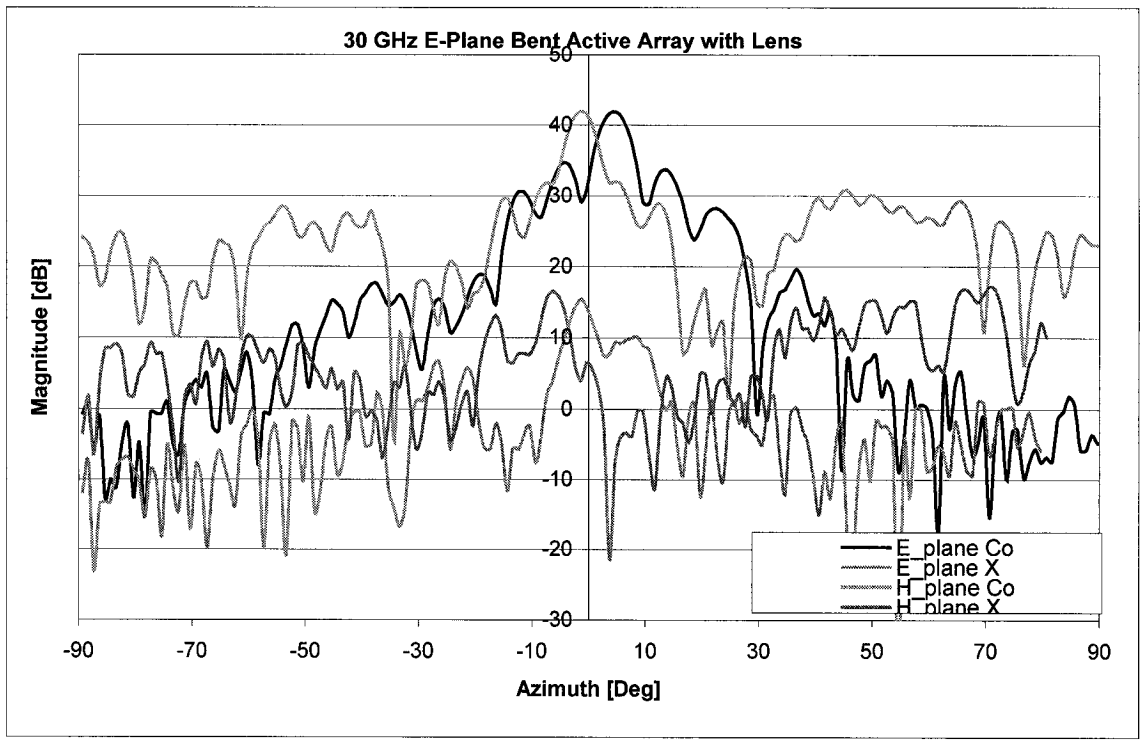

Figure 5.17:Linear active array with lens radiation patterns

The patterns as plotted are excellent. Beam shaping is now occurring in both planes (In the E-plane due to array multiplication and in the H-plane due to the lens) giving an overall pencil beam. There is a small offset due to the difficulties encountered in accurately positioning the array and lens combination. The gain increases due to the lens from a value of 35.11 dB to 42.53 dB an increase of 7.52 dB. The cross-pol levels are still within specification at 12 dB and 7 dB for the E and H-planes respectively. Spatial combining with beam forming is occurring. The entire system works.

The lens was nominally rated to provide a gain of 10 dB, which should result in an expected overall gain of 45dB. The 2.5 dB shortfall is attributed to the fact that the focal distance could not be adjusted as minutely as desired. This was due to the fact that each adjustment required the shutdown of the entire

array, adjustment of the lens, repositioning of the test head to account for the offset in elevation and then finally remeasurement. Such an arduous test scheme had to be employed for safety due to the high RF power levels involved. This meant that the number of possible focal distances tested was limited.

5.4.3 EIRP for 16 Element Bent Active Array with Lens

An important specification that requires verification is the EIRP of the array. This parameter is a difficult to measure considering that at saturation the array is capable of generating over a 150 Watts of effective radiated power. At these power levels there is significant risk to both health and test equipment. In order to avoid these difficulties an alternate test setup is considered. The active array was tested over the linear portion of its P_{in} vs. P_{out} curve up to an input power of -5 dBm. Verifying that the relationship is linear over these portions allows for easy extrapolation to higher power levels. Since power combining is happening in free space, the gain of the array and lens can be added to the amplifier's gain curve, this results in an EIRP curve shown in Figure 5.18. As the patches and lens are only passive elements, there should be no added distortion.

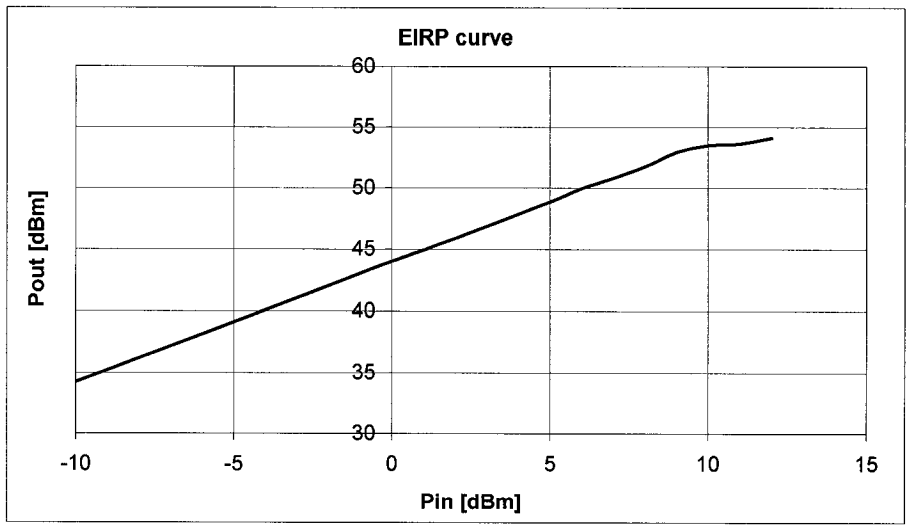

Figure 5.18: EIRP for 16-element active array with lens

The EIRP curve shows a peak gain of 53 dBm at the 1 dB compression point. This is 8 dB above the minimum required EIRP of 45 dBm.

5.5 Conclusion – 16 Element Active Array Final Design

The linear active array and lens design represents the successful culmination of several disparate techniques studied in previous sections into a coherent whole.

Distribution and division of power over a network of distributed amplifiers with subsequent spatial recombination has been successfully demonstrated. A high gain and EIRP are observed. The idea of doing away with a reflector and replacing it with an array and lens combination has realized the focused beam that was required. The linear array produces the fan shaped pattern with a narrow beam in the array plane and a wide beam in the orthogonal element plane. The one-dimensional linear lens can then be observed to focus the broad element pattern to a narrow beam, thus yielding a high gain pencil beam over all planes.

The one significant advantage of the linear array and lens configuration over a competing reflector antenna system is that it performs the same function in a much more compact package. As an example, for the reflector based system used as a reference for this design, the overall dimensions are 0.45m x 0.45m x 0.225m*[Shak02]*. The linear array with lens combination on the other hand occupies a volume of 0.15m x 0.15m x 0.205m. This represents a volume that is 10 times smaller, i.e. only occupies 10% of the original volume. Although the output power of the linear array and lens combinations is not as high as the baseline reflect-array system, it is foreseeable that the volume savings would still be large for a lens and linear array combination with the same output power. However it must be kept in mind that this comparison is valid only for EIRP. For the same beam width as a reflect array the linear array would have to be scaled up to have the same aperture size.

In terms of cost the spatially combined distributed amplifier structure offers a distinct advantage over a comparable reflector and single high power amplifier configuration. This can be seen by examining Table 5.3:

Table 5.3:Comparison of single vs. distributed amplifiers

	Device name	Cost [U$]
1 x 4 watt amplifier	TGA 4517-EPU	270
4 x 1 watt amplifier	TGA 4509-EPU	160

Additionally if larger EIRP were required from the system the linear array can easily be extended to a larger number of radiating elements, or the active elements replaced with higher power amplifiers. This is not as conveniently done with a reflector-based antenna. Additionally although not undertaken in this

work, phase shifters can be integrated with the linear array thus allowing for beam scanning, which can not be done using a reflector.

Finally bending the array was also successfully implemented. This eased active element integration with the linear passive array. Bending made it possible to reduce interference to the radiation patterns from the heat sink. This novel method has applications in many future active array designs.

CHAPTER 6

CONCLUSION AND FUTURE WORK

6.1 Summary of Research Conducted

The use of microstrip patch elements in conjunction with integrated amplifiers for the design of an EHF SATCOM terminal has been investigated in detail. The principal focus has been on the feasibility of spatially combined arrays and on effective design techniques for successfully harnessing spatial power combining concepts, for use with the feed structure in low cost portable SATCOM terminals. To this end, a number of practical microstrip element and array configurations were explored. The various configurations were initially characterized using theory and simulations, with subsequent experimental validation of the simulated results.

In addition to this primary thrust, effort was directed towards investigation of the design and implementation of microstrip power combiners in Chapter 3, and towards novel mechanical shaping methods for integration of active devices and their associated thermal management mechanisms in Chapter 4. Although not detailed in the main body of the thesis, the design of multi-frequency capable

Fresnel zone lens for beam shaping has also been undertaken in Appendix E. The first two topics were investigated through simulation as well as experimental verification.

6.2 Summary of Results

The principal conclusion of this research has been the successful demonstration of spatial power combining with an active linear array and an associated beam shaping lens, for practical use in a SATCOM terminal. The design demonstrates the stated aim of creating an economical alternative for a portable terminal design. This was mainly achieved by spatially combining a distributed low cost, low power, amplifier structure into a coherent high power beam. Further cost savings were realized by implementing the solution on microstrip technology, which in itself is inherently low cost due to ease of manufacturing. The minimum required EIRP of 45 dBm was successfully obtained. The pencil beam pattern desired was also seen.

The full-scale demonstration was confined to only the transmit section of the terminal. However workable alternatives for a complete design i.e. both transmit and receive sections were also designed and tested. This included low axial ratio on the circularly polarized patches as well as a large gain and low cross-pol levels on a half scale dual frequency, passive array. This successfully demonstrated simultaneous operation at both 20 GHz and 30 GHz.

Significant knowledge was gained on the design of practical active arrays. This was done through not only the investigation of various array topologies but also through the characterization of manufacturing methods that would make

practical the integration of active devices with an array. Mechanical shaping of Duroid was shown to be possible without adverse impact on the electrical performance of the array.

Finally a Fresnel lens was successfully used with the active array for beam shaping the broad element pattern into a focused beam. The combination of the lens and array factor correctly focused the overall antenna pattern into a pencil beam over all azimuthal angles. The lens tested was also only built for operation at the 30 GHz transmit frequency, however viable methods for design of dual frequency lens are further discussed.

6.3 Areas for Additional Research

The evolution of the design was based much more on practical aspects rather than simply theoretical considerations only. Though the theoretical understanding of spatial power combining was an important thrust to the research, of paramount importance was the use of these concepts in implementing a practical design. Thus many avenues, which may initially seem unrelated to the main area of research, were explored.

This did however mean that not all research paths were fully explored. The three main design concepts still requiring additional research in order for a capable portable SATCOM terminal prototype include:

- The replacement of the linear patch elements used with the circular polarized patch elements already designed. The majority of this work has already been completed in the present research. All that is required is the correct matching of the array with the patches.

- The manufacture of an active dual frequency 16 elements circularly polarized array. Once again the individual parts of such an array have already been designed i.e. an active 16 element array, a dual frequency array and circularly polarized elements. The paucity of time and resources prevented the full-fledged array from being built, but all major aspects of the design have already been characterized. This is not an area of additional research but rather, a manufacturing exercise that needs to be completed once resources are available.
- As undertaken in Appendix E, the refinement of the multi-frequency lens design to make it more practical for manufacturing is required. The theory behind the idea is sound; however, it still needs to be experimentally verified.

Should these additional objectives be met for the linear array with lens, the final hurdle that would remain would be the packaging of the entire system. The system can be enclosed in a ruggedized/weatherized box, with little additional difficulty. Thus another area for additional work would be the packaging of the array and lens.

Recall that simple manufacturing techniques were utilized over the entire design cycle in order to have a low cost design. This in itself should allow the entire system to be very quickly and very easily developed commercially and deployed in the future. This work is however beyond the scope of this thesis and is left for future implementation.

APPENDIX A

Appendix A1

The following figures illustrate the effect of varying inter element spacing on antenna pattern. Results from section 4.2.2

A1.1 Case 2: Spacing of 5.45mm

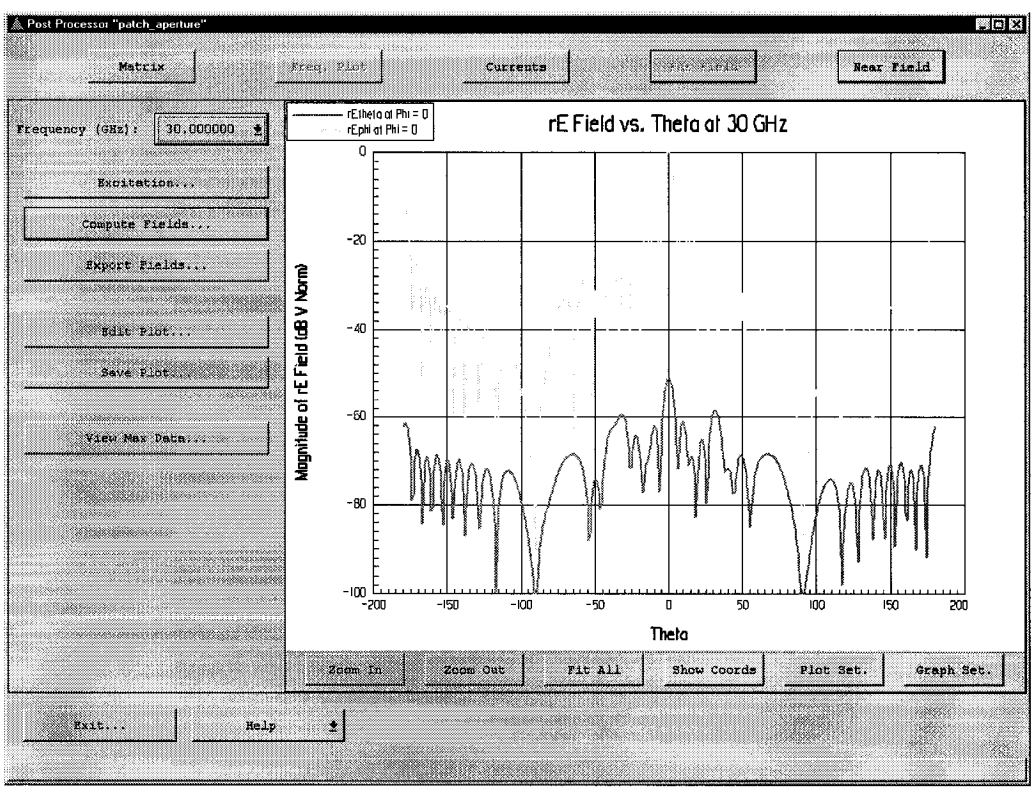

Figure A1.1: Simulated results for inter-element spacing of 5.45mm

A1.2 Case 3: Spacing of 6.6mm

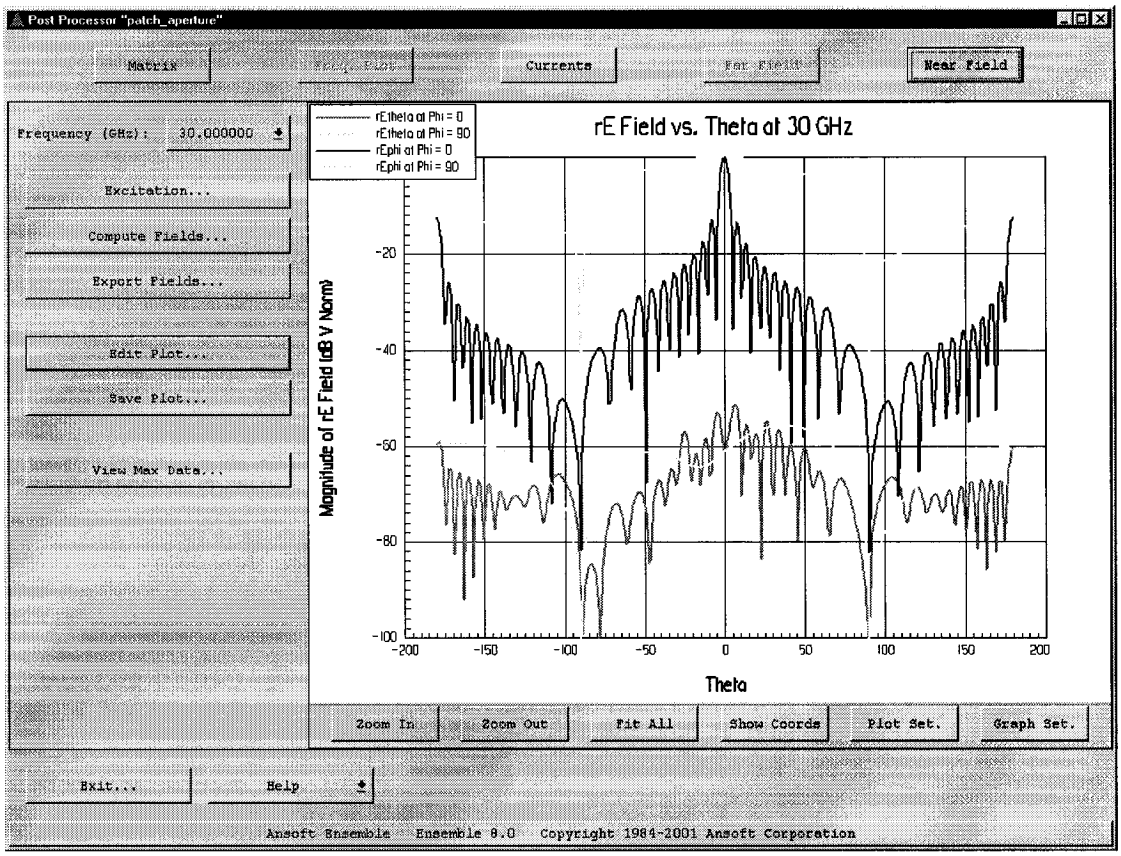

Figure A1.2: Simulated results for inter-element spacing of 6.6mm

A1.3 Case 4: Spacing of 11.1mm

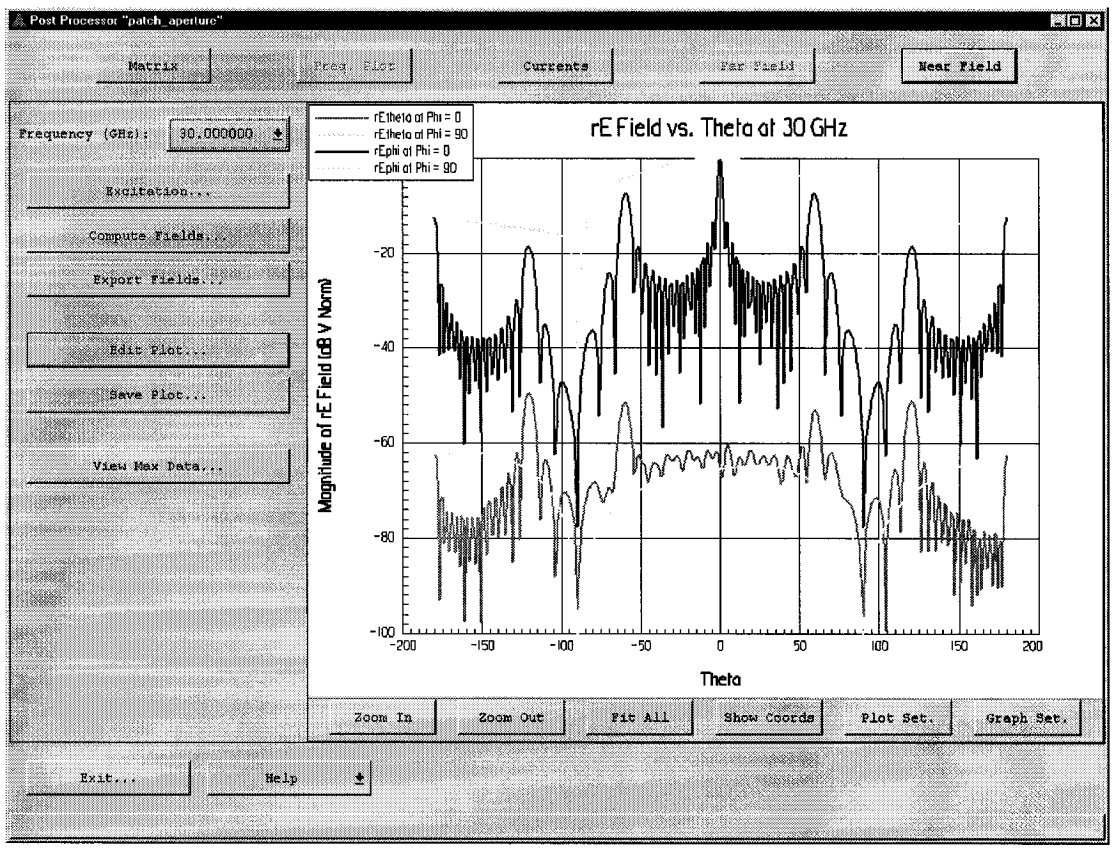

Figure A1.3: Simulated results for inter-element spacing of 11.1mm

Appendix A2

The following figures illustrate the effect on the S-parameters when Duroid is bent over various radii. This continues the data presented in Section 4.3.3.

A2.1 Line 2 – 0.75 inch bend

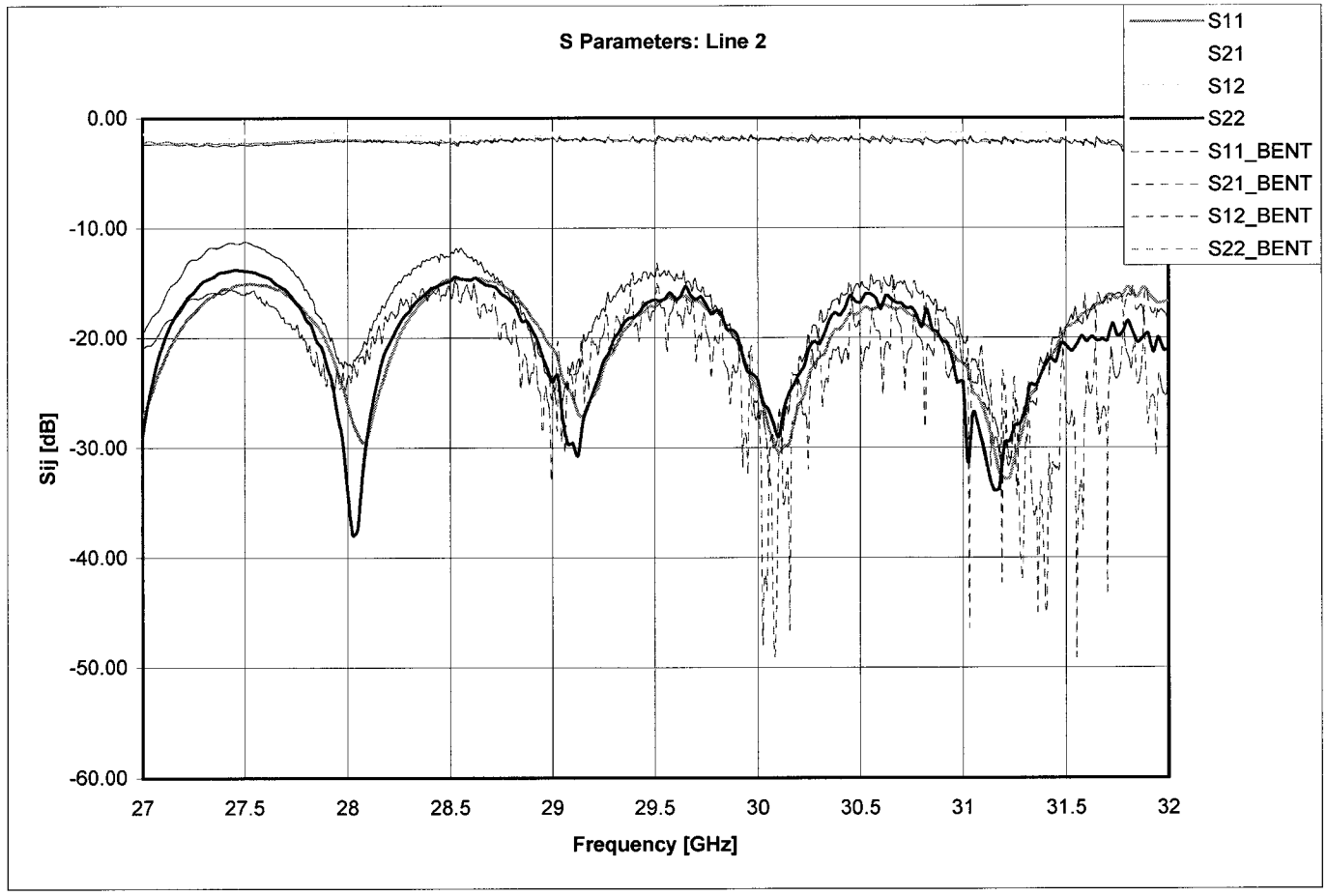

Figure A2.1: S-parameters for 0. 75 inch bent line

A2.2 Line 3 – 1.0 inch bend

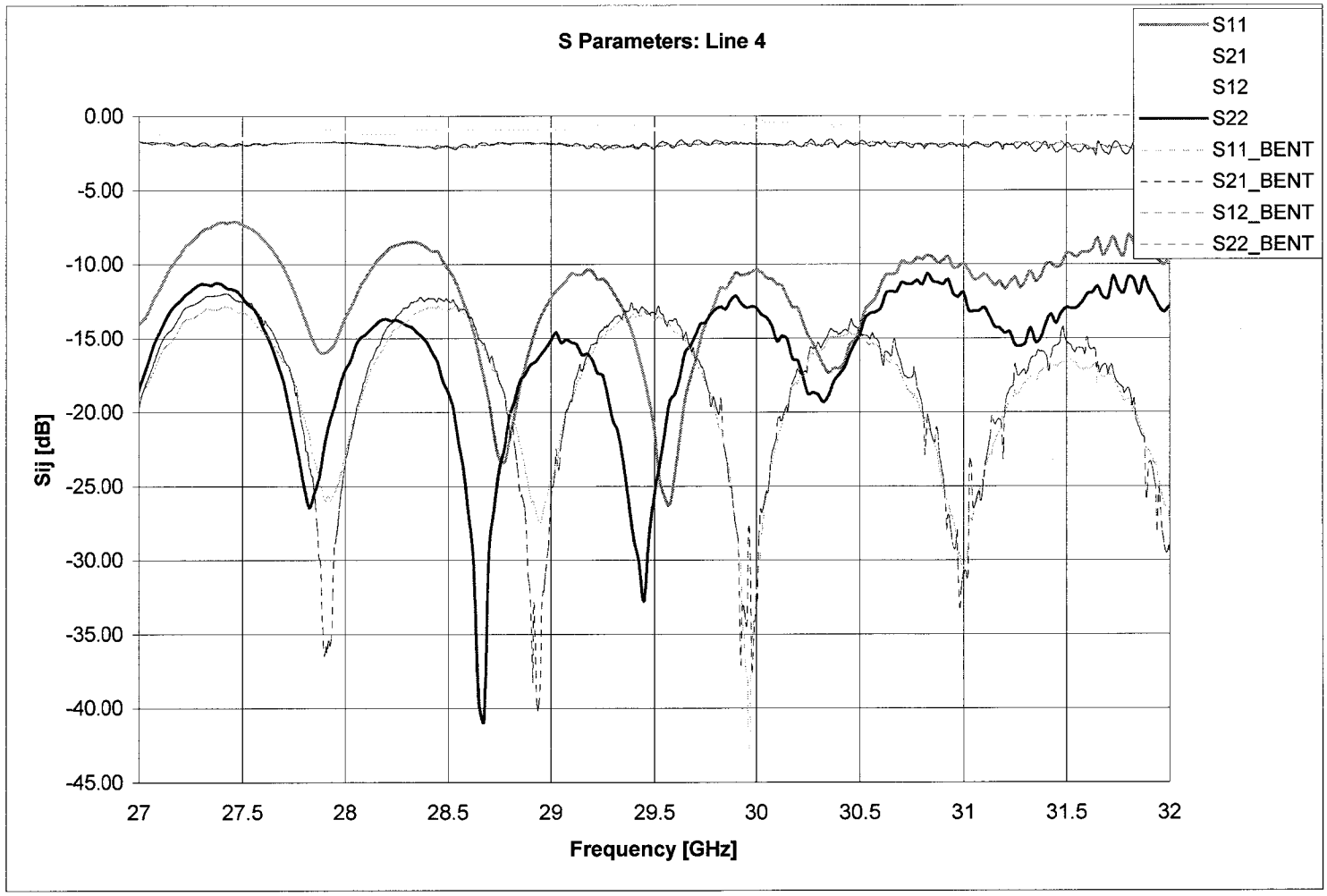

Figure A2.2: S-parameters for 1.0 inch bent line

A2.3 Line 4 – 1.5 inch bend

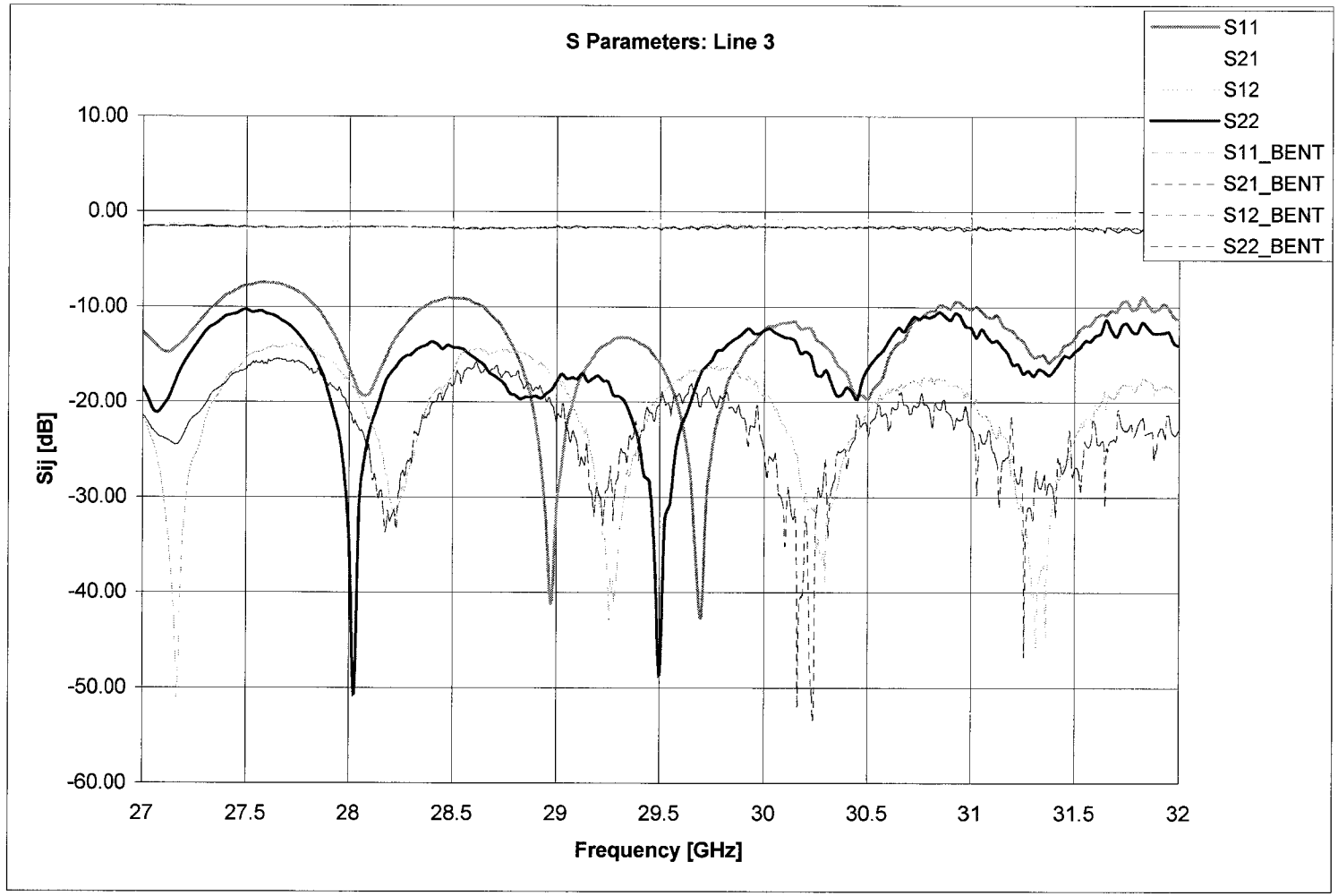

Figure A2.3: S-parameters for 1.5 inch bent line

A2.4 Line 5 – 2.0 inch bend

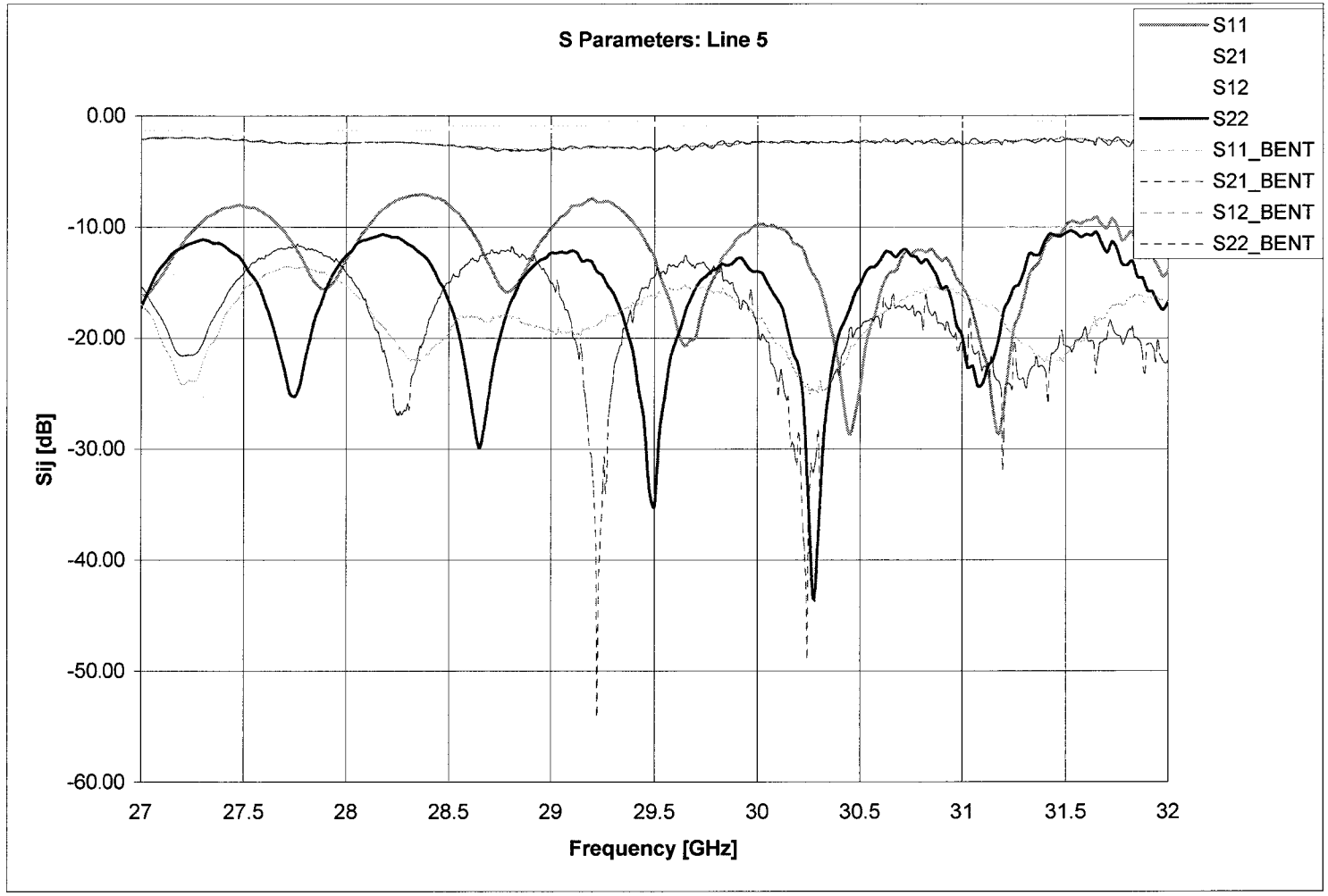

Figure A2.4: S-parameters for 2.0 inch bent line

A2.5 Line 6 – 2.5 inch bend

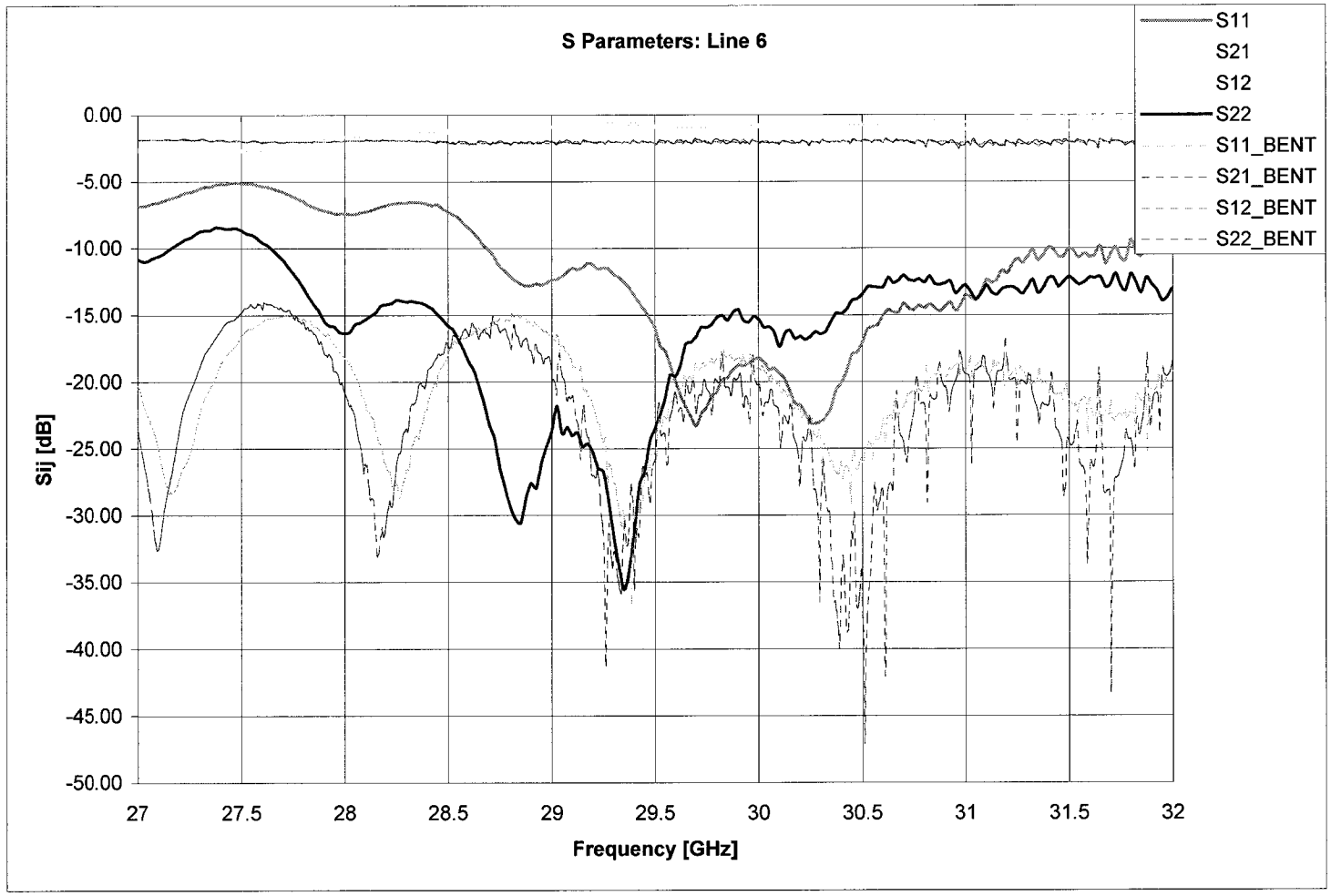

Figure A2.5: S-parameters for 2.5 inch bent line

APPENDIX B

Appendix B1 – Example Patch Design

$\varepsilon_r = 2.2$

h = 0.762 mm

f_0 = 30GHz

$$W = \frac{c}{2f_0}\sqrt{\frac{2}{\varepsilon_r + 1}}$$

c = 3 x 10^8 m/s

W = 3.95mm

$$\varepsilon_{eff} = \frac{\varepsilon_r + 1}{2} + \frac{\varepsilon_r - 1}{2}\left[1 + \frac{10h}{W}\right]^{-1/2}$$

ε_{eff} = 1.9507

To compensate for fringing fields need to work out Leff and ΔL to get L

$$\Delta L = \frac{0.42h(\varepsilon_{eff} + 0.3)\left[\frac{W}{h} + 0.264\right]}{(\varepsilon_{eff} - 0.258)\left[\frac{W}{h} + 0.8\right]}$$

ΔL= 0.38 mm

For TM_{010} mode

$$f_0 = \frac{c}{2L_{eff}\sqrt{\varepsilon_{eff}}}$$

$$L_{eff} = \frac{c}{2f_0\sqrt{\varepsilon_{eff}}}$$

L_{eff} =

L = (L+2ΔL)

L = 2.8 mm

Check with approximation

$$L \approx \frac{\lambda_0}{2\sqrt{\varepsilon_r}}$$

L ≈ 3.37 mm

Within the same range but obviously with more detailed calculation that take into account fringing fields a better value of L = 2.8mm is obtained.

Location of feed point

$$G_s = \frac{W}{120\lambda_0}\left[1 - \frac{1}{24}(k_0 h)^2\right]$$

$$k_0 = \frac{2\pi}{\lambda_0}$$

G_s = 0.0033 S

$$R_{in}(s) = \frac{1}{2G_s}\cos^2\left(\frac{\pi}{L}s\right)$$

$$s = \frac{L}{\pi}\cos^{-1}\sqrt{2G_s R_{in}}$$

We want R_{in} = 50Ω

∴s = 0.8642 mm

APPENDIX C

Appendix C1 – Microstrip Line Width

The following MATLAB program is used to calculate the width of microstrip line for any required characteristic impedance.

```
%Relative Dielectric of Board
Er = 2.2
%Characteristic Impedances to be calculated
Zo = [70.71 51.49 43.87 39.53 36.63 34.51 32.86 102.99 131.61
158.11 50]

%Calculations begins
B = (60*pi^2)./(Zo*sqrt(Er));
WoverH1 =(2/pi)*(B-1-log(2*B-1) + ((Er-1)/(2*Er))*(log(B-1) + 0.39
-(0.61/Er)));
WoverH1'

A = (Zo./60)*sqrt((Er+1)/2) + ((Er-1)/(Er+1))*(0.23 + (0.11/Er));
WoverH2 = (8*exp(A))./(exp(2*A)-2);
WoverH2'

eff1 = (Er+1)/2 + ((Er-1)/2)*((1 + (10*(1./WoverH1'))).^(-0.5))
eff2 = (Er+1)/2 + ((Er-1)/2)*((1 + (10*(1./WoverH2'))).^(-0.5))


for i = 1: length(Zo)

if (Zo(i) <= (89.91/sqrt(eff1(i))))
   WH(i) = WoverH1(i);
   eeff(i)= eff1(i);
elseif (Zo(i) > (89.91/sqrt(eff2(i))))
   WH(i) = WoverH2(i);
   eeff(i) = eff2(i);
else
   WH(i) = 0;
   eeff(i) = 0;
  end
end

disp('        Zo  Z<89.81/eff Z>89.81/eff   W/h     Eeff')
disp('-------------------------------------')
X = [Zo', WoverH1', WoverH2',WH',eeff'];
disp(X)

disp('        Zo      W/h      W        Eeff      LambdaG 1/4
Trans')
Y = [Zo',            WH',   WH'*0.010*25.4    ,    eeff',
sqrt(1./eeff'), (1/4)*sqrt(1./(eeff'))*10];
disp(Y);
```

Appendix C2 – Patch Dimensions and Radiation Pattern

The following MATLAB code is used to automate the calculation of the dimension of a single patch antenna and to plot the theoretical radiation pattern of the aforesaid patch.

```
%Patch Design and Radiation Pattern%
Rin = 50
f = 30e9
c = 3e8
lambda = c/f
k = 2*pi/lambda
%L = 29.570e-3%
theta = -pi/2:0.01:pi/2
phi = 0
phi1 = pi/2
er = 2.2
h = 0.762e-3%mm%
%W = 2.5-3 %mm%

W = (c/(2*f))*sqrt(2/(er+1))
eeff = ((er+1)/2) +((er-1)/2)*(1+ (10*(h/W)))^-0.5
Leff = c/(2*f*sqrt(eeff))
WoverH = W/h
DL = (0.412*h*(eeff+0.3)*(WoverH+0.264))/((eeff-0.258)*(WoverH + 0.8))
L = Leff - (2*DL)

% for phi = 0 or E-plane cut%
Wk = 0.5*k*W*sin(theta).*sin(phi)
Lk = 0.5*k*(L+(2*DL))*sin(theta).*cos(phi)
Etheta = (-cos(Lk).*cos(phi).*(eeff - (sin(theta)).^2))./((eeff-
(sin(theta)).^2.*(cos(phi).^2)))
Ephi = (cos(Lk).*eeff.*cos(theta).*sin(phi))./(eeff-
((sin(theta).^2).*(cos(phi).^2)))
E = sqrt((Etheta.^2) + (Ephi.^2))

%for phi = pi/2 or H-plane cut %
Wk1 = 0.5*k*W*sin(theta).*sin(phi1)
Lk1 = 0.5*k*(L+(2*DL))*sin(theta).*cos(phi1)
Etheta1 = 0
Ephi1 = (sin(Wk1).*eeff.*cos(theta))./(Wk1.*(eeff))
E1 = sqrt((Etheta1.^2) + (Ephi1.^2))

%Location of feed point%
Gs = (W/(120*lambda))*(1-((1/24)*(k*h)^2))
s = (L/pi)*acos(sqrt(Rin*2*Gs))

%Plot radiation pattern
title('Normalized Radiation Pattern for Microstrip Patch at f= 2.9 Ghz')
polar(theta,(E1/max(E1)), 'g')
hold on
polar(theta,(E/max(E)), '-.b')
```

Appendix C3 – Perforated Fresnel Zone Lens Layout Code

The following MATLAB code is used to generate zone width, perforation diameter and perforation placement for the perforated zoned Fresnel lens

```
%Perforated Lens Design
f = 30 %in GHz
t = 10.16   %Lens Thickness
P =   12    %Number of zones desired
er = 10      %Dielectric strength of lens material
lambda = 3e8/(f*1e9)*1e3;

%Calculation of the Eeffn for the various zones
Eeff(1) = er
for z = 2:P+1
Eeff(z) = (sqrt(Eeff(z-1)) - (lambda/(P*t)))^2;
end
Eeff'
for z = 1:P+1
alpha(z) = ((Eeff(z)/er)-1)/((1/er)-1);
ds(z) = sqrt(alpha(z)*2*sqrt(3)/pi);
AoA(z) = alpha(z)*2;
end
%End of alculation of the Eeffn for the various zones

%Specify the bit sizes available
bs = [2 5 7 9 11 13 15 17 19 21 23 25]  %bitsize

%Based on the bitsizes available calculate the horizontal
%and vertical seperation between holes
for z = 2:P+1
s(z-1) = bs(z-1)*2/ds(z);
end
h = sqrt(s(12)^2 - (s(12)/2)^2)
% End of calc
x_new = 0;
y_new = 0;
z = length(bs)
for t = 1:z
%Begin Tiling Calculations
delta(t) = s(t)/4
L=floor(h/delta(t)) %Specify the number of tiles to be layed out
%L = 2
%Loop that does the drawing of the tiles
for i = 1:L
   %Horizontal Tiles
    x_new = 4*delta(t) + x_new;
    y_new = 0;
    circle (bs(t),x_new,y_new)
    circle(bs(t), x_new+(2*delta(t)),y_new+(2*sqrt(3)*delta(t)))
         for j = 1:L
         %Vertical Tiles
         y_new = 4*sqrt(3)*delta(t) + y_new;
         circle (bs(t),x_new,y_new)
         circle(bs(t),
x_new+(2*delta(t)),y_new+(2*sqrt(3)*delta(t)))
     end
end
x_new = x_new + delta(t)
end
```

APPENDIX D

Appendix D1 – Chip Carrier

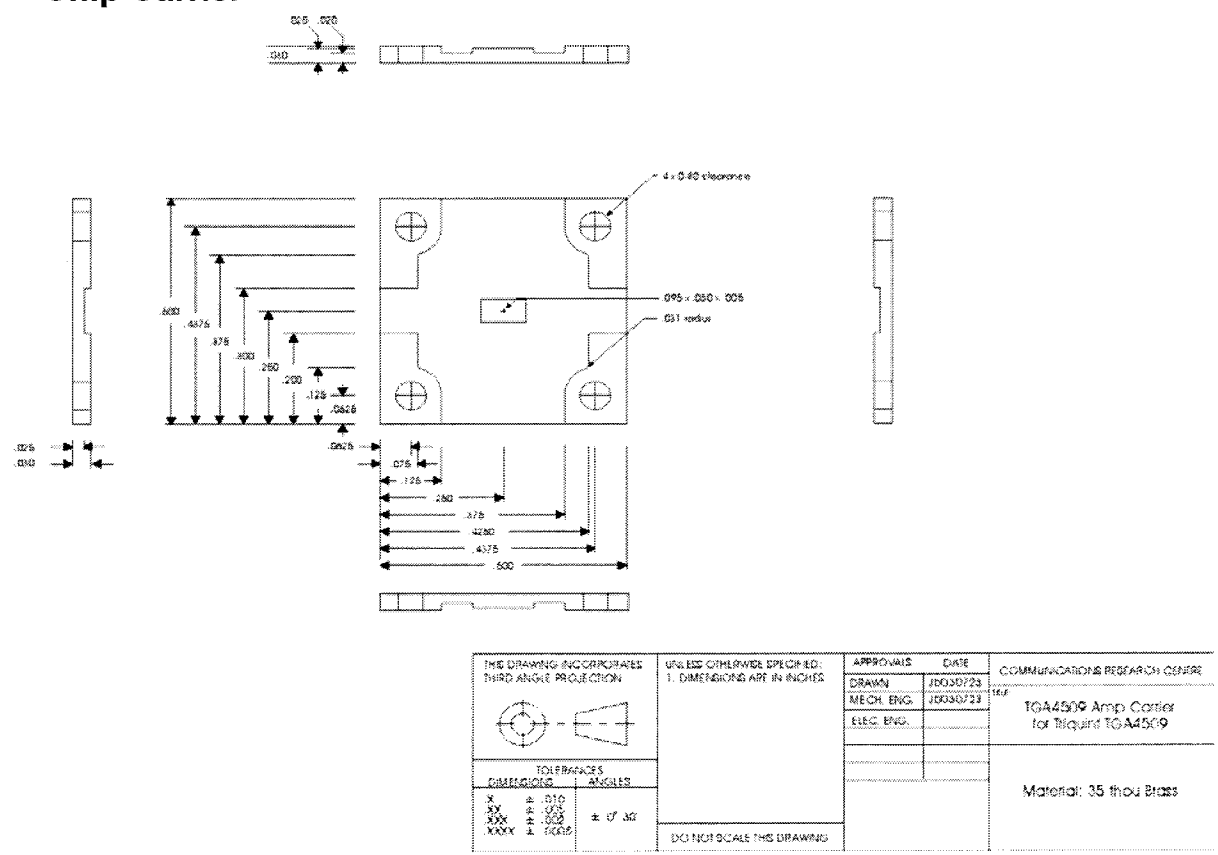

Appendix D2 – 2 Element Prototype Board

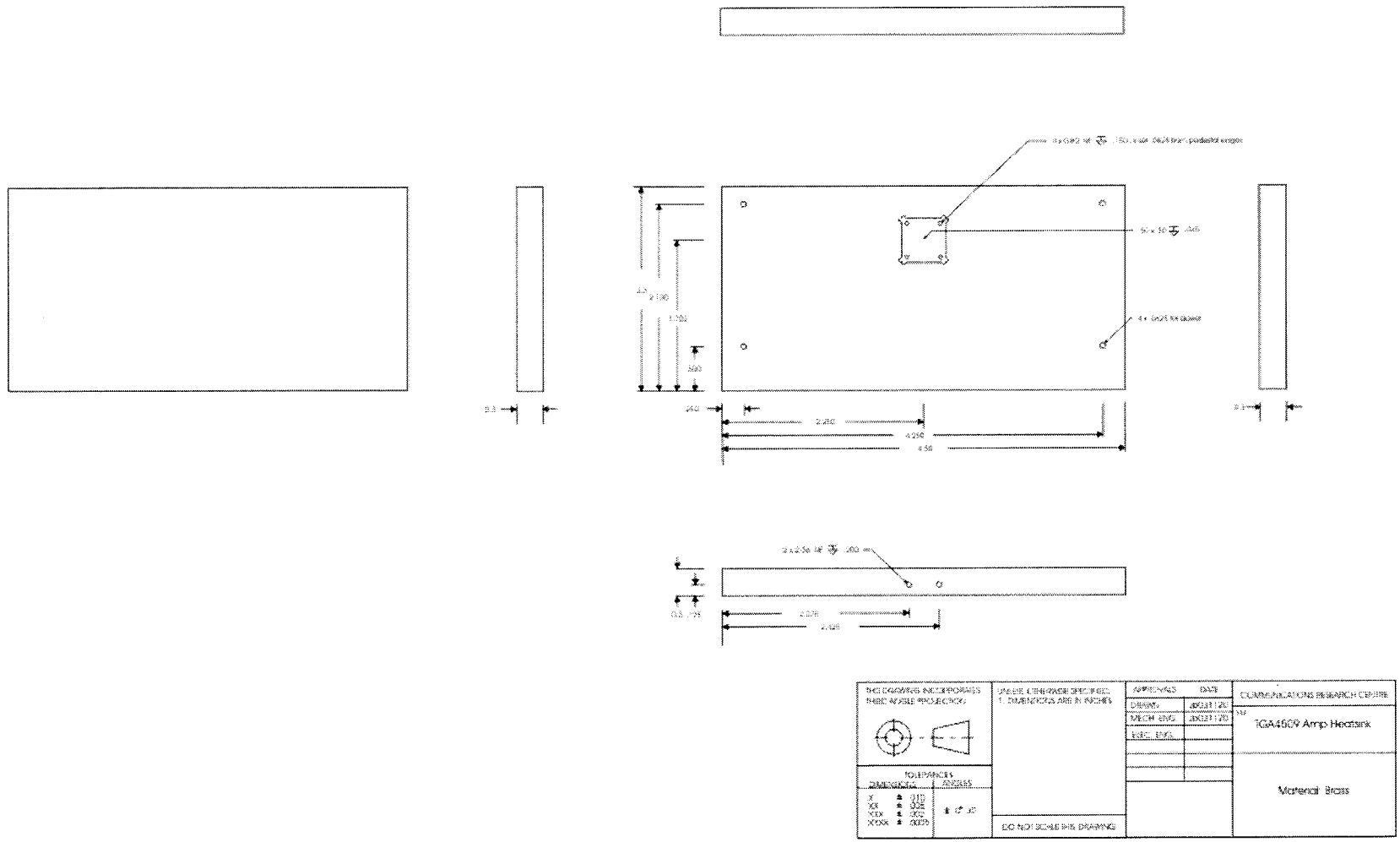

Appendix D2 – 16 Element Final Board

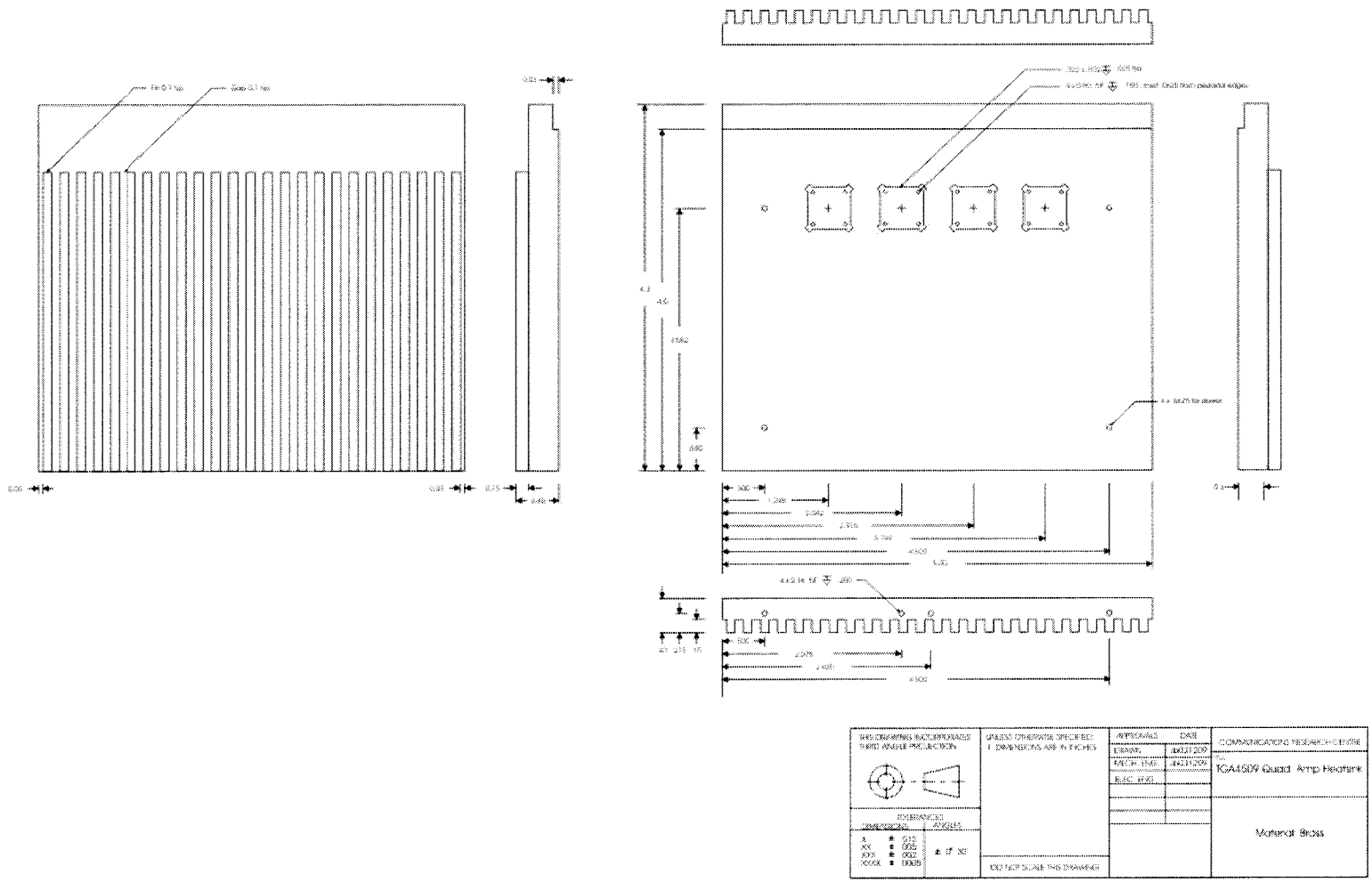

APPENDIX E

LENS DESIGN

A very viable alternative to traditional reflector and reflect array antennas are dielectric lens. A lens antenna with a feed offers significant savings in terms of cost and size when compared to parabolic dishes. The cost savings are realized because dielectric lenses are typically made of inexpensive plastics, which can easily be machined and/or molded. Machining a lens is further simplified as the tolerance requirements are much less stringent than those required for a reflector antenna. The weight savings in a lens are realized due to the fact that the lens, are usually thin and significant weight savings can be traded off with aperture efficiency if required. Electrically, lens antennas can be very broad-band and offer wide scan angles. These advantages can be traded off for weight savings if required. They do not suffer from aperture blockage that is associated with similar reflector antennas.

E.1 Fresnel Lens

A variety of lenses exist amongst which an important class of lens is the Fresnel lens. A Fresnel lens antenna consists of two basic elements – a transmission or reflection zone plate and a feed. The feed design and performance has been discussed exhaustively in the previous sections. The Fresnel zone plate converts the transmitted (received) signal from a spherical (plane) wave into a plane(spherical) wave. There exist two types of Fresnel zone plate antennas.

- The Soret type – This type of Fresnel lens consists of metallic rings that selectively block some zones and allow waves to travel through other zones thus allowing constructive addition and a focusing effect. Soret type zone lenses are flat but they suffer from poor aperture efficiency in that they block at least 50% of the power. (See Figure E.1)

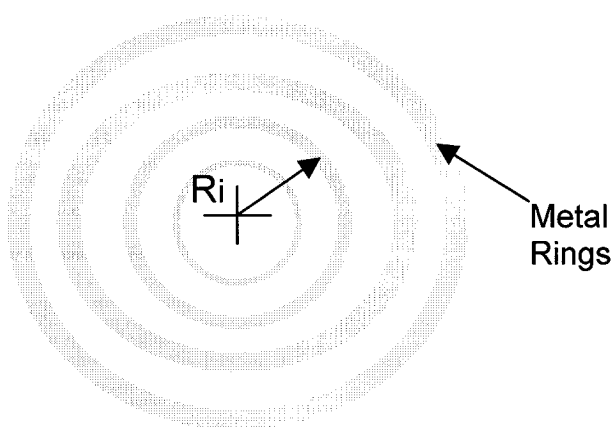

Figure E.1: Soret type zone lens

- The Wood type – The Wood type lens on the other hand consists of phase corrected dielectric zones. The zones alternate in thickness

such that adjacent rings correct the phase of the feed antenna at discreet locations. The addition of extra material to the different zones ensures that all the wave fronts that exist the lens are phase matched which converts a spherical wave to a planar wave. A Wood type lens does not suffer from the blockage associated with a Soret type zone lens. All the design work that was done was exclusively on Wood type lens. See Figure E.2.

E.2 Wood Type Fresnel Zone Lens

There are two important design factors for a zone lens. The first one is the radius of each Fresnel zone and the second is the thickness or height of each zone.The radius of each Fresnel zone is set so that the maximum phase error at the edge of the lens is $360^0/P$ where P is an integer.

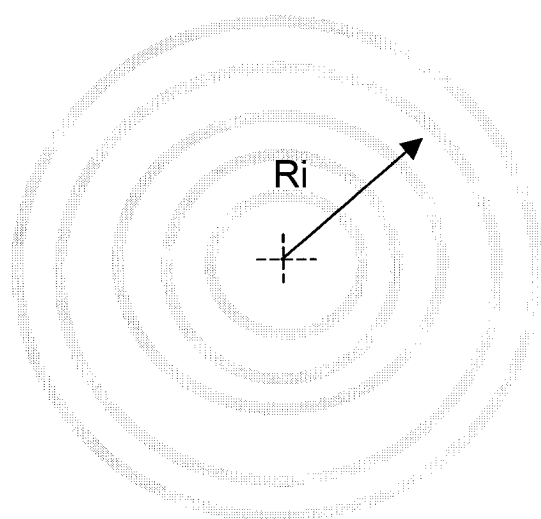

Figure E.2: Wood type zone lens

The radius of each zone can be calculated using the equation below where R_i is the radius of the ith zone.

$$R_i = \sqrt{2fi\Delta + (i\Delta)^2}$$
$$\Delta = \lambda_0 / P \qquad \text{[E.1]}$$

f is the focal distance.

The groove height *s* of each zone as seen in Figure E.3 is setup such that the phase adjustment that occurs for a wave traveling through the zone and one traveling through free space is 360^0/P where again P is an integer.

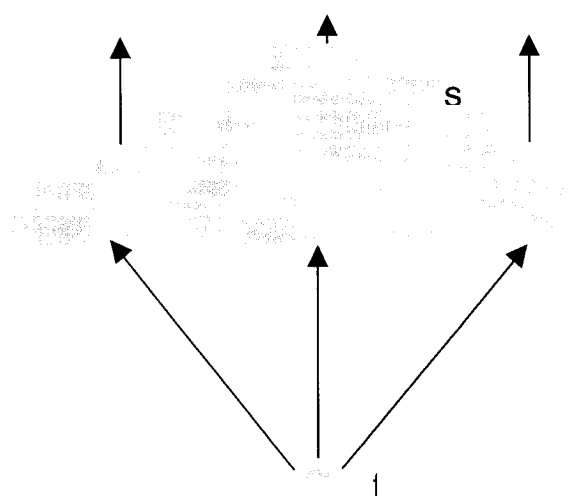

Figure E.3: Cross-section of zoned Wood type Fresnel lens

The height of each zone can be calculated using the equation below:

$$s = \frac{\lambda_0}{P(\sqrt{\varepsilon_r} - 1)} \qquad \text{[E.2]}$$

where ε_r is the relative permittivity of the material chosen for the lens.

The integer P sets the desired amount of phase correction. A larger P yields better phase correction but at the same time increase the number of steps required in the lens.

E.3 Making the Lens Multi-Frequency Capable

The only shortcoming of this approach is that the lens operates at a single frequency. This presented a significant challenge that would invalidate the entire feed design. It was important to have a lens that would not only shape the received wave at 20GHz but also the transmitted wave at 30GHz. Conventionally this can only be done by using a full homogenous lens that works at all frequencies. However doing so would counter the potential cost and weight savings that can be accrued by using a zoned Fresnel lens. In order to address this issue the following novel idea was proposed.

Examining the above equations it can be seen that using two separate frequencies of operation would yield two different lens dimensions. In order to have a single lens the equations must be manipulated so that the final zone height and zone radius remains the same irrespective of whether a 20GHz or a 30GHz wave illuminated the lens. The trick to doing this was to adjust the phase correct factor P. If P was intelligently varied the ratio λ/P could be made into a constant. Once this was achieved the equations would give exactly the same dimensions for the lens for both a 20GHz design and a 30GHz one. This is illustrated in the Figure E.4 below:

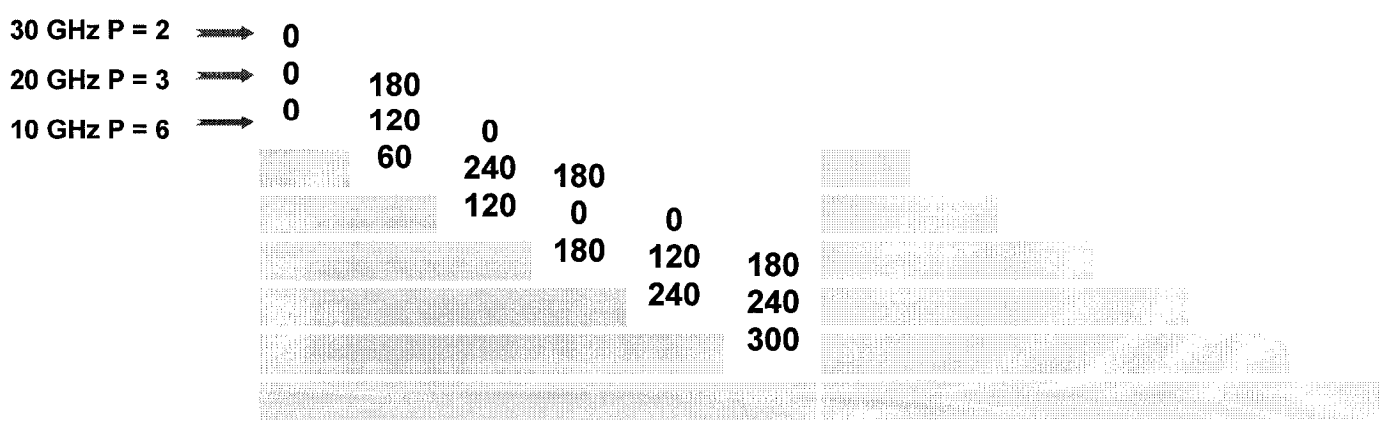

Figure E.4: Phase compensation for 3 discrete frequencies

Setting P=2 for the 30GHz signal and P=3 for the 20GHz signal ensured that the ratio λ/P was equal to a constant 5. This in turn meant that the groove height and radius was identical for both the frequencies. The down side of this approach is that the phase adjustment that occurs for the two frequencies is not equal. As illustrated in the figure above the 30GHz signal is phase compensated every 180^0 while the 20GHz signal is phase compensated every 120^0, carrying on to a hypothetical 10GHz signal the phase compensation is even better at every 60^0. This does mean that the lens displays a greater focusing effect for the lower frequencies that for the higher frequencies. However if this can be tolerated then it is not a great price to pay for the increased versatility of the lens. Using this method the lens shown in Figure E.5 was designed:

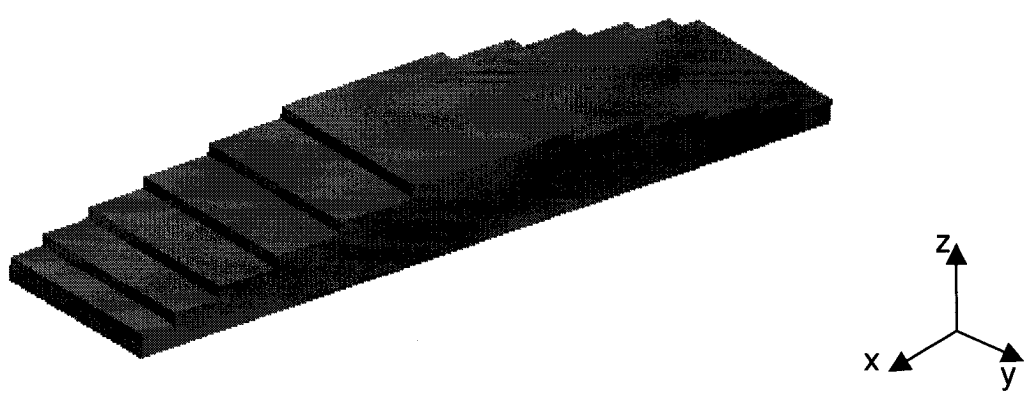

Figure E.5: Illustration of 6 step 1-D lens – Simulation setup

Table E.1 is a summary of the critical dimensions.

Table E.1: 6-step Fresnel Lens critical dimensions

Frequency	10/20/30 GHz	
εr	2.2	
P	6/3/2	
Step size	10.34 mm	
Step #	**Radius R_i – X axis [mm]**	**Step location –Y axis [mm]**
1	32.01	10.34
2	45.82	20.69
3	56.78	31.04
4	66.33	41.28
5	75.0	51.73
6	83.06	62.08

Despite the promise displayed by the above innovation there still remained a problem. For the design at hand the phase correction factor of P=2 for the 30GHz signal was not considered sufficient to obtain the focusing required. This meant that a higher P was required. The next available multiple of P that can take advantage of the ideas outlined above would be a P=4 for 30GHz and a P=6 for 20GHz. The problem with doing this though meant that a twelve-step lens would be required (This is the next possible step number where the dimensions for a 20GHz and a 30GHz lens will converge). This is not desirable as it leads to a thicker lens, which cancels out the initial weight savings that were being aimed for. In search for a solution to this problem it was decided to investigate the use of perforated lenses.

E.4 Perforated Lenses.

Another alternative to phase correcting a wave by using different height zones is to maintain each zone at a single height but then utilize different dielectrics for the various zones. Doing so ensures that the required phase compensation occurs while getting rid of the grooves. However it is not a trivial

task to machine and integrate a variety of dielectrics of different mechanical properties to form the aforesaid lens. What can be done instead is to use a single dielectric slab and then strategically perforate the lens so that the combination of the dielectric constant of air in the perforation and the dielectric constant of the slab material yield a third effective dielectric constant.

An effective dielectric constant can achieved by proportioning, the size of the perforation to its occupied unit area (also known as the filling factor). For a triangular lattice as in Figure E.6 the following equations describe the relationship between the effective dielectric constant and filling factor α of a unit cell.

$$\varepsilon_{eff} = \varepsilon_r(1+\alpha)+\alpha$$

$$\alpha = \frac{A_0}{2A} = \frac{d^2\pi/4}{2(\sqrt{3/4})s^2} = \frac{\pi}{2\sqrt{3}}\left(\frac{d}{s}\right)^2 \qquad \textbf{[E.3]}$$

α is the filling factor, A_o is the area of the hole, A is the area of the unit cell, s is the spacing between the holes and d is the hole diameter

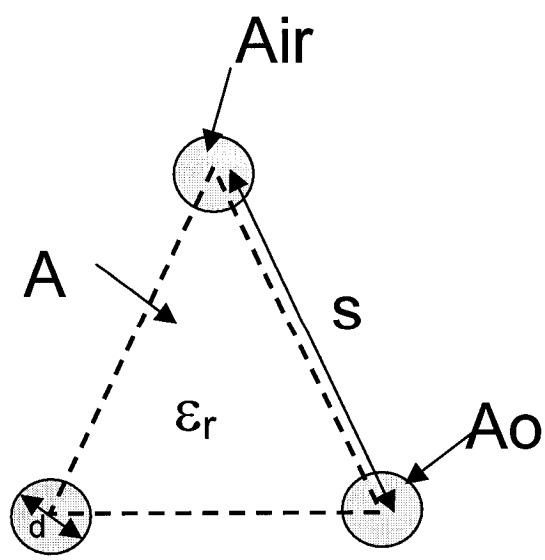

Figure E.6: Perforated lens unit cell

E.5 Multi frequency Perforated Lens

With the above design equations in hand the goal was now to make the perforated lens multi frequency capable by combining it with the ideas presented in section E.3.

The main aim was to use a perforated lens to increase the phase correction factor P to P=4 for the 30 GHz signal. For a multi-dielectric lens (where the lens thickness (t) remains constant), the required values of permittivity (ε_m) are obtained using:

$$t = \frac{\lambda_0}{P(\sqrt{\varepsilon_{rn}} - \sqrt{\varepsilon_{rn-1}}} \qquad \textbf{[E.4]}$$

Instead of 12 steps now we require 12 different dielectric constants so that the phases align at both 20GHz and 30GHz. The lens thickness is set by the maximum and minimum permittivites allowed:

$$t_{\min} = \frac{(N-1)\lambda_0}{P(\sqrt{\varepsilon_{r\max}} - \sqrt{\varepsilon_{r\min}}} \qquad \textbf{[E.5]}$$

It is desirable to start as high as possible with the ε_{rmax} in order to have the widest range of effective dielectric constants. For this design a material known as Stycast with an ε_r=10 was selected. The ε_{rmin} was set by the mechanical properties of the Stycast. From previous experience it was known that the maximum allowable d/s ratio was 11/12 after which the Stycast lens would begin cracking. With a d/s =11/12 the ε_{rmin} = 19.78mm.

Using these numbers and plugging into equation E.5 recursively yield the results shown in Tables E.2 for 30 GHz and E.3 for 20GHz.

Table E.2: 12 zone perforated Fresnel lens – Perforation size and placement @ 30GHz

Frequency	30 GHz			
λo	10.00mm			
Lens Thickness	19.78mm			
P	4			
ε_{rmax}	10			
Step #	ε_{eff}	α	**d/s**	**Ao/A**
0	10.00	0	0	0
1	9.22	0.087043	0.31	0.174086
2	8.47	0.170536	0.434	0.341073
3	7.75	0.25048	0.526	0.500959
4	7.06	0.326873	0.6	0.653746
5	6.40	0.399717	0.664	0.799433
6	5.78	0.46901	0.719	0.93802
7	5.19	0.534754	0.768	1.069508
8	4.63	0.596948	0.811	1.193896
9	4.10	0.655592	0.85	1.311184
10	3.60	0.710686	0.885	1.421372
11	3.14	0.76223	0.917	1.52446

Table E.3: 12 zone perforated Fresnel lens – Perforation size and placement @ 20GHz

Frequency	20 GHz			
λo	15.00mm			
Lens Thickness	19.78mm			
P	6			
$\varepsilon_{r\,max}$	10			
Step #	ε_{eff}	α	**d/s**	**Ao/A**
0	10.00	0	0	0
1	9.22	0.087043	0.31	0.174086
2	8.47	0.170536	0.434	0.341073
3	7.75	0.25048	0.526	0.500959
4	7.06	0.326873	0.6	0.653746
5	6.40	0.399717	0.664	0.799433
6	5.78	0.46901	0.719	0.93802
7	5.19	0.534754	0.768	1.069508
8	4.63	0.596948	0.811	1.193896
9	4.10	0.655592	0.85	1.311184

10	3.60	0.710686	0.885	1.421372
11	3.14	0.76223	0.917	1.52446

As can be seen from the above tables the dielectric constants and therefore the filling factor α can be made to converge by appropriately selecting the right phase correction factor P.

The design work presented above made it clear that it was possible to manufacture a 12 zone perforated lens to work at multiple frequencies. Other advantages of a perforated lens as opposed to the step zoned Wood design are that the weight and complexity of a 12 variable height zone lens was avoided, greater focusing was achieved than a 6-zone variable height lens, the cost and weight of a full homogenous lens was avoided and finally a novel new application for a perforated lens was discovered.

With the dimension ratios worked out to obtain the desired effective dielectric constants for the different zones a MATLAB program was written to automate the layout (See Appendix C). Since the ratio of the hole diameter to spacing was already calculated all that remain was to select an appropriate bit to drill the required diameter. From the d/s ratio calculated above the spacing between holes could then easily be calculated. In the figure below the hole diameters i.e. the drill bits have been varied over the different zones. An easier approach would be to select the same bit size and vary the spacing. For a 12 step lens, the hole dimensions and spacings for the required ε_{eff} . are shown in Table E.4.

Table E.4: 12 zone perforated Fresnel lens – Critical dimensions

Step #	ε_{eff}	Hole diameter – d [mm]	Spacing – s [mm]
0	10.00	N/A	N/A
1	9.22	0.254	0.82
2	8.47	0.254	0.59
3	7.75	0.254	0.48
4	7.06	0.254	0.42
5	6.40	0.254	0.38
6	5.78	0.254	0.35
7	5.19	0.254	0.33
8	4.63	0.254	0.31
9	4.10	0.254	0.30
10	3.60	0.254	0.29
11	3.14	0.254	0.27

Using these values a cross section of the lattice can be seen in Figure E.7. As can seen the spacing between the holes for the final zone is approaching the maximum of d/s ratio of 11/12 (This maximum has been obtained from the work done previously at the CRC with perforated lens. When d/s > 11/12 the Stycast begins to crack)

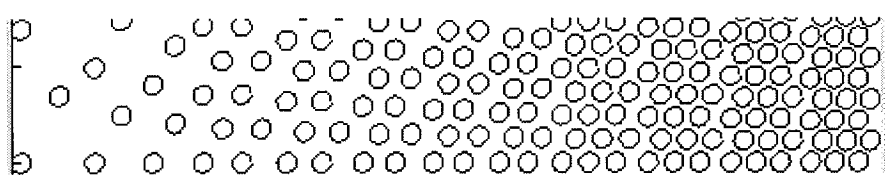

Figure E.7: Performated lens with constant diameter holes

An alternate method of building the lens then is to vary both the bit size, which sets the *d* and therefore the spacing *s*. An example lens is shown bin Figure E.8 for such a case.

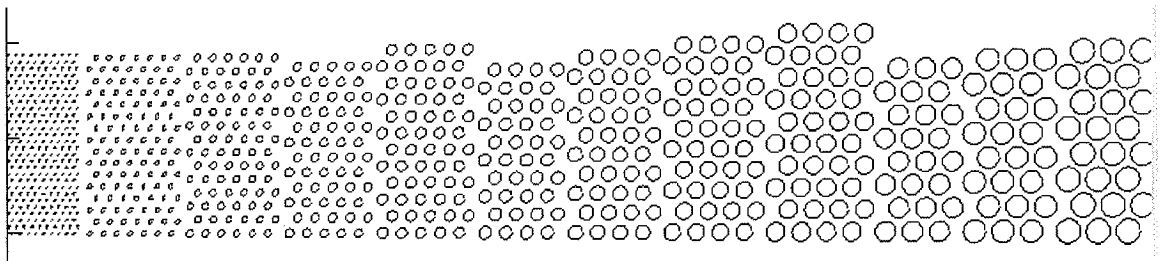

Figure E.8: Perforated lens with diameter of holes varied

E.6 Conclusion

Unfortunately despite the novelty and the elegance of the design it was not possible to machine the perforated lens. This was mainly due to the time constraints that were present on availability of milling machines. Milling such a lens would require a long time due to the large number of perforations required while at the same time ensuring that the material does not crack. Despite this setback it is hoped that the ideas presented above would find an application in the future. Measurements that were carried out of a 4 zone perforated lens indicated that the focusing effect for multiple frequencies that were outlined in the previous sections will occur should the lens be designed correctly i.e. the measurements were promising but are not presented here due to the fact that lens tested was not purposely built for the 20/30GHz range.

For the present it was decided to use just a grooved zoned lens working at a single frequency of 30 GHz to finalize the design.

REFERENCES:

[Arps00] Antenna Radiation Patterns Software Version 3.0, Farfield Corporation.

[Asho92] H. Ashoka, "Practical Realisation of Difficult Microstrip Line Hybrid Couplers and Power Dividers". *IEEE Microwave Theory Tech Digest.* Vol. MTT-S pp. 273 – 276, September 1992.

[Bala82] C. Balanis, "Antenna Theory – Analysis and Design". *John Wiley & Sons,* 1982.

[Chou02] Gerald Chouinard, "Rural and Remote Broadband Access – CRC R&D Program," *CRC Internal Presentation*, pp. 22. Ottawa Canada, Dec. 2002.

[Deck00] B. Deckman, D.S. Deakin Jr., E. Sovero, D. Rutledge, "A 5-Watt, 37-GHz Monolithic Grid Amplifier". *International Microwave Symposium Boston.* June 2000.

[Deli02] M.P. DeLisio, R.A York, "Quasi-Optical and Spatial Power Combining". *IEEE Trans. Microwave Theory Tech.* Vol. 50, MTT-3 pp.929 – 936, March 2002.

[Garg01] R. Garg, P. Bhratia, I. Bahl, A. Ittipiboon, "Microstrip Antenna Design Handbook". *MA Artech House,* Boston, 2001.

[Guo01] Y. Guo, K. Luk, K. Lee, R. Chair, "A Quarter-Wave U shaped Patch Antenna with Two Unequal Arms for Wideband and Dual

Frequency Operation". *IEEE Trans. on Antennas & Propogation.* Vol.50, No.8 pp.1082 – 1087, Aug 2002.

[Hans98] R.C. Hansen, "Phased Array Antennas". *Wiley Series in Microwave and Optical Engineering,* John Wiley & Sons,1998

[Harv00] J. Harvey, E.R. Brown, D.B. Rutledge, R.A. York, "Spatial Power Combining for High Power Transmitters". *IEEE Microwave Magazine.* ISSN 1527-3342 pp.48 – 58, Dec. 2000

[Hrist00] H.D. Hristov, "Fresnel Zones in Wirless links, Zone Plate Lens and Antennas". *Artech House,* Boston, 2000

[Jame88] J.R. James, G. Andrasic, "Superimposed Dichroic Microstrip Antenna Arrays". *IEE Proceedings.* Vol.135, No.5 pp.304 – 312, Oct. 1988

[Krau88] J.D. Kraus, "Antennas". *McGraw Hill,* Second Edition, 1988.

[Lim01] J.S. Lim, S.W. Lee, C.S. Kim, J.S. Park, D. Ahn, S. Nam, "A 4:1 Unequal Wilkinson Power Divider". *IEEE Microwave and Components Letters*, Vol.11, No.3 pp.124 – 126, March 2001.

[Loso90] F.G. Loso, "US Army Tactical EHF Communications Overview" *Tactical Communications Conference*, Tactical Communications - Challenges of the 1990's, Vol.1 24-26, pp. 217 –234, April 1990.

[Maci97] S. Maci, G. B. Gentili, "Dual-Frequency Patch Antennas". *IEEE Antennas and Propagation Magazine.* Vol. 39, No. 6 pp.13 – 20, Dec. 1997

[Mehr78] R. Mehran, "Calculation of Microstrip bends and Y-Junctions with

Arbitrary Angle". *IEEE Trans. Microwave Theory Tech.* Vol. MTT-26 pp. 400 – 405, June 1978.

[Peto01] A.Petosa, A. Ittipiboon, "A Fresnel Lens Designed Using a Perforated Dielectric". *Symposium on Antennas Technology and Applied Electromagnetics ANTEM*, Montreal, Canada, pp.399 – 403 Aug. 2002.

[Peto99] A. Petosa, A. Ittipiboon, M. Cuhaci, "Low Profile Dielectric Resonator Antenna Arrays for Reflector Feeds". *29th European Microwave Conference*, Munich Germany, pp. 171 – 174, Oct. 1999.

[Poza98] D.M. Pozar, "Microwave Engineering". *John Wiley & Sons,* Second Edition, 1998.

[Rutl99] D.B. Rutledge, N. Cheng, R.A. York, "Failures in Power Combining Arrays". *IEEE Trans. Microwave Theory Tech.* pp.1 – 7, Jan. 1999.

[Shaf93] L. Shafai, H. Moheb, D. Roscoe, "Microstrip Antenna design Candidates for 20/30GHz Personal Communications" *2nd International Conference on Universal Personal Communications,* Vol. 2 12-15. pp. 906 –908, Oct. 1993.

[Shak00] J. Shaker, S. Jette, A. Petosa, J. Bradley, M. Cuhaci, "A novel bifocal dual-frequency, dual orthogonal polarisation planar reflector for SatCom applications," *AP2000,* pp. 603, Davros, Switzerland, Vol. 1, April 2000.

[Shak02] J. Shaker, A. Petosa, S. Thirakoune, C. Pike, M. Cuhaci,

"Investigation of the performance of a reflectarray fed by an active feed block to establish link with ACTS," *ANTEM 2002*, pp. 506 – 509. Montreal, Canada, Aug. 2002.

[Stou00] S. Stout, "Compact Dielectric-Loaded Patch Antennas for L-Band Mobile Satellite Applications". *CRC Report No. CRC-RP-2000-003*. Appendix 3, Jan.2000